WCAP-9736

MULTIFLEX 3.0
A FORTRAN-IV COMPUTER PROGRAM FOR
ANALYZING THERMAL-HYDRAULIC-STRUCTURAL
SYSTEM DYNAMICS (III) ADVANCED BEAM MODEL

K. Takeuchi, D. J. Kowalski,
D. R. Bhandari, and L. T. Gesinski

July, 1982

APPROVED: _F. F. Cadek_

F. F. Cadek, Manager
Safeguards Engineering and Development

TABLE OF CONTENTS

TABLE OF CONTENTS (CONTINUED)

TABLE OF CONTENTS (CONTINUED)

LIST OF TABLES

LIST OF ILLUSTRATIONS

LIST OF ILLUSTRATIONS (CONTINUED)

LIST OF ILLUSTRATIONS (CONTINUED)

ACKNOWLEDGEMENTS

ABSTRACT

MULTIFLEX is a computer code to calculate hydraulic force for structure evaluation during a LOCA type transient. This report describes the program and the mathematical representation of the thermal-hydraulic system interacting with the mechanical structure system. While the original beam model is described in the previous report, WCAP-8708^{+}, and the code description of the shell model and the projector method is given in WCAP-8920^{++}. The present report describes the advanced beam model; i.e., the network downcomer model equivalent to two-dimensional fluid-structure interactions, the non-linear boundary conditions with impact damping, the relative modal analysis for vessel motion, the sliding friction loss, and the possible application of the external loads. It also covers the pre-processor, RELMØDE.

[+] The version of the code for the original beam model is referred to as MULTIFLEX 1.0.

[++] The corresponding version of the code is referred to as MULTIFLEX 2.0.

1.0 INTRODUCTION

The MULTIFLEX program is an engineering tool for calculation of hydraulic loads on the reactor internals structure and the pressure vessel during rapid thermal hydraulic transients caused by an imposed driving force on the system. The driving force is taken, throughout this report, to be a break of a primary or secondary loop in a PWR system or simulation of the experiments related to rapid depressurizations. The hydraulic loads are computed in this code by taking into account the hydraulic-structural interactions. It is constructed by incorporating structural models into the thermal-hydraulic code, BLØDWN-2A (see Reference 1).

The thermal-hydraulic portion of MULTIFLEX is based on the 1-dimensional homogeneous model[1,2] which is expressed in a set of mass, momentum, and energy conservation equations. These equations are quasi-linear first order partial differential equations which are solved by the method of characteristics[1,3,4,5, 40]. The employed numerical method is the explicit scheme. Consequently, time steps for stable numerical integration are restricted by sonic propagation[6].

The walls surrounding a hydraulic path may deviate from their neutral positions depending on the force differential on the wall. Usually thermal-hydraulic programs such as BLØDWN-2A ignore this displacement thereby considering the wall as rigid, i.e., rigid wall treatment. In the MULTIFLEX[7-9] code, the wall displacements are represented by those of 1-dimensional mass points which are described by mechanical equations of vibration. A variety of structural models have been incorporated in MULTIFLEX. The independent mass model was reported in Reference 7. The second MULTIFLEX report[8] describes the original beam model. The third report[10] covers description of 2-directional beam models, shell models, and projector models. All of these models are available as options in the present MULTIFLEX code. The beam model option and the shell model option are frequently referred to as BEAMFLEX and SHELLFLEX, respectively. These structural equations are solved by means of the Laplace transformation over the small time step determined by the numerical stability of the hydraulic system. Verification of the code as a general analysis tool for a fluid-structure interaction system is given in References 9 and 11. Sensitivity study of the original beam model is made in Reference 12.

When the original beam model was developed, the gap size between the core barrel flange and the pressure vessel was regarded as very small (on the order of 30 mils).

In this situation, the linear MULTIFLEX structural model was proven to respond to a LØCA transient consistent with the non-linear DARI-WØSTAS model[13]. Recently, however, the consistency can no longer be attained as the gap size is realized to be fairly large (on the order of 120 mils). Moreover, the boundary is non-linear even after the gap is closed. In addition, a method of network downcomer modeling with fluid-structure interaction has been developed for a more realistic representation of the downcomer annulus[14-16]. In order to improve the calcula-tional technique, an advanced beam model has been developed, which is reported in the present paper. This advanced beam model deals with

i)   the non-linear boundary conditions by the intermediate pseudo-force method[17],
ii) the vessel motion by the relative modal analysis[18],
iii) the downcomer annulus by the network modeling.

These are described in the following.

In Section 2.1, the problem to be solved is expressed in a mathematical form by presenting the thermal-hydraulic conservation equations, the mechanical equation of vibration, and the coupling term between the two systems. However, the detailed discussions in deriving characteristic equations and in using the steam tables are rendered to Reference 8. The methods of solving the mechanical equations are dis-cussed in Section 2.2. The advanced beam model is discussed in Section 2.2. First, the conventional modal analysis is given to introduce development and formulation of the relative modal analysis. In this new formulation, the external loads can be also introduced. Finally, the intermediate pseudo-force method is presented. In Section 2.3, the one-dimensional network formation is briefly reviewed that is equivalent to two-dimensional fluid-structure interactions.

Presented in Section 3 is a brief summary of the code structure and the functional relations of MULTIFLEX to structure codes such as WECAN[27] and DARI-WØSTAS[28,29]. The input data instructions are presented in Section 4.1. To supplement the in-structions, sample input data for all IØSTYPs are explained in Section 4.2 and a method of computing the advanced beam structural data is also discussed.

Discussed in Section 5 is a detailed description of structural input data computa-tion. The structural models for non-linear boundary conditions at the barrel and vessel flanges are discussed in Section 5.1. This is followed by the normal mode analyses for the relative modal analyses, in Section 5.2 and Appendix A. An ap-

plication of the advanced beam model is explained with an example of a thermal shield three-loop plant in Section 4.2 and it is briefly summarized in Section 6.1. The MULTIFLEX non-linear boundary condition is verified in Section 6.2 by comparison of barrel/vessel relative displacements computed by MULTIFLEX and WECAN codes. Results of a sensitivity study is presented in Section 6.3 in terms of the magnitudes of the maximum vessel support loads and the maximum fuel grid impact loads. A detailed description of the modeling of a three-loop neutron panel plant which has distinguished features from the thermal shield plant is given in Section 7.1. Computed pressure differentials, hydraulic forces, and structural response are given in Section 7.2. Computed results are also analyzed in this section.

2.0 MATHEMATICAL DESCRIPTION OF THERMAL-HYDRAULIC-MECHANICAL SYSTEMS

This code obtains the thermal-hydraulic state of a system and calculates hydraulic loads on the internal structure by solving the conservation equations shown in Section 2.1, coupled with the structural dynamic equations for the advanced beam model discussed in Section 2.2: The conventional modal analysis is summarized in Section 2.2.1, which is then developed to the relative modal analysis in Section 2.2.2. The non-linear boundary conditions are treated by the intermediate pseudo-force method in Section 2.2.3. The rules of one-dimensional network formation is summarized in Section 2.2.4.

2.1 CHARACTERISTIC EQUATIONS AND STRUCTURAL DYNAMICS

The dynamic variables that specify the thermal-hydraulic state of the fluid are density $\rho(z,t)$, mass flow rate $G(z,t)$, pressure $p(z,t)$, and enthalpy $h(z,t)$, at a certain point in space z and time t. For a one-dimensional homogeneous model, the conservation laws become as follows:

Conservation of mass:

$$\frac{\partial}{\partial t} (\rho A) + \frac{\partial}{\partial z} (GA) = 0 \qquad , \tag{2-1}$$

Conservation of momentum:

$$\frac{\partial}{\partial t} (GA) + \frac{\partial}{\partial z} (uGA) + Ag_c \frac{\partial}{\partial z} p = - \rho FA \qquad , \tag{2-2}$$

Conservation of energy:

$$\frac{\partial h}{\partial t} + u \frac{\partial h}{\partial z} - \frac{1}{J\rho} \left(\frac{\partial p}{\partial t} + u \frac{\partial p}{\partial z} \right) = Q + \frac{uF}{Jg_c} \qquad , \tag{2-3}$$

where u is the fluid velocity, conversion factors g_c and J are the gravitational constant (32.2 $lb_m ft/lb_f sec^2$) and the mechanical-thermal conversion ratio (778 $lb_f ft/Btu$), respectively. The F stands for the sum of frictional and gravitational contributions,

$$F \equiv \frac{f}{2 D_{eff}} u|u| + g \cos \alpha \qquad , \tag{2-4}$$

when a pipe of effective diameter D_{eff} with friction factor f is elevated at an angle α, where g is the acceleration of gravity (32.2 ft/sec^2). The heat deposition rate per unit mass is denoted by Q.

2-1

By the method of characteristics, the above partial differential equations are reduced to ordinary differential equations. The detailed derivation is shown in Reference 8. The "C+ and C- characteristic equations"

$$\frac{dG}{dt_+} + \frac{g_c}{c}\frac{dp}{dt_+} = u\frac{d\rho}{dt_+} - \rho F + \frac{g_c}{c}Q''' - c\rho\frac{\dot{A}}{A} \tag{2-5}$$

and

$$\frac{dG}{dt_-} - \frac{g_c}{c}\frac{dp}{dt_-} = u\frac{d\rho}{dt_-} - \rho F - \frac{g_c}{c}Q''' + c\rho\frac{\dot{A}}{A} \tag{2-6}$$

are valid respectively on the C+ and C- characteristics determined by

$$\frac{dz}{dt_\pm} = u \pm c \qquad . \tag{2-7}$$

These two equations are for the acoustic signal transportation at the sonic velocity c. The "CH- characteristic equation"

$$\frac{dh}{dt_o} = Q + \frac{uF}{Jg_c} + \frac{1}{J\rho}\frac{dp}{dt_o} \tag{2-8}$$

is defined on the material characteristics

$$\frac{dZ}{dt_o} = u \qquad . \tag{2-9}$$

The quantities, p, G, and h are computed as above and then ρ and the sonic velocity c are determined by the use of the steam table (References 8 and 11).

The effect of the flow area variation appears in the last terms of Eqs. (2-5) and (2-6). The flow area is a function of the structural deformation, vector [x], which is obtained by solving the equation of structural motion,

$$\{M\}[\ddot{x}] + 2\eta\sqrt{\{M\}\{K\}}[\dot{x}] + \{K\}[x] = [f(p)] \tag{2-10}$$

subjected to the hydraulic force on the right hand side, where {M} and {K} are mass and stiffness matrices respectively and η is the damping ratio. In these matrices, one may employ the independent mass model, the beam model, or the shell model which is discussed in the following sections.

The hydraulic force $[f(p)]$ and $\rho c \dot{A}/A$ in Eqs. (2-5) and (2-6) constitute the coupling between the hydraulic and the structural systems. If the coupling terms are ignored, Eqs. (2-5) and (2-6) are reduced to the conventional characteristic equations in Reference 1 (A = constant, rigid walls). In order to specify the coupling terms, consider N mass points representing the structure, i.e., the structural wall is discretized into N walls. Their displacements from the neutral positions have been denoted by the vector $[x]$ in which the i-th element corresponds to mass point i.

(2-11)

(2-12)

(a,c)
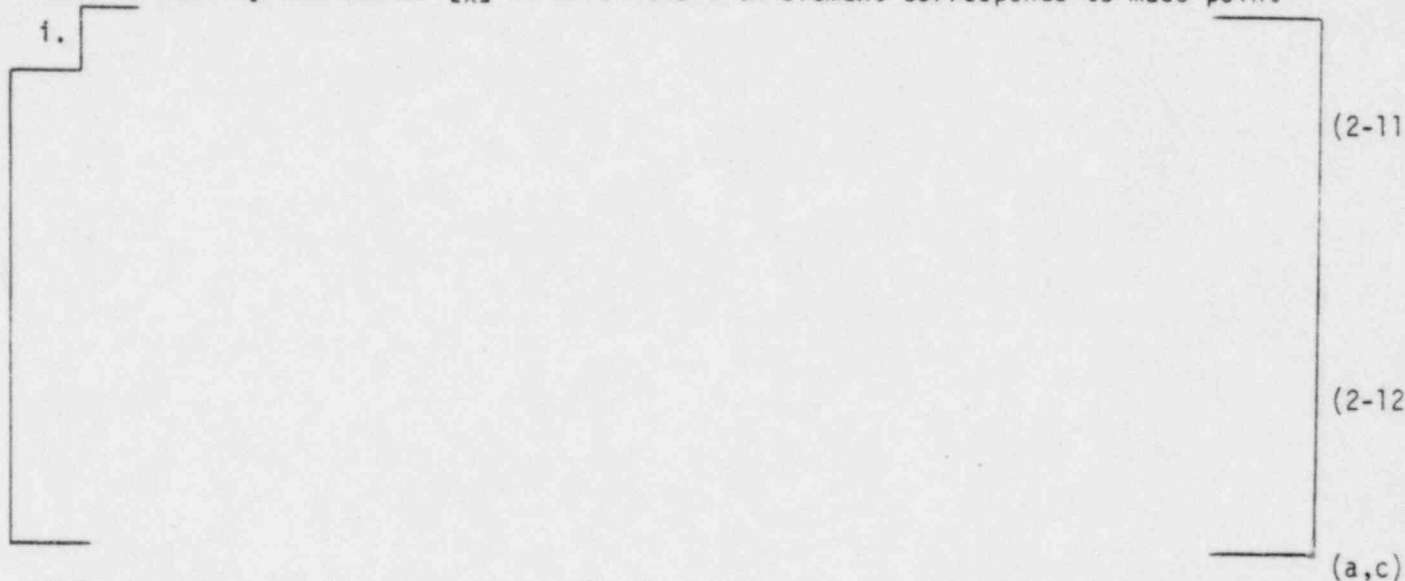
With the above coupling terms, Eqs. (2-5) - (2-10) are simultaneously solved. In practice, the explicit-scheme difference equations are derived from the characteristics (see Reference 8). The von-Neumann stability condition is found to be the Courant-Friedrich-Lewy criterion. Although the numerical stability of the combined hydro-structural system equations has not been analyzed, it is found by experience that the stability is regulated by the condition for the explicit hydraulic equations[8].

2.2 STRUCTURAL MODELS

Methods for constructing Eq. (2-10) and its solution technique are discussed in this section. In the case of independent mass model, M and K matrices are diagonal and so Eq. (2-10) can be solved straight-forwardly.

For beam and shell models, M and K are non-diagonal and various solution techniques are available in the current version of MULTIFLEX. The options developed in the past are:

1) Independent Mass Model in References 8 and 10 is applied to analyses of steam generators (see References 7, 19, 20, and 21).

2) <u>One-Directional Beam Model</u> extensively discussed in Reference 8 is applied to most design computations (see, for example, Reference 22).

3) <u>Two-Directional Beam Model</u> is explained in Reference 10 and its application can be found in conjunction with the projector method.

4) <u>Shell Model</u> discussed at length in Reference 10 is applied to design computation of the reactor internals (see Reference 23).

5) <u>Projector Method</u> much discussed in Reference 10 is applied to analyses of experiments of the 1/24-th scale RPV model[16].

These subjects are discussed in the previous reports, References 8 and 10. In the present report, the advanced beam models are discussed. Introduced in Section 2.2.1 is the conventional beam model which is developed in Section 2.2.2, the relative modal analysis to take into account the vessel motion. The non-linear boundary conditions are solved by means of the intermediate modal analysis in Section 2.2.3 and it is incorporated into the relative modal analysis.

The rules of one-dimensional network formation are summarized in Section 2.2.4, but the practical method of the network downcomer modeling is illustrated in later sections.

2.2.1 MODAL TECHNIQUE, IN GLOBAL COORDINATE SYSTEM

Modal analysis[11,12] can be used to solve the eigenvalue problem,

$$M^{-1} K \phi_i = \omega_i^2 \phi_i \qquad (2-13)$$

with ortho-normality relation,

$$\phi_i^T M \phi_j = m_i^* \delta_{ij} = \omega_i^{-2} \phi_i^T K \phi_j \qquad . \qquad (2-14)$$

The i-th eigenvector ϕ_i is the mode shape, and m_i^* is called the generalized mass. The eigenvectors are collectively expressed by a matrix $\phi = [\phi_i]$.

Then, the solution of Eq. (2-10) is expressed by the eigenfunction expansion,

$$x = \sum_i q_i (t) \phi_i = \phi q \qquad . \qquad (2-15)$$

2-4

The equation for the expansion vector q is obtained by applying Eq. (2-15) to Eq. (2-10) and then operating by ϕ^T from the left hand side,

$$\ddot{q} + 2 \eta \Omega_o \dot{q} + \Omega_o^2 q = \not{f} \qquad (2\text{-}16)$$

where use is made of Eq. (2-14) and the definitions,

$$\Omega_o^2 \equiv (M\star)^{-1} \phi^T K \phi \qquad , \qquad (2\text{-}17)$$

$$\not{f} \equiv (M\star)^{-1} \phi^T f \qquad , \qquad (2\text{-}18)$$

and

$$M\star \equiv \phi^T M \phi \qquad . \qquad (2\text{-}19)$$

$$\qquad (2\text{-}20)$$

$$\qquad (2\text{-}21)$$

$$\qquad (2\text{-}22)$$

(a,c)
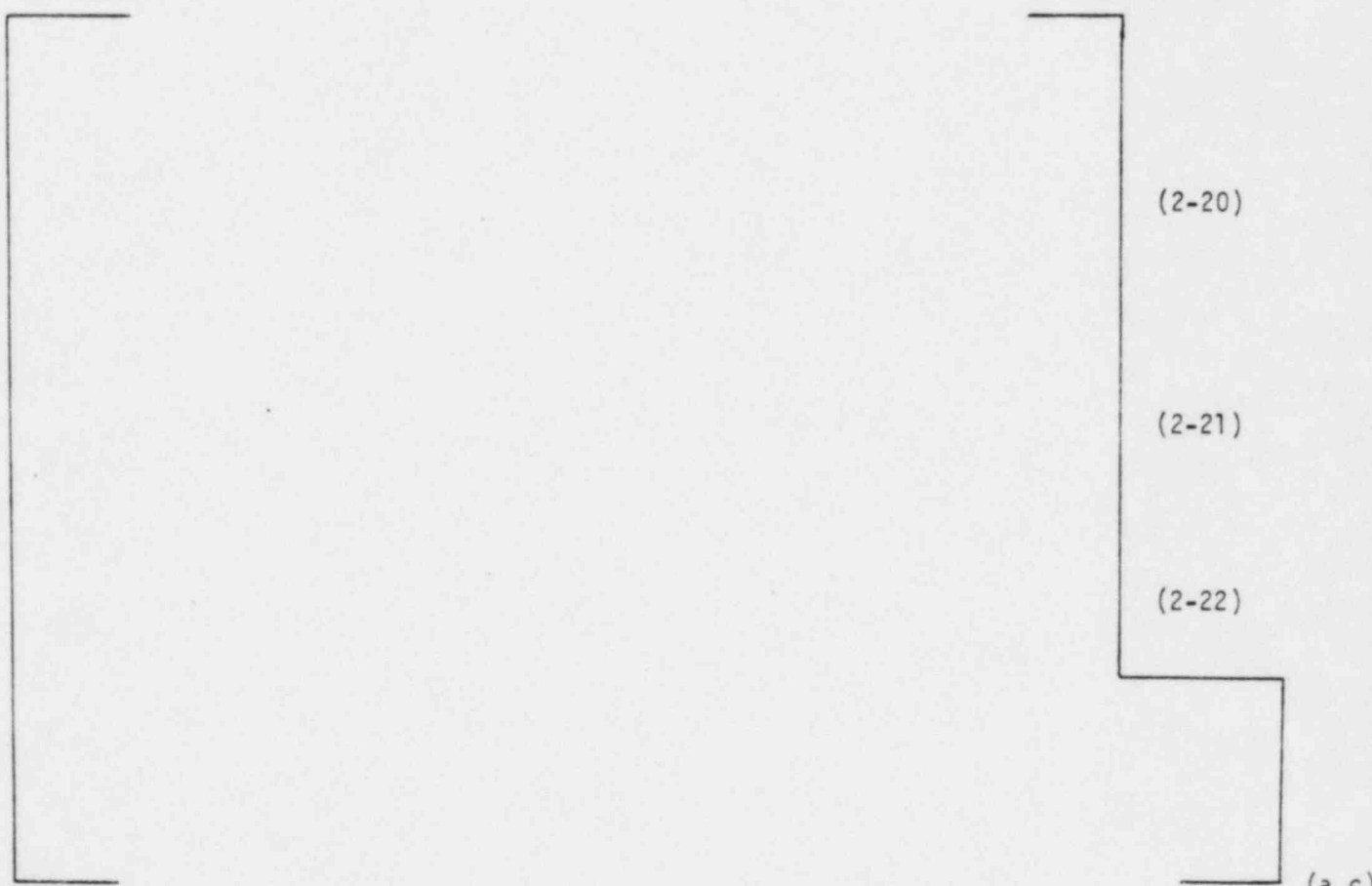
2.2.2 RELATIVE MODAL ANALYSIS

The fluid structure interactions in the downcomer annulus are effective only

when the core barrel displaces or deforms relative to the vessel. The original beam model is developed based on the conventional modal analysis (see Section 2.2.1) for the absolute barrel displacements, under the assumption that the vessel is motionless. To take into account the vessel motion, a relative modal analysis is developed below. Consequently, it is found that the formulation of the conventional modal analysis can be utilized without changes, but the structural input data must be computed by the use of the relative modal analysis.

2.2.2.1 Fluid Structure Interactions In A Deformable Coaxial Cylinder

In order to introduce the problem, consider that beam motion of the barrel and the vessel in the annulus region are described by displacement vectors X_B and X_V for n nodes each, respectively. For linearized boundary conditions, the structural equation for these displacements is

$$M \frac{d^2}{dt^2} \begin{pmatrix} X_V \\ X_B \end{pmatrix} + 2n \sqrt{MK} \frac{d}{dt} \begin{pmatrix} X_V \\ X_B \end{pmatrix} + K \begin{pmatrix} X_V \\ X_B \end{pmatrix} = \begin{pmatrix} f_V \\ f_B \end{pmatrix} \qquad (2\text{-}24)$$

subjected to the hydraulic forces f_V and f_B acting respectively on the vessel and the barrel. Feedback of the structural motion to the fluid system is expressed by changing rate of local volume, Equations (2-5) and (2-6)

$$\text{Hydraulic Cons.} = -\rho c \frac{\dot{V}}{V} \ (= -\rho c \frac{\dot{A}}{A}) \qquad (2\text{-}25)$$

and

$$\dot{V} = W_B \dot{X}_B - W_V \dot{X}_V \qquad (2\text{-}26)$$

where the direction cosines of the beam motion and the barrel surface normal are inclusive in the wall areas W_B and W_V, respectively.

2.2.2.2 Conventional Modal Analysis

The conventional modal analysis is applied to Eq. (2-24) as follows: Transform the displacement vector to the generalized coordinate q by the mode shape matrix ϕ, as Eq. (2-15),

$$\begin{pmatrix} X_V \\ X_B \end{pmatrix} = \phi q \qquad (2\text{-}27)$$

where ϕ is obtained by solving the eigenvalue problem,

$$M^{-1} K \phi = \phi \, \Omega_o^2 \qquad . \tag{2-28}$$

The eigenvalues in the diagonal matrix Ω_o are the in-air frequencies. Suppose m mode shapes are chosen for the calculation. Then, ϕ is a ($2n \times m$) matrix, Ω_o is a ($m \times m$) matrix, and q is a vector ($m \times 1$). Applying Eqs. (2-27) and (2-28) to Eq. (2-24), one finds the equation for the generalized coordinate, Eq. (2-16),

$$\ddot{q} + 2\eta \, \Omega_o \dot{q} + \Omega_o^2 \, q = (M^*)^{-1} \, \phi^T \begin{pmatrix} f_V \\ f_B \end{pmatrix} \tag{2-29}$$

where M^* is the generalized mass matrix. After solving Eq. (2-29), q is substituted to Eq. (2-27) to get the displacements,

$$X_V = \phi_V \, q \tag{2-30}$$

$$X_B = \phi_B \, q \tag{2-31}$$

where ϕ is blocked,

$$\phi = \begin{pmatrix} \phi_V \\ \phi_B \end{pmatrix} \qquad . \tag{2-32}$$

In the above expressions, the vessel and the barrel components of displacements, mode shapes, and forces are explicitly written out of the modal analysis in Section 2.2.1. But these notations are introduced to clarify the following discussions.

2.2.2.3 Relative Modal Analysis

A relative coordinate for MULTIFLEX computation is chosen as

$$r \equiv X_B - \frac{W_V}{W_B} X_V \tag{2-33}$$

such that Eq. (2-26) becomes

$$\dot{V} = W_B \, \dot{r} \qquad . \tag{2-34}$$

Its dyadic coordinate is defined by

$$R \equiv X_B + \frac{W_V}{W_B} X_V \qquad . \tag{2-35}$$

In summary, the transformation between these two coordinate system is achieved by (2n x 2n) matrix U,

$$\begin{pmatrix} r \\ R \end{pmatrix} = U \begin{pmatrix} X_V \\ X_B \end{pmatrix} \tag{2-36}$$

where

$$U \equiv \begin{pmatrix} -\ W_V/W_B & -1 \\ -\ W_V/W_B & -1 \end{pmatrix} \tag{2-37}$$

and its inverse matrix

$$U^{-1} = \frac{1}{2} \begin{pmatrix} -\ W_B/W_V & W_B/W_V \\ -\ 1 & 1 \end{pmatrix} \qquad . \tag{2-38}$$

Applying Eq. (2-27) to Eq. (2-26), one gets a new mode shape matrix Ψ,

$$\begin{pmatrix} r \\ R \end{pmatrix} = \Psi q \tag{2-39}$$

where

$$\Psi \equiv U\phi = \begin{pmatrix} \phi_B - \frac{W_V}{W_B} \phi_V \\ \phi_B + \frac{W_V}{W_B} \phi_V \end{pmatrix} = \begin{pmatrix} \psi_r \\ \psi_R \end{pmatrix} \tag{2-40}$$

Thus, the relative coordinate becomes

$$r = \psi_r\, q \qquad . \tag{2-41}$$

Next, the force term in Eq. (2-29) is transformed,

$$(M^\ast)^{-1}\ \phi^T \begin{pmatrix} f_V \\ f_B \end{pmatrix} = (M^\ast)^{-1}\ \phi^T\ (U^{-1}\ U)^T \begin{pmatrix} f_V \\ f_B \end{pmatrix}$$

$$\tag{2-42}$$

$$= (M^\ast)^{-1}\ \Psi^T \begin{pmatrix} \frac{1}{2} [f_B - \frac{W_B}{W_V} f_V] \\ \frac{1}{2} [f_B + \frac{W_B}{W_V} f_V] \end{pmatrix}$$

Now that the hydraulic force acting on the vessel is related to that on the barrel by $f_v = -\frac{W_V}{W_B} f_B$, Eq. (2-29) for the generalized coordinate becomes

$$\ddot{q} + 2\eta \, \Omega_o \, \dot{q} + \Omega_o^2 \, q = (M*)^{-1} \, \psi_r^T \, f_B \quad . \tag{2-43}$$

Thus, once the relative mode shapes in Eq. (2-40) are obtained, the generalized coordinate is calculated by Eq. (2-43). Then, the relative coordinates are computed by Eq. (2-41) and the feedback by Eq. (2-34). These equations are identical to the set of conventional model analysis except that the mode shape matrix ϕ in Eqs. (2-15) - (2-19) is replaced by the relative mode shape matrix.

The computational procedure is summarized as follows:

1. Perform modal analysis of a dry linearized structural model including the vessel motion.

2. Use the calculated eigenvalues and generalized masses as the input data.

3. Compute the relative mode shape ψ_r, by taking weighted difference of vessel and barrel displacements.

Figures 2-1 and 2-2 compare WECAN structural models for the conventional and relative modal analyses. Figure 2-1 cited from Reference 8 depicts the beam model of thermal shield, core barrel and fuel assembly, but the pressure vessel is assumed motionless. For the relative modal analysis, the vessel supported at the node of the inlet nozzle/downcomer joint is included in the model. The relative mode shapes are computed by the weighted difference of the displacements at nodes 2 and 32, 3 and 31, etc., of each mode.

2.2.2.4 Absolute Displacements

Notice that the generalized coordinate computed by Eq. (2-43) is identical to the one in Eq. (2-29) as is evident from the derivation of the former equation shown in the previous section. So, the absolute displacements can be computed by the use of Eqs. (2-30) and (2-31). For example, the distance between the barrel flange and the vessel can be obtained by

$$(X_B - X_V)_b = (\phi_B - \phi_V)_b \, q \tag{2-44}$$

where subscript b indicates the values at the boundary node.

2.2.2.5 External Loads

During a LOCA, the external loads of loop and cavity forces are exerted on outside the pressure vessel in addition to the internal hydraulic forces. In order to take into account the effect of these external loads to the fluid structure interactions, the relative modal analyses in the previous section are generalized below.

Denote the external vessel force by f_{ext} and the internal hydraulic forces by f_V and f_B as before. Then, Eq. (2-42) that is the force term in Eq. (2-29) becomes

$$
(M^*)^{-1} \phi^T \begin{pmatrix} f_V + f_{ext} \\ f_B \end{pmatrix} = (M^*)^{-1} \psi^T \begin{pmatrix} f_B - \frac{1}{2} \frac{W_B}{W_V} f_{ext} \\ \frac{W_B}{W_V} f_{ext} \end{pmatrix}
$$

$$
= (M^*)^{-1} \{ \psi_r^T f_B + \phi_V^T f_{ext} \}
$$

where use has been made of the force relations above Eq. (2-43) in the first equality and Eq. (2-40) in the second equality. ϕ_V is the conventional mode shape at the pressure vessel. So, Eq. (2-43) becomes

$$
\ddot{q} + 2\eta \, \Omega_0 \, \dot{q} + \Omega_0^2 \, q = (M^*)^{-1} \{ \psi_r^T f_B + \phi_V^T f_{ext} \} \quad . \tag{2-45}
$$

In practice, the external loads can be lumped to a lateral force and a moment effective at the node of the inlet nozzle/downcomer joint. The moment is then broken into two lateral forces acting at two nodes neighboring that joint node so that the mode shapes ϕ_V at the three nodes are necessary in computation.

2.2.3 INTERMEDIATE PSEUDO-FORCE METHOD FOR NON-LINEAR BOUNDARIES

Some structural non-linearity in fluid-structure interactions[24] can be taken into account by the pseudo-force method that solves the structural dynamic equation with the non-linear term incorporated in the external force term. Furthermore, time dependent modal analysis is demonstrated in References 25 and 26 to be capable of solving a structural non-linear boundary problem by the use of the pseudo-force method (known also as modal superposition). This method is generalized in this section so as to include linearized boundary conditions in the modal analysis and the difference between the non-linear and the linearized boundary condi-

tions in the pseudo-force term; the intermediate pseudo-force method.

2.2.3.1 Pseudo-Force Method On Modal Analysis

The equation of motion of a structure is

$$\{M\} [\ddot{X}] + \{C\} [\dot{X}] + \{K\} [X] = [F] \tag{2-46}$$

subjected to the hydraulic force $[F]$, where $\{M\}$, $\{C\}$, and $\{K\}$ are respectively mass, damping and stiffness matrices. The damping and stiffness matrices can be composed of linear and non-linear parts;

$$\{C\} = \{C_\ell\} + \{C_{n\ell}\} \tag{2-47}$$

and

$$\{K\} = \{K_\ell\} + \{K_{n\ell}\} \tag{2-48}$$

$$= \{\bar{K}_\ell\} + \{K'_{n\ell}\} \tag{2-49}$$

In Eq. (2-46), the non-linear stiffness is factored into the linearized stiffness and the remainder,

$$\{\bar{K}_\ell\} \equiv \{K_\ell\} + \{\bar{K}_{n\ell}\} \tag{2-50}$$

and

$$\{K'_{n\ell}\} \equiv \{K_{n\ell}\} - \{\bar{K}_{n\ell}\} \tag{2-51}$$

where $\{\bar{K}_{n\ell}\}$ represents the linearized boundary conditions, for example. Then, Eq. (2-46) is written,

$$\{M\} [\ddot{X}] + \{C_\ell\} [\dot{X}] + \{\bar{K}_\ell\} [X] = F - \{C_{n\ell}\} [\dot{X}] - \{K'_{n\ell}\} [X] \tag{2-52}$$

This equation can be solved as follows:

In the input structural data computation, the eigenvalue problem with the linearized stiffness

$$\{M\}^{-1} \{\bar{K}_\ell\} \{\phi\} = \{\phi\} \{\Omega_o\}^2 \tag{2-53}$$

2-11

is solved for the mode shape matrix $\{\phi\}$ and the in-air frequency $\{\Omega_o\}$. Then, the generalized mass matrix is computed,

$$\{M^*\} = \{\phi\}^T \{M\} \{\phi\} \quad . \tag{2-54}$$

Now that the structural displacement is related to the generalized coordinate $[q]$ by

$$[X] = \{\phi\} [q] \quad , \tag{2-55}$$

Equation (7) becomes

$$[\ddot{q}] + 2\eta \{\Omega_o\} [\dot{q}] + \{\Omega_o\}^2 [q] = \{M^*\}^{-1} \{\phi\}^T ([F] + [N]) \quad , \tag{2-56}$$

where the non-linear pseudo-force is

$$[N] = - \{C_{n\ell}\} [\dot{X}] - \{K'_{n\ell}\} [X] \quad . \tag{2-57}$$

In Reference 24, these equations are solved for the case that $\{C\} = 0$ and the stiffness is a bi-linear or quadratic representation of plastic deformation of a pipe: The elastic stiffness is included in $\{\bar{K}_\ell\}$ and the remainder enters in $\{K'_{n\ell}\}$. The term $\{K'_{n\ell}\} [X]$ in Eq. (11) is taken into account by explicit integration and the result of computation is found satisfactory as shown in Reference 24. This same computation technique is recently applied to water hammer analyses of a steam generator in which the stiffness increases discontinuously in contrast to the case of plastic deformation where the stiffness sharply decreases beyond a yielding point. The result of computation is also found satisfactory. This pseudo-force method is now applied to the non-linear boundary condition calculation.

There are probably three non-linear boundaries in the beam model illustrated in Figure 2-3; the upper core barrel support, the hot leg nozzles, and the lower core support plate. The solid line in Figure 2-4 illustrates a force-displacement relation at a boundary with a gap g. The dashed lines illustrate possible choices of the linearized boundary condition: Lines AA' and BB' are the upper and lower limits, in practice. An intermediate case would be line CC' between these two limiting cases. For the chosen linearized stiffness $\bar{K}_{n\ell}$, the pseudo-force becomes

$$N = \bar{K}_{n\ell}\, r_N - \begin{cases} K_{n\ell}(r_N - g) + C_{n\ell}\,\dot{r}_N & \text{for } r_N > g \\[2mm] K_{n\ell}(r_N + g) + C_{n\ell}\,\dot{r}_N & \text{for } r_N < -g \\[2mm] 0 & \text{otherwise} \end{cases} \qquad (2\text{-}58)$$

where r_N is the relative displacement between the barrel and the vessel at a particular boundary point. Notice that this relative displacement is not the weighted relative displacement in Eq. (2-33) but the difference of absolute displacements in Eq. (2-44);

$$r_N = (\phi_B - \phi_V)_b\, q \qquad (2\text{-}59)$$

2.2.3.2 Relative Modal Analysis

The above formulation is based on the conventional modal analysis corresponding to Section 2.2.1 which is transformed to the relative modal analysis according to Section 2.2.2. Let us block the relative mode shape matrix defined by Eq. (2-40) into two parts, one for the internal nodes ψ_B and another for the boundary nodes ψ_n.

$$\psi_r = \left\{ -\frac{\psi_B}{\psi_n}- \right\} \qquad (2\text{-}60)$$

Then, the weighted relative displacement in Eq. (2-41) becomes

$$r = \left[-\frac{r_B}{r_N}- \right] = \left\{ -\frac{\psi_B}{\psi_n}- \right\} [q] \qquad (2\text{-}61)$$

and the equation for the generalized coordinate:

$$[\ddot{q}] + 2n\,\{\Omega_o\}[\dot{q}] + \{\Omega_o\}^2[q] = \{M^*\}^{-1}\{\psi_B{}^T \mid \psi_n{}^T\} \left[\frac{f_B}{f_n + N(r_N)} \right] \qquad (2\text{-}62)$$

where f_B and f_n are the hydraulic force exerted on the internal and the boundary nodes, respectively. Eq. (2-62) is solved by the use of the Laplace transformation between a time step for numerical computations of the hydraulic system. The pseudo-force term $N(Y_N)$ is computed from Eqs. (2-58) and (2-59) given q in the previous time step.

2.2.3.3 Impact Damping And Sliding Friction

The impact damping is the non-' .ar damping in the pseudo-force term of Eq. (2-58). The damping coefficient is proportioned to the non-linear stiffness;

$$C_{n\ell} = 2\eta \frac{1}{\omega_0} K_{n\ell} \tag{2-63}$$

where η is the damping ratio and ω_0 is the impact frequency.

A sliding force term can be also included in the pseudo-force term,

$$N_s = - \text{sign} (\dot{r}_N) \mu w_s \qquad , \tag{2-64}$$

where μ is the kinetic friction coefficient, w_s is the weight of the barrel or the vertical force acting between the barrel and the vessel flanges. The symbol sign $(\dot{r}_N)$ means the sign of the relative velocity so that the friction force acts in the opposite direction of the velocity.

2.2.4 ONE-DIMENSIONAL NETWORK

The downcomer annulus is represented by the one-dimensional network that is equivalent to two-dimensional fluid-structure interactions[14-16]. The rules for the network formation are:

1. The flow area of an axial leg is equal to the flow area of the circumferential leg.

2. The sonic velocity in the network legs is scaled by a multiplication factor $\sqrt{2}$.

3. The coupling terms $\dot{A}/A$ in Eqs. (2-5) and (2-6) are scaled by a factor 1/2.

Rules 2 and 3 are incorporated in the code and Rule 1 is taken care of in the modeling as illustrated in Section

The basic theory for the above rules is developed for a uniform sheet of hydraulic volume in References 14 and 15. The rules are applied to model the uniform annulus of the Fritz-Kiss shaker experimental facility. The computed in-water frequency agrees very well with the measured value, verifying the method of network formation (see Reference 15). This method is further applied to analyses of

the experiment performed with a 1/24-th scale reactor pressure vessel model (see Reference 16). Detailed description of downcomer network formation for a PWP downcomer can be seen in Sections 4.2.1 and 4.2.2.

$$(a,c)$$
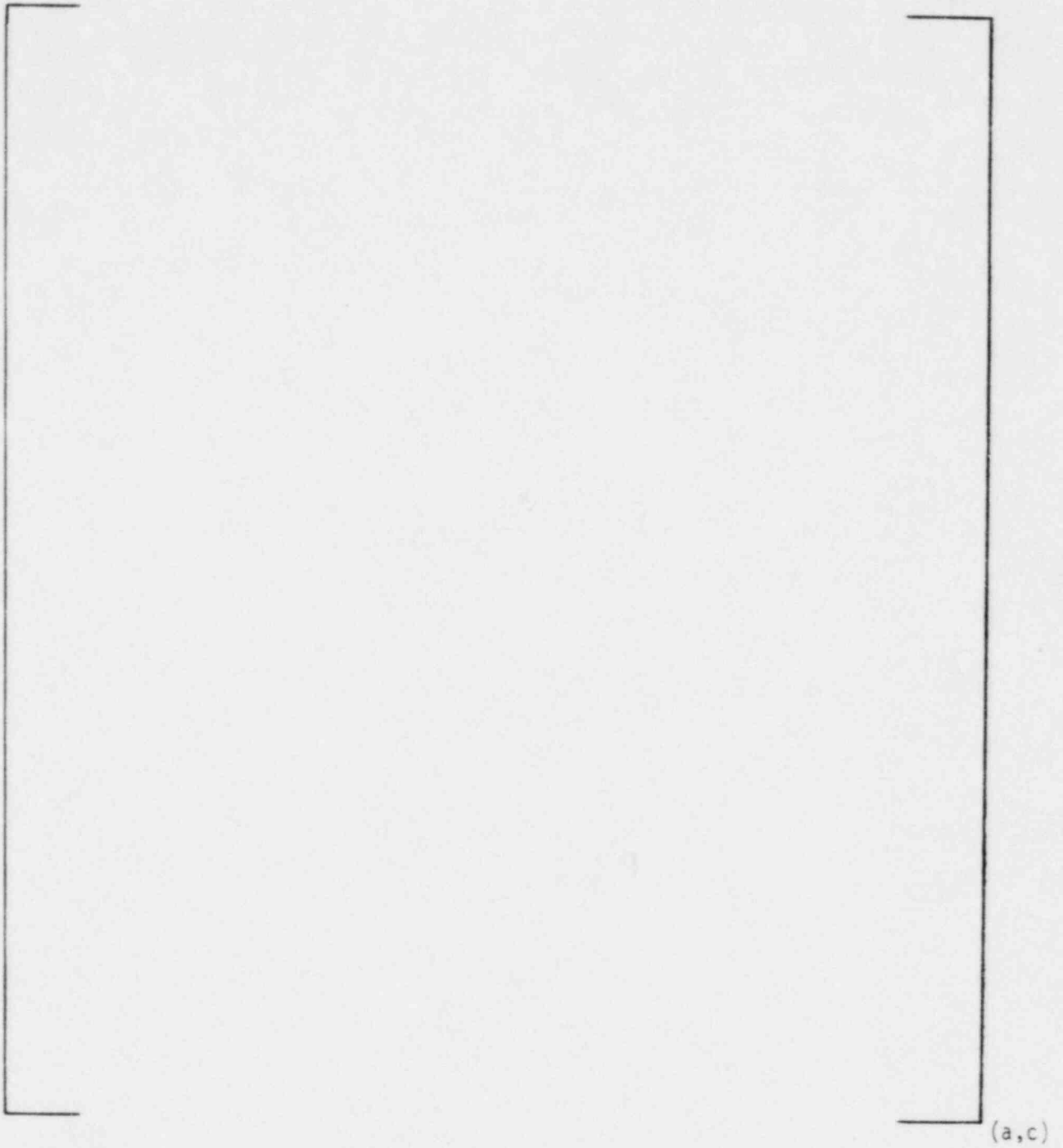
Figure 2-1. Previous Structural Model

Figure 2-2. Model for Relative Modal Analysis
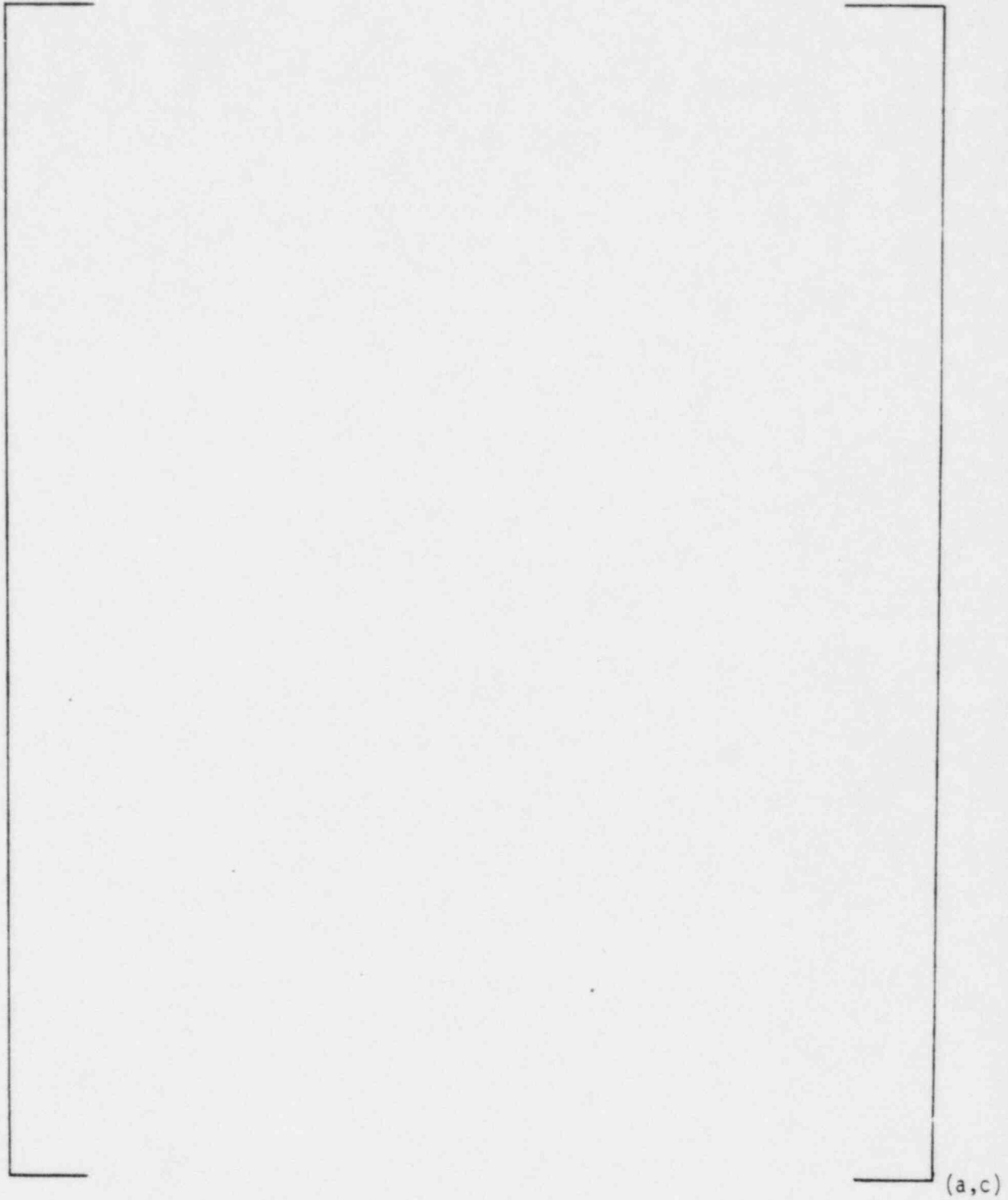
Figure 2-3. Beam Model With Possible Non-Linear Boundaries Between Barrel And Vessel

(a,c)
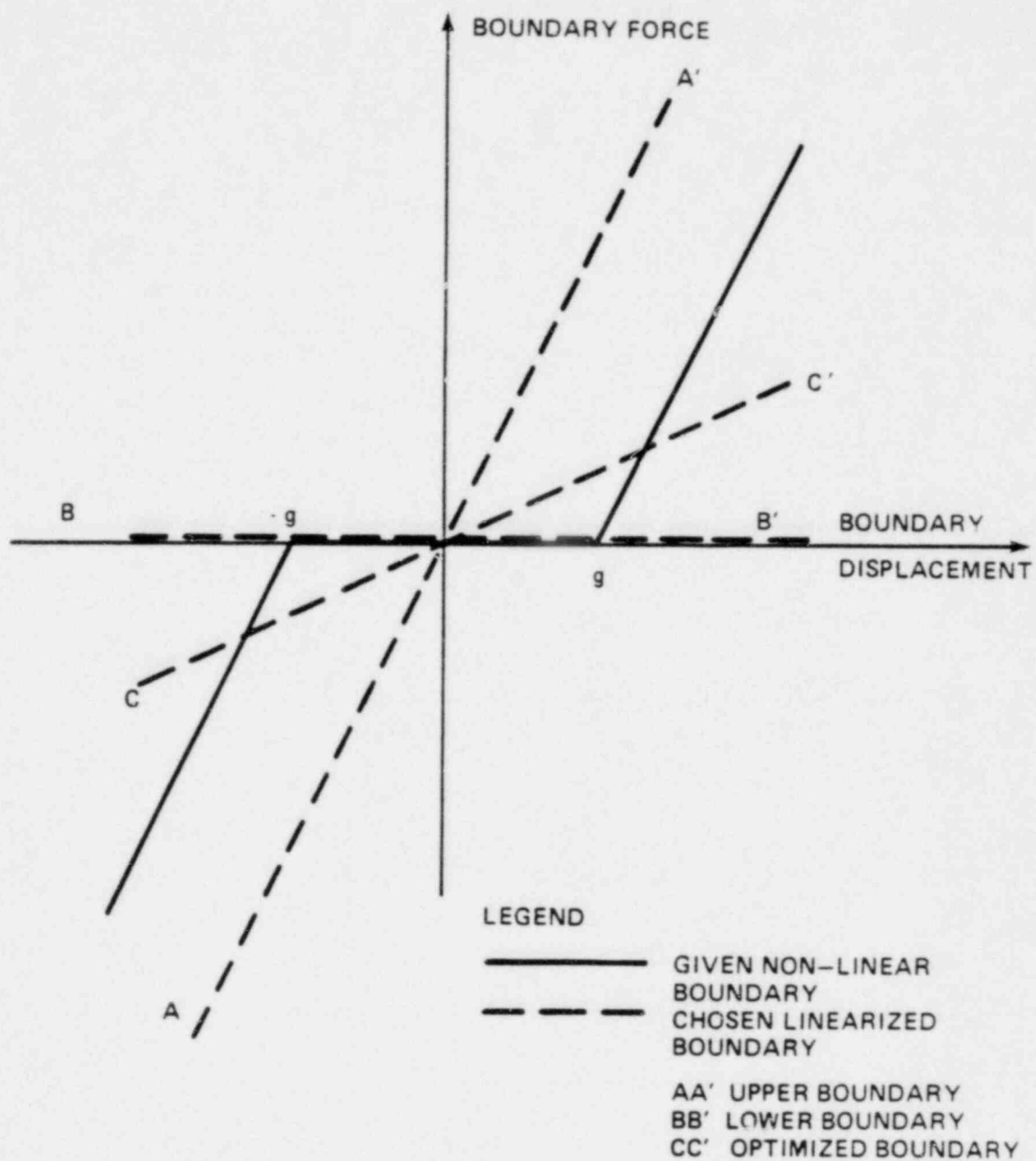
Figure 2-4. Force-Displacement Relations at a Non-Linear Boundary With Gap Size g

3.0 GENERAL PROGRAM DESCRIPTION

A general description of the overall MULTIFLEX organization and major subroutines is presented. Then the role of MULTIFLEX is shown in relation to the other codes for a complete stress analysis.

3.1 STRUCTURE OF PROGRAM

Flexible use of input-output devices is implemented in this program as can be seen below.

3.1.1 Table Of Subroutines

The source program is written in FORTRAN-IV, single precision for the CDC-7600. It currently utilizes approximately 150K of the small core. Computer time ranges from 30 to 300 seconds for analysis of a simple system and approximately 20 minutes for a typical reactor internals analysis. It may take 1 hour for an advanced beam model computation. The program is composed of four overlays as shown in Table 3-1.

3.1.2 Input-Output In General

The subroutine DATAS reads in the card input data and also prints out the results of the steady state hydraulic and heat balancing calculations, if executed. The structural data are provided by an input data deck to be read in STRUCDT and by the tapes to be attached, TAPE7 or TAPE15 and TAPE18. The subroutine MAINTR prints out the results of the transient calculation, it may write COMMON blocks on TAPE11, if requested. For restarts, TAPE11 is read in subroutine MAINST.

At each time step, MAINTR may dump the computed hydraulic information at printout stations on TAPE10 and TAPE12 to be plotted by program BLOPLOX. The hydraulic information at the first and the last nodes of all the legs are written on TAPE1 to provide input data to LATFORC, FORCE-2, or BLOPLT code. The computed pressure differentials and wall displacements are dumped on TAPE4 to be plotted by a subroutine DIRPLT on the third overlay or by a separate code DIRPLT.

3.2 FUNCTION OF SUBROUTINES AND MAJOR NOTATION

The subroutines may be grouped into property, thermal, hydraulic, structure, and boundary routines for their computational roles. Major subroutines and the quantities to be computed are described below.

3-1

3.2.1 Property Routines

The fluid properties (see Reference 8) are computed in the property routines PROP, SATURE, SUB, SUP, and TMP. SUB and SUP computer partial derivatives of specific volume for subcooled water and superheated steam respectively. The subroutine PROP, associated with the SATURE, computes fluid quality $X(I,J,K)$, density $R(I,J,K)$, and sonic velocity $C(I,J,K)$ at the I-th node of the J-th leg during the K-th timestep. (K=2 for the present time, K=1 for time at previous timestep.) These subroutines are called from all the major subroutines and, therefore, with the exception of TMP which computes fluid temperature, are located in overlay level (0,0).

3.2.2 Thermal Routines

The heat source-sink terms are computed in the thermal routine HTCOEF, CORE, STMGN, and (PIPE) (see References 1 and 2).

The subroutine HTCOEF computes the physical heat transfer coefficients (H.T.C.) for the core and the steam generator whenever wall temperature exceeds fluid temperature. Otherwise, these constants are computed in CORE and STMGN, respectively. The key notation appearing in HTCOEF is rather obvious, QDNB -- the heat flux to departure from nucleate boiling, TCRIT - the critical wall temperature for nucleate boiling, and TSAT - the water saturation temperature.

Although the primary function of PIPE is not the calculation of H.T.C., both H.T.C. and heat flux between the wetted wall and fluid are computed there.

3.2.3 Hydraulic Routines

In the hydraulic routines, pressure, flow rate, and enthalpy are computed for all nodes except for those at the boundary points. They are computed in the subroutines PIPE, LEAK, and CHAR.

The subroutine PIPE solves the characteristic equations to get the pressure $P(I,J,K)$, the flow rate $G(I,J,K)$, and enthalpy $H(I,J,K)$ for the internal nodes of each leg, specified by the subscripts (i.e., same as R, etc., in Section 3.2.1).

Hydraulic specification of leg J is given in terms of the number of nodes, $NO(J)$, the node spacing, $DX(J)$, and the effective diameter for friction, $DIAM(J)$. In addition, the leg elevation with an angle θ is stored in $ELEV(J)$, which equals $g \cos \theta$.

The dynamic variables at the point R are involved in the C+ characteristic equation and those at the point S in the C- characteristic equation. They are calculated in CHAR by a linear interpolation. The quantities at points R and S are denoted by making these letters the last alphanumeric character in the variable name throughout the entire program. For example, the pressure at R is denoted by PR and the pressure at S by PS. The subroutine LEAK computes the fluid state in a leakage element. A leg is required to be composed of at least two nodes.

3.2.4 Structure Routines

The structure routines are PIPE, the STRUCDT series (MAINI, MAINB, MAIN2DB, MAIND, MTRXDAT, ZORGEN, ISIMEQ, MMAT, BMAT), the FORCE series (FORCEI, FORCEB, FORCE2B, FORCED) and the STRUCT series (STRUCTI, STRUCTB, STRUC2B, STRUCTD). In the STRUCDT subroutines, mechanical structure information is read in. After reading the hydraulic data and establishing the steady state in DATAS, MAINST calls STRUCDT which calls the structural data reading routines MAINI, MAINB, MAIN2DB, and MAIND according to the options of the independent mass model, the beam model, the 2-D beam model, and the shell model, respectively. In the case of the projector method, MAIN2DB and then MAIND are called. As an option, MAIND may call MTRXDAT, the structural data processor, which further calls ZORGEN to print out matrix data, ISIMEQ to take inverse of a mass matrix, MMAT for matrix multiplication, and BMAT to generate the B matrix for the $A^T B$ treatment of the shell model and of the projector method.

Differential pressures across flexible walls are computed in PIPE. Hydraulic forces due to the differential pressures are computed in the appropriate FORCE and STRUCT routines, which solve the mechanical structure equations of vibrations, Equation (2-10). The $\dot{A}/A$ in the right hand side of Equations (2-5) and (2-6) is calculated. The corresponding pressure change is computed in PIPE.

3.2.5 Boundary Routines

Most of the engineering devices are modeled at boundaries and their characteristics are represented by the boundary values. The subroutine names imply their functions; DEAD for the dead-end boundary, JOINT for two-leg joints, TEE for 3-6 leg junction, PUMP for the pump, FREE for pre-determined boundary conditions.

The subroutine CROSS chooses one of these boundary routines at each boundary in accordance with the pre-selected boundary type NND2(J) at the last node of leg J.

The subroutines XIT and DXIT compute fluid discharge rate through the broken end.

3-3

In XIT the broken end is set up at the first node so that the C- characteristic is utilized; the first leg in the model is always assumed to have this broken end although its open area can be controlled by an input value, AORIF. On the other hand, DXIT places the broken end at the last node, using the C+ characteristic; the leg I.D. number is arbitrary in this case. Furthermore, the DXIT broken end can be excluded from the system by the choice of Ø-type break.

3.3 STRUCTURAL ANALYSIS PROCEDURE

The computational procedure for stress analysis is illustrated in Figure 3-1. Hydraulic models generally follow those developed and accepted in the previous rigid wall hydraulic force computation carried out by the BLØDWN-2 code. For a simple structure model, the mass and the spring constant are obtained directly from the material properties. For a beam model, modal analysis is carried out by the use of the WECAN code[27] to get generalized masses, modal frequencies, and mode shapes which are inputted to MULTIFLEX. For a shell model, the stiffness, mass, and A^T matrices computed by the WECAN code are processed by either MULTIFLEX or MØDES (see Appendix F) to yield TAPE7, to be read in MULTIFLEX.

MULTIFLEX solves thermal-hydraulic conservation equations together with mechanical equation of vibration to yield pressure values at all the locations in the hydraulic system written on TAPE1, and structural displacements, written on TAPE4 (see Section 3.1.2).

From TAPE1, LATFORC or FORCE-2 (see Reference 8) selects pressure differentials and mass velocities at necessary locations and converts them to hydraulic forces for the purpose of structure analysis. The X-component of hydraulic forces generated by LATFORC coincide with those used in structure computation done by the MULTIFLEX beam model.

The hydraulic forces are the forcing functions for the detailed structure analysis carried out by WECAN, DARI-WOSTAS, BOSOR, IENA, etc.[28,29].

Configuration absolute files can be attached as follows:

MØDES

    ATTACH (MØDES,MØDES)

MULTIFLEX

    ATTACH (BLØW,MULTIFLEX)

DIRPLT
   ATTACH (DIRPLT,DIRPLT)

BLØPLØX
   ATTACH (BLØPLØX,BLØPLØX)

3.4 STRUCTURAL OUTPUT

The structural output of MULTIFLEX includes a listing of all input quantities, including K and M matrices where appropriate, at the beginning of a problem. The structural printout then appears with the same frequency as the thermal hydraulic output (see NPRINT on input card No. 4). This periodic printout includes, for each wall: Wall number, LCHAN, JCHAN (see Section 4), pressure differential, displacement (in), velocity (in/sec), channel area (ft^2), and the quantity $\frac{DA}{A}$ where A is the channel area. Additionally, for IOSTYP=9, 10, 59, and 60, a modal analysis is performed on both the displacements and differential pressure, and the results printed.

If the structural results are plotted, a plot will be produced for the displacement and for the differential pressure across each wall. If the modal analysis option is chosen, each level in the core will have its results (both displacements and forces) decomposed into 8 modes. Thus, for example, a typical IOSTYP=9 run would produce 160 plots: 40 wall pressure differentials, 40 wall displacements, 40 (8 modes X 5 levels) displacement decompositions and 40 force decompositions.

TABLE 3-1
SUBROUTINES

OVERLAY(BLOW,0,0)

PROGRAM	BLDWN2
SUBROUTINE	EXPLAIN
SUBROUTINE	PROP
SUBROUTINE	SATM
SUBROUTINE	SUB
SUBROUTINE	SUP

OVERLAY(BLOW,1,0)

PROGRAM	MAINST
SUBROUTINE	DATAS
SUBROUTINE	STRUCDT
SUBROUTINE	MAINB
SUBROUTINE	MAIN2DB
SUBROUTINE	MAIND
SUBROUTINE	MAINI
SUBROUTINE	MTRXDAT
SUBROUTINE	ZORGEN
SUBROUTINE	ISIMEQ
SUBROUTINE	MMAT
SUBROUTINE	BMAT

OVERLAY(BLOW,2,0)

PROGRAM	MAINTR
SUBROUTINE	XIT
SUBROUTINE	DXIT
SUBROUTINE	PIPE
SUBROUTINE	FORCE2B
SUBROUTINE	FORCEI
SUBROUTINE	FORCEB
SUBROUTINE	FORCED
SUBROUTINE	LEAK
SUBROUTINE	CROSS
SUBROUTINE	DEAD
SUBROUTINE	JOINT
SUBROUTINE	TEE
SUBROUTINE	PUMP
SUBROUTINE	FREE
SUBROUTINE	CORE
SUBROUTINE	STMGN
FUNCTION	HTCOEF
FUNCTION	TMP
SUBROUTINE	STRUC2B
SUBROUTINE	STRUCTI
SUBROUTINE	STRUCTB
SUBROUTINE	STRUCTD
SUBROUTINE	CHAR

TABLE 3-1 (CONTINUED)

SUBROUTINES

OVERLAY(BLOW,3,0)

PROGRAM	DIRPLT
SUBROUTINE	DPLOT
SUBROUTINE	MODAL
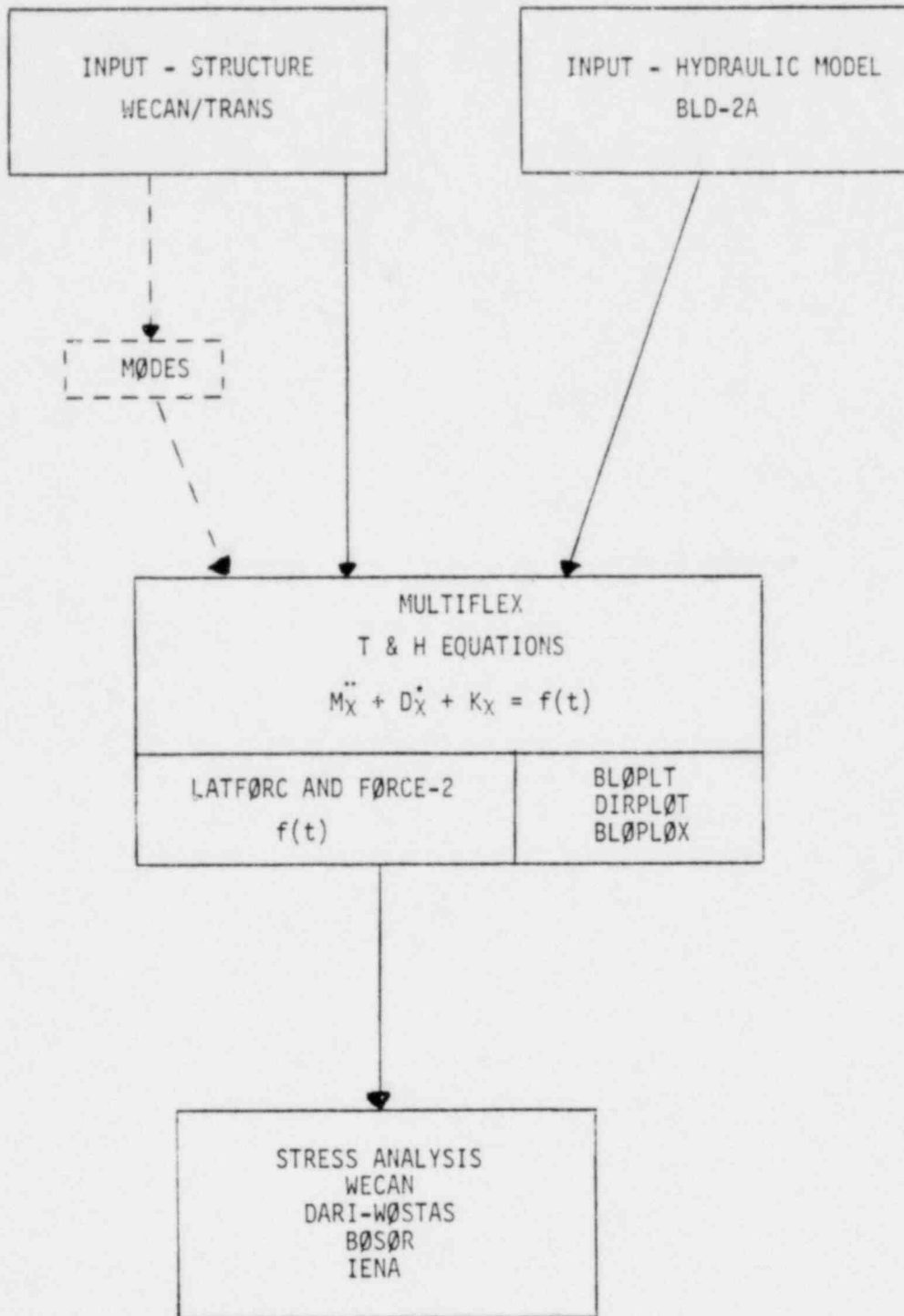
FIGURE 3-1   Chart Of Fluid-Structure Computation For Structural Analysis

4.0 MODELING AND INPUT DATA PREPARATION

In this section rules for modeling and input data preparation are described. The input data instructions in Section 4.1 provide the outline of modeling as well as the FORTRAN notation. The details of reactor component modeling are given in Reference 8.

In Section 4.2, structural input data and interface modeling are explained.

4.1 INPUT DATA INSTRUCTIONS

The required input data are listed in Table 4-1. The fundamental units are lb, ft, sec, psi, and Btu. Those cards with asterisks must be provided for any type of computation. A card group may be composed of more than one physical card. The number of required cards is generally indicated in the parenthesis at the Card Number; for example, Card Group No. 11 (X NØLEG) indicates that NØLEG cards must be prepared. Most of the notation appearing in the table is used throughout the FORTRAN program.

The data can be divided into two general categories, thermal hydraulic and structural. Although the required hydraulic input is the same for each type of structural analysis (IØSTYP), the data necessary for each structural option may differ not only in the values but in the kind of information needed. Beginning with Card Group Number 50, therefore, the input for each type of structural model and analysis will be described separately. It should be noted that several of the basic types (IØSTYP = 1-10) can be modified to use a generalized mass simply by adding 50 to the value of IØSTYP. All necessary input is on cards, except that the direct and projector methods also require the matrices $M^{-1}K$ and $M^{-1}(1 + A^TB)$ read in from the attached TAPE7. If, however, IPREP=1 is provided on Card No. 53, then $M^{-1}K$ and $M^{-1}(1 + A^TB)$ are computed (see Appendix C) provided that the M and K matrices and A^T matrix are attached to TAPE15 and TAPE18, respectively. Afterwards, the normal transient computations are carried out. At the same time the computed matrices are written on TAPE7 to be catalogued for future usage. The B matrix necessary in the computation is automatically generated without an additional specification. The plotting program, DIRPLT, may be run either as an integral part of MULTIFLEX or as a separate program. Directions for its use follow the structural data description. Rigid wall computations can be performed with a blank card placed after Card No. 49.

The calculated results are written on tapes in different ways than those described

4-1

in Reference 8 and so, detailed descriptions are given here. The pressure differentials across core barrel walls and the wall displacements are written on TAPE4 to be plotted by DIRPLT. The results at the first and the last nodes of all the legs are written on TAPE1 to be plotted by BLØPLT, if NTPLØX $\geq$ 0. If NTPLØX < 0 , none is written on TAPE1. If NTPLØX $\neq$ 0, the results of the first 20 plot stations are written on TAPE10 and the remaining on TAPE12, to be plotted by BLØPLØX. These plot stations are specified by the printout stations (JD, ID) if NST = 0 by the separately specified stations (JST, IST) as many as NST (0 < NST $\leq$ 40).

4.2 ADVANCED BEAM MODELING

The fundamental modeling technique for fluid-structure interaction systems is described in References 5, 8, and 10. In this section, the technique for the advanced beam modeling is described in relation to the input data instruction in Table 4-1 and it is illustrated with a three-loop thermal shield plant. First, a method of network downcomer modeling is described in Section 4.2.1. The fluid-structure interface is discussed in Section 4.2.2 followed by the structural input data preparation in Section 4.2.3.

4.2.1 Advanced Beam Modeling

The rules for the one-dimensional network that is equivalent to two-dimensional fluid-structure interaction are summarized in Section 2.2.4. The geometry of the PWR downcomer is somewhat more complicated than the experimental situation in References 14-16: (1) The annulus gap is not uniform, and (2) the downcomer of two-dimensional annulus is connected to the one-dimensional inlet nozzles and to the three-dimensional lower plenum. So, the method is generalized as described below. Network formation and flow area computation are described in Section 4.2.1.1. A method to help attaining an acceptable steady state condition in the downcomer is discussed in Section 4.2.1.2. Scaling of the sonic velocity and an inlet nozzle/downcomer joint modeling are contained in Sections 4.2.1.3 and 4.2.1.4, respectively.

4.2.1.1 Network Formation And Flow Area Computation

(a,c)

(4-1)

(4-2)

(4-3)

(4-4)

(4-5)

(4-6)

(a,c)

4-3
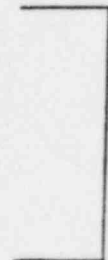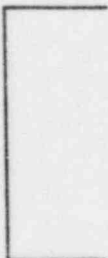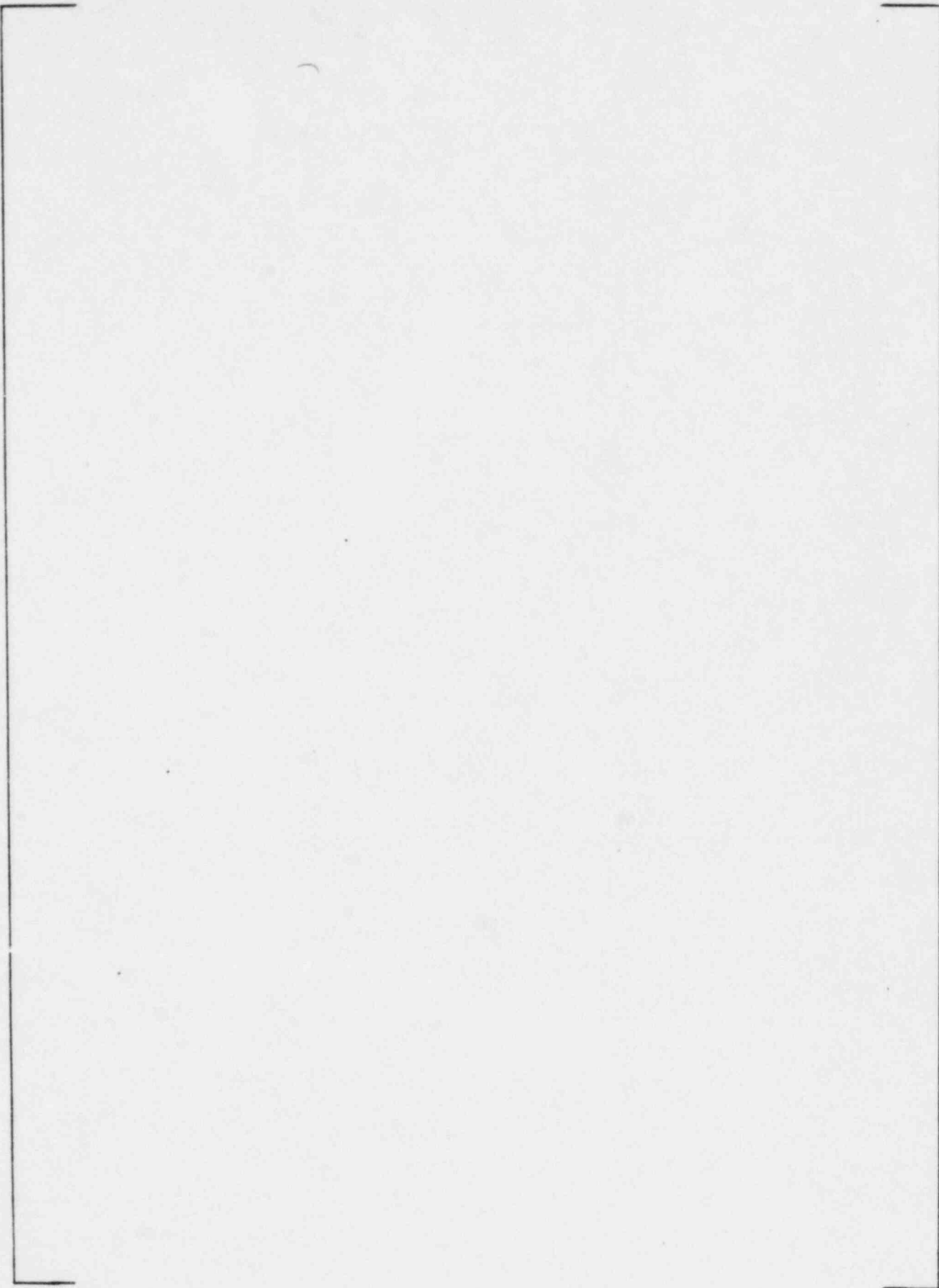
4.2.1.2 Steady State Balancing

Compare the downcomer network in Figure 4-2 with the original modeling in Reference 8. The downcomer/lower plenum joint, made symmetric in the new model, and lateral flow paths have been added at three elevations: the top and the bottom of the thermal shield and its midpoint. With the increased number of lateral flow paths, difficulties were encountered with excessive flow unbalances during the steady state calculations at the junctions in the thermal shield region.

To aid the current flow balancing computation, artificially small hydraulic diameters ($\simeq 0.01$) are used in these lateral legs only during the steady state calculations. This is achieved by the input data NSØNIC = 1 in the input data Card No. 4 followed by the data Card No. 20a with DIAMT = 0.01 at the lateral legs at the mid-point and the bottom of the thermal shield J1 = 121 and J2 = 138 in the case of the model in Figure 4-2.

4.2.1.3 Scaling Of Sonic Velocity

The sonic velocity in the downcomer network can be scaled according to two input data cards. NSØNIC = 1 in Card No. 4 and the second card is added immediately before the geometry input cards, Card No. 10a. The sonic velocity in the legs numbered from JC1 to JC2 is scaled by the multiplication factor FACTØR ($= \sqrt{2}$). In the case of Figure 4-2, JC1 = 55 and JC2 = 138.

4.2.1.4 Modeling Of The Inlet Nozzle/Downcomer Joint

At the inlet nozzle/downcomer joint, one leg having sonic velocity c and flow area A_1 joins three or four legs with sonic velocity $\sqrt{2}c$. The penetration factor at this joint becomes

$$\beta = 2\sqrt{2}\, A_1 / (\sqrt{2}\, A_1 + \sum_{i \neq 1} A_i) \qquad . \qquad (4-7)$$

So, the flow areas in the downcomer must be adjusted so as to get a desirable penetration factor, $\beta \simeq \beta_{th}$. The theoretical penetration factor β_{th} is defined in Reference 9,

$$\beta_{th} = 2r^2 / \{ r^2 + 2h\, (r + \frac{\pi}{4}\, h) \} \qquad . \qquad (4-8)$$

4-4

where r and h are the radius of the inlet nozzle and the gap of the downcomer annulus, respectively.

The flow areas in the downcomer, at the joint must be adjusted such that

$$A_i L_i = A_i^{(o)} L_i^{(o)} \tag{4-9}$$

where $A_i^{(o)}$ and $L_i^{(o)}$ are the values originally determined according to the method described in Section 4.2.1.1.

The effects of the sonic discontinuity are illustrated by the peak total hydraulic force (THF) on the vessel, computed by the following five models,

CASE 1   Original downcomer model ($\beta = 0.69$; WCAP-8708).

CASE 2   Network downcomer model w/o scaling the sonic velocity ($\beta = 0.62$).

CASE 3 (Base)   Network downcomer model with the scaled sonic velocity ($\beta = 0.777$).

CASE 4   Network downcomer model with the scaled sonic velocity and with a reduced nozzle area ($\beta = 0.641$).

CASE 5   Sonic velocity scaled in the network downcomer, the lower plenum, and the barrel interior ($\beta = 0.777$).

Results of computations are summarized in Table 4-2 and in Figure 4-3, indicating that:

(1) The peak THF is determined fairly well by β at the inlet nozzle/downcomer joint.

(2) The sonic discontinuity at the lower plenum/downcomer joint does not have a significant effect.

(3) The peak THF is decreased by approximately 20% and the force frequency is reduced by about 25%, by forming the network.

4.2.2 MODELING OF FLUID-STRUCTURE INTERFACE

The structural surface interfacing with the fluid in the downcomer is the outer surface of the thermal shield and of the barrel and the inner surface of the vessel. But the fluid-structure interactions in the channel between the thermal shield and the barrel are assumed to be insignificant. Among the interfacing walls, the effect of the vessel inner surface is incorporated in the weighted relative displacement and only the thermal shield and barrel walls are explicitly modeled. The details of the network interface modeling are described below, but the fundamental aspects of the modeling are rendered to the previous reports[5,8,10].

(4-10

(4-11

(a,c)

4.2.3 STRUCTURAL INPUT DATA

Structural input data for the advanced beam model are the relative mode shapes, the generalized masses, the modal frequencies, and the data for the non-linear boundary conditions. Preparation of the modal analysis data is discussed in Sections 4.2.3.1 through 4.2.3.3. Then, the data preparation for the boundary conditions are discussed in Sections 4.2.3.4 and 4.2.3.5.

4.2.3.1 WECAN Modal Analysis And LATFØRC Modeling

The structural input data are obtained by the modal analysis performed by the WECAN code on the linearized structural model illustrated in Figure 4-6. In this model, the barrel, the thermal shield, and the fuel assembly are the same as the original model shown in Reference 8, where node Nos. 21 and 32 were fixed at the ground. To take into account the vessel motion, the pressure vessel is modeled by a beam which is fixed to a ground via springs of the vessel support. This part of the model is equivalent to the DARI-WØSTAS model in Reference 22 in the example. The values of

the linear and rotary springs are $k^{(v)} = 69.92 \times 10^6$ $1b_f/in$ and $k_{ROT}^{(v)} = 12.68 \times 10^{11}$ $1b_f/rad$. The top boundary of the barrel is joined to the vessel by a rotary spring $k_{ROT}^{(Top)} = 1.8 \times 10^{11}$ $1bf/rad$. The linear springs at the top and bottom boundaries are shown to be $k^{(Top)} = 15 \times 10^6$ $1b_f/in$ and $k^{(Bot)} = 10 \times 10^6$ $1b_f/in$ which fill $\{\bar{K}\}$ in Eq. (2-52).

Elevation of the nodes is important to maintain a fair consistency in the models of WECAN model analysis, MULTIFLEX, LATFØRC, and WECAN dynamic analysis. Nodal elevations of these models in the downcomer area are listed in Table 4-3.

The origin is taken at the level of the inlet nozzle center line. Nodal elevations of WECAN model and dynamic analyses are identical to each other. The mass points of MULTIFLEX are located at the elevations of the circumferential legs and the mid-points of the axial legs in the downcomer network, Figure 4-5. There are slight discrepancies in the nodal elevations of WECAN and MULTIFLEX: The top node of WECAN is located at the mid-point of 3.25" thick barrel flange, while the upper bound of fluid volume is at most the bottom of the flange. Similarly, the bottom WECAN node is located at the mid-point of the core support plate of 16" thickness, while the downcomer volume extends to the lower end of the core plate. Another discrepancy is due to the top thermal shield level; the structural node is at the thermal shield/barrel joint and the fluid branching point is the top of the thermal shield. The elevations of the LATFØRC boundaries are obtained by dividing the axial downcomer lengths in proportion to the areas of MULTIFLEX walls. Computed hydraulic forces are applied to the WECAN node from the top to the bottom without interpolation.

4.2.3.2 Relative Modal Analysis

By the modal analysis of the structural model in Figure 4-6, system eigenfrequencies, generalized masses, and mode shapes are computed. According to the relative model analysis developed in Section 2.2.2.3, the generalized masses are input to EFFMAS of Card Group No. 55a with MASPNT=10 and IEFF=1. The eigenfrequencies are provided to FREQ of Card Group No. 56. But the mode shapes, PHI in Card Group No. 57, are the relative mode shapes illustrated below.

The relative mode shape ψ_r is defined by Eq. (2-40) and it is computed from the weighted difference of barrel displacements and the barrel displacements. In the case of the model in Figure 4-6, the weight is 1.138 for the top four nodes and the bottom node. With this weight, the relative modal displacement at the top mass

point is computed by difference of displacements of nodes 2 and 32 for each mode, and so on. The weight value is 1.061 for the thermal shield nodes and the relative displacement at the 6th mass point is the difference of modal displacements of nodes 10 and 36. The weight at the thermal shield edges is 1.098. The computed relative mode shapes are illustrated in Table 4-4.

4.2.3.3 Boundary Mode Shapes

In Table 4-4, boundary mode shapes are also shown to be used for the pseudo-force calculation in Section 2.2.3. In this example, the number of the non-linear boundary conditions are two; NLBC=2 in Card Group No. 59. The weighted relative displacements, ψ_n, at the boundaries appear in Eqs. (2-61) and (2-62). The data are input to PHIB in Card Group No. 60. The difference of the absolute displacements are applied to the pseudo-force term in Eqs. (2-58) and (2-59). The data are supplied to RPHIB in Card Group No. 61.

4.2.3.4 Boundary Conditions

The top and bottom boundaries of the core barrel are non-linear. The top boundary is comprised of the barrel flange and the vessel flange. The gap sizes are 0.104, 0.120, and C.144 in. respectively for typical two-, three-, and four-loop plants. As their relative distance increases beyond the gap, the two flanges deform and the surface area in contact increases. Consequently, the force-displacement relation becomes non-linear even after the gap is closed, as shown in Figure 4-7 (see Reference 32). However, it is possible to approximate the curve by a bi-linear relation or by two linear springs with different gap sizes. For example, of three loop plant, the two springs are:

$$k_1 = 3.939 \times 10^6 \, lb_f/in \text{ with } g_1 = 0.12 \text{ in}$$

and

$$k_2 = 37.916 \times 10^6 \, lb_f/in \text{ with } g_2 = 0.196 \text{ in} \quad .$$

(4-13)

These data are input to Card Group Nos. 62 and 63. As described in Section 4.2.3.1, the linearized spring at the top boundary (N = 1) is $15 \times 10^6 \, lb_f/in$, so that

    XKLIN = 15 x 10⁶
    XFJUMPO = XJMP = XFJMP = 0
    GAP1 = 0.12

$$XKNL1 = 3.939 \times 10^6$$
$$GAP2 = 0.196$$
$$XKNL2 = 37.916 \times 10^6$$

The input data for XCNL and SLIDEF are described later.

At the bottom boundary, the core support plate closes a gap ($\simeq 0.007$ in) of one of the six radial keys as the core support plate displaces. Then, gaps of the other keys are closed at approximately 0.135 in. The force-displacement relation is illustrated in Figure 4-8. As the first gap is closed, the key deforms elastically to the yielding point at $\simeq 1 \times 10^6$ lb_f and then it deforms plastically, $k = 3.481 \times 10^6$ lb_f/in, until the second gap is closed. The second yielding point is 3.46×10^6 lb_f and the spring constant in the following plastic deformation is 15.424 lb_f/in. The elastic deformations are approximated by step functions and the first gap is ignored. Then, these data for the bottom boundary (N = 2) are input in Card Group Nos. 62 and 63:

$$XKLIN = 10 \times 10^6 \quad \text{(see Section 4.2.3.1)}$$
$$XKJMPO = 1 \times 10^6$$
$$XJMP = 0.135$$
$$XFJMP = 1.99 \times 10^6$$
$$GAP1 = 0$$
$$XKNL1 = 3.481 \times 10^6$$
$$GAP2 = 0.135$$
$$XKNL2 = 11.943 \times 10^6$$

4.2.3.5 Impact Damping And Sliding Friction

The impact damping is expressed in the form of Eq. (2-63). The recommended value of the damping coefficient η is 12.5%[33] and the frequency ω_o is the actual system frequency according to Reference 34. As is seen later, the system frequency is on the order of 10 Hz and so:

$$XCNL = 2\eta/\omega_o = 0.003979$$

is input to Card Group No. 62 for both top and bottom boundaries (N = 1 and 2). A constant sliding friction force can be input to SLIDEF for the top boundary (N = 1). During the transient, the weight at the flange may vary, but the average value is computed to be on the order of 0.1×10^6 lb_f[35].

4-10

TABLE 4-1

MULTIFLEX CODE INPUT DATA INSTRUCTIONS

NOTATION	FORMAT	DESCRIPTION
*Card No. 1		
NGO	I5	Re-start Indicator Blank -- if not re-start case
NDUMP	I5	Common Dump Indicator NDUMP>0 - the COMMON area is dumped on TAPE11 for re-start calculation at the real time limit (TEND) Blank -- dump is not required
TLIM	F10	Computer Time Limit (sec.) specified in the JOB CARD TLIM-5 > Computer Running Time (CP) -- the common dump is executed TLIM $\leq$ CP + 5 - dump is not executed
TEND1	F10	Real Time Limit (TEND) for the re-start case Blank -- if not re-start case
TDBG	F10	Real Time (sec.) after which debug printout takes place at each time increment Blank -- for normal printout as specified through NDEBUG and NPRINT
TTDMP	F10	Real Time (sec.) Limit for reading the data of TAPE11. The value must be just slightly smaller ($\sim 10^{-6}$) than the desired time limit Blank -- if not re-start case
*Card No. 2 And No. 3		
TITLE1	12A6	Any message for the computation title
TITLE2	12A6	
*Card No. 4		
NDATA	I5	The number of stations for which results are printed. The stations are specified by JD(K) and ID(K) below NDATA is restricted to be $\leq$ 40
NPRINT	I5	Print Interval Multiplier NPRINT = 1 -- print after every time computa- tion = 2 -- after every other time computa- tion

TABLE 4-1 (CONTINUED)

NOTATION	FORMAT	DESCRIPTION
	I5	NPRINT 10^{-5} = real time (sec.) increment for printing NPRINT = 10000 -- printout interval is 0.1 sec.
NDEBUG	I5	Print Type Indicator NDEBUG = 0 -- only for specified stations (JD(K), ID(K)) NDEBUG $\geq$ 1 -- for additional edits of thermal properties at each node in the reactor core NDEBUG $\geq$ 2 -- for debug printout from sub-routines XIT and LEAK when T > TDBG NDEBUG < 0 -- for edit steady state convergence
NTAPE	I5	NTAPE = 1 -- results are printed on TAPE1 (used for plotting); otherwise enter 0
NHEAT	I5	NHEAT = 1 -- heat transfer calculations for the core and S.G. are performed; otherwise enter 0
NPUMP	I5	Pump Operator Mode Indicator NPUMP = 0 -- pump power is turned on at time T = 0 NPUMP = -1 -- pump is absent
NLOOPS	I5	Number of external loops in the model NLOOPS must be $\leq$ 3
NWINDOW	I5	Pre-determined Boundary Condition Indicator NWINDOW > 0 -- Tables of special boundary conditions are read in (see TTBL(K), WTBL(K), HTBL(K), PTBL(K) on Card No. 51)
NST	I5	Plot Station Specification for BLOPLOX = 0 -- the printout stations specified by Card No. 5 are the plot stations > 0 -- the plot stations must be specified on Card No. 7a.
NSONIC	I5	> 0 -- for network computation = 0 -- otherwise

*Card Group No. 5 (x NDATA/7)

| | 14I5 } | The leg and node I.D. numbers specifying the stations for printing out the results (NDATA stations) |

TABLE 4-1 (CONTINUED)

NOTATION	FORMAT	DESCRIPTION
*Card No. 6		
W	F10	Time (sec.) to reach steady state. During the time interval from -W to 0, the transient routines are run to settle the oscillations
AORIF	F10	Final flow area (ft^2) of rupture or break at the first node of the first leg
CD	F10	The discharge coefficient at the rupture (0.61 - 1.0)
CBACK	F10	
TSTAR	F10	Rupture or Break Opening Time (sec.)
TEND	F10	Real Time (sec.) for the end of transient calculation
TPUMP	F10	Real Time Duration (sec.) for which pump power is on
*Card No. 7		
NOLEG	I5	Total number of legs ($\leq$ 200)
NTPLOX	I5	Mode indicator for dumping results NTPLOX > 0 -- for dumping the plot stations on TAPE10 and TAPE12 for BLOPLOX NTPLOX = 0 -- for dumping on the first and last nodes of all legs on TAPE1 for BLOPLT NTPLOX < 0 -- TAPE10 and TAPE12 for BLOPLOX and TAPE1 for BLOPLT
DTR	F10	Time Increment Divider. The increment is given by DT = DT'/DTR, where DT' is determined internally. DTR = [ ] is recommended
FCOEF	F10	Mean Friction Coefficient FCOEF = 0.015 is recommended
TOL	F10	Tolerance for pressure calculations in subroutines PIPE and JOINT TOL $\geq$ 0.05 is recommended
NITER	I5	Maximum times of iterations in subroutines JOINT, TEE, and PIPE 2 $\leq$ NITER $\leq$ 5 is recommended

(a,c)

TABLE 4-1 (CONTINUED)

NOTATION	FORMAT	DESCRIPTION

If NST = 0 (Card No. 4), then skip Card No. 7a.

Card No. 7a (x NST/7)

| JST (K) | 14I5 | The leg and node I.D. numbers specifying the plot stations. |
| IST (K) | | |

*Card No. 8

BRKTYP	A1	Break Type Designator BRKTYP = ₿ -- for small orifice break BRKTYP = D -- for guillotine break, either complete or partial BRKTYP = S -- for propagating longitudinal split, modeled through multiple orifices
NORIF	I4	Number of legs with orifice break Blank -- for BRKTYP = ₿ NORIF = 2 -- for BRKTYP = D NORIF = 6 -- for BRKTYP = S
KBRK	I5	= 1 For Piccolo break analyses Blank otherwise
NØSPLT	I5	= 0 If it is split = 1 If the unbroken inlet nozzle is not split

If KBRK = 0, skip Card No. 8a.

Card No. 8a

| AØRIF1 | F10 | The second break area for Piccolo break |
| TSTAR1 | F10 | Break time |

If BRKTYP = ₿, Card No. 9 should be skipped. Prepare Card No. 9a for BRKTYP = D and No. 9b for BRKTYP = S.

Card No. 9a

| JBRK2 | I5 | The leg I.D. number other than 1 to which orifice break is attached |
| IBRK2 | I5 | The last node of leg JBRK2 |

Card No. 9b

| VCRACK | F10 | Maximum crack propagation velocity (inch/sec.)
VCRACK = 4600. -- is suggested |
| PAREST | F10 | Crack tip arrest pressure (psia) |

TABLE 4-1 (CONTINUED)

NOTATION	FORMAT	DESCRIPTION
DPIPE	F10	Pipe internal diameter (inch)
ORIFSP	F10	Spacing of orificed leg axes (inch)
CRACKL	F10	Initial crack length (inch)

If NSONIC $\leq$ 0, skip Card No. 10.

Card Group No. 10

JC1	I5	Multiplication factor (FACTOR = $\sqrt{2}$); sonic
JC2	I5	velocity in the legs J (JC1 $\leq$ J $\leq$ JC2) is scaled by this multiplication factor
FACTOR	F10	FACTOR*C

*Card Group No. 11 (XNOLEG)

J	I5	Leg no. The first leg must have an orifice break at its first node
NO(J)	I5	The number of nodes in leg J ($\leq$ 10)
NND1(J)	I5	Type of boundary condition at the first node of leg
NND2(J)	I5	Boundary condition type at the last node of leg J NND2 = 1 -- Dead end (Accumulator SIS/Deluge system) NND1, NND2 = 2 -- Two leg joint NND1, NND2 = 3-6 -- 3-6 leg junction. The Y-junction is registered as if a 3-leg junction. NND2 = 7 -- Pressurizer tank NND1, NND2 = 8 -- Pump NND1, NND2 = 9 -- Accumulator NND1, NND2 = 10 -- Rupture NND1(1) = 10 always and NND2(J) = 10 for J $\neq$ 1 NND2 = 11 -- Core spray ** NND2 = 12 -- p(t) in table PTBL (see Card No. 51) NND2 = 13 -- w(t) and h(t) in table WTBL and HTBL (see Card No. 51)

**n.b. - These boundary conditions are specified internally by the program. As input data, NND2 = 1 for accumulator and SIS/Deluge system and NND2 = blank for core spray system.

LEG(J,1)	I5	Junction I.D. number at the first node.
LEG(J,2)	I5	Junction I.D. number at the last node
A(J)	F10	Flow area (sq. ft.)
DX(J)	F10	Node spacing (ft.)
ELEV(J)	F10	32.174 * cos θ for angle θ between the leg direction and the upward vertical line

TABLE 4-1 (CONTINUED)

NOTATION	FORMAT	DESCRIPTION
	A1 (Col. 61)	Letters H, C, or M indicating that leg J belongs to the hot, cold or mean portion of the system. The core and S.G. belong to the M category.
AMIN (J)	F10	Orifice flow area (sq. ft.) at the last node of leg J (= 0 if there is no orifice)

*Card Group No. 12 (XNOLEG)

J	I5	Leg no.
OK(J)	F10	Hydraulic Loss coefficient at the last node of leg J
TOK(J)	F10	For NND1(J) = 2 -- An adjusting constant for sudden expansion or contraction loss For NND1(J) ≠ 2 -- Hydraulic loss coefficient at the first node of leg J
DIAM(J)	F10	Effective diameter = blank -- DIAM = $\sqrt{4*A(J)/\pi}$ applied internally Suggested values: = 2 · gap thickness -- downcomer = 4 · A/P -- core legs, where A is flow area and P is wetted perimeter = a large value -- plenums
NM	I5	= 1 -- the last card of this set = 0 -- otherwise

*Card No. 13

NLEL	I5	Total number of leakage elements

If NLEL = 0, Cards No. 14 and 15 should be skipped.

Card Group No. 14 (x NLEL) (each card is followed by the corresponding Card Group No. 15)

LEL	I5	The leakage element I.D. number
JLEL(LEL)	I5	Leg I.D. number of system leg representing leakage element LEL
NODE(LEL)	I5	Junction I.D. number at the first node of the above system leg
NLINK(LEL)	I5	Number of legs connecting with leakage element LEL

TABLE 4-1 (CONTINUED)

NOTATION	FORMAT	DESCRIPTION
VOL (LEL)	F10	Volume of the leakage element LEL

Card Group No. 15 (x NLINK(LEL))

LINK(LEL,I)	I5	Leg I.D. number of the I-th path connecting to the leakage element LEL
LINKTYPE(LEL,I)	I5	Leakage path type indicator = 0 -- normal path (another system leg) = 1 -- abnormal path (another leakage element)
ALEAK(LEL,I)	F10	Orifice flow area at the joint of path I (ft^2)
ALOSS(LEL,I)	F10	Hydraulic loss coefficient at the orifice

*Card No. 16

JCOR	I5	The I.D. number of the first leg in a series of legs representing the core region (bottom of core) In the case of multi-channel, it must be the bottom leg in the average channel
JINSG1	I5	The leg I.D. number of the first of S.G. legs in external loop No. 1
JOUTSG1	I5	The leg I.D. number for the last of S.G. legs in external loop No. 1
JINSG2	I5	Same as JINSG1 for loop No. 2
JOUTSG2	I5	Same as JOUTSG1 for loop No. 2
JCLAST	I5	Last leg number in the core (or in the average channel for the case of multi-channel option)
NCHAN	I5	Number of core channels ($\leq$ 3)
NCVERT	I5	Number of legs forming one of the core channels
JINSG3	I5	Same as JINSG1 for loop No. 3
JOUTSG3	I5	Same as JOUTSG1 for loop No. 3
IW5	I5	Heat flux correlation indicator = 1 -- W5B critical heat flux correlations = 0 -- W3 + GE correlation

4-17

TABLE 4-1 (CONTINUED)

NOTATION	FORMAT	DESCRIPTION
*Card No. 17		
HOTCF	F10	Ratio of the mean power density in the hot channel to that in the core
AVGCF	F10	Ratio of the mean power density in the average channel to that in the core
HOTCFR	F10	Axial hot channel factor If HOTCFR = 10, then u^2 sin u axial heat profile is chosen instead of cut-off cosine and the value of (HOTCFR - 10) becomes the hot channel factor
SPUT	F10	Exponent for sputtering effects
*Card No. 18		
JBOTPL JTOPPL	I5 I5	The first and last leg I.D. numbers in the sequence of series-connected legs around the core
JCRBYP	I5	= blank -- for no core bypass = the I.D. number of the leg connected to the lower plenum in the peripheral leg series
*Card No. 19		
PM	F10	The expected initial value of fluid pressure (psia) in the system
WM	F10	The initial flow rate (lb/sec) = .1 -- presence of closed loop = 0. -- for open loop ($\neq$ 0 implies that the steady state balancing calculation is requested)
ENTHOT	F10	Initial fluid enthalpy (Btu/lb) in the hot legs
ENTCLD	F10	Same as ENTHOT for cold legs
PSATHOT	F10	Initial saturation pressure in the hot legs (psia)
PSATCLD	F10	Same as PSATHOT for cold legs
DENSHOT	F10	Initial fluid density (lb/ft^3) in the hot leg

TABLE 4-1 (CONTINUED)

NOTATION	FORMAT	DESCRIPTION
*Card No. 20		
DENSCLD	F10	Same as DENSHOT for cold legs
TEMPHOT	F10	Fluid temperature (°F) in the hot legs
TEMPCLD	F10	Fluid temperature (°F) in the cold legs
*Card Group No. 21		
J1	I5	DIAM(J) inputted on Card No. 12 may be updated;
J2	I5	DIAM(J) = DIA for J ranging from J1 to J2. This is useful for the downcomer and plenum
DIA	F10	regions.
		Blank -- a) no need of this operation
		b) ending the series of these cards

If NSONIC $\leq$ 0, skip Card No. 22.

Card Group No. 22

J1	I5	Temporary hydraulic diameter of legs J
J2	I5	(J1 $\leq$ J $\leq$ J2) for improved steady statem computation.
DIAMT	F10	

If NPUMP (Card No. 4) < 0, then the following Cards No. 23-25 for the pump characteristic data should be skipped.

Card Group No. 23 (a card for each table)

HAN(I)	9F5 For the HAN curve	⎫
HAD(I)	9F5 For the HAD curve	⎪
HVN(I)	9F5 For the HVN curve	⎬ Pump head (speed, discharge rate) characteristics
HVD(I)	9F5 For the HVD curve	⎪
HVT(I)	9F5 For the HVT curve	⎭
BAN(I)	9F5 For the BAN curve	⎫
BAD(I)	9F5 For the BAD curve	⎪ Pump torque (speed,
BVN(I)	9F5 For the BVN curve	⎬ discharge rate) characteristics
BVD(I)	9F5 For the BVD curve	⎭

TABLE 4-1 (CONTINUED)

NOTATION	FORMAT	DESCRIPTION
BVT(I)	9F5 For the BVT curve	Pump torque (speed, discharge rate) characteristics
HAT(I)	9F5 For the HAT curve	
BAT(I)	9F5 For the BAT curve	

Card No. 24

HR	F10	Nominal pump head (total, ft)
QR	F10	Nominal discharge rate (gpm · 10^{-4})
ENR	F10	Nominal pump speed (rpm)
TR	F10	Nominal torque (ft · lb)
XITER	F10	Inertia of all rotating parts attached to the pump rotor including motor (lb · ft^2)
APUMP	F10	Pump inlet flow area (ft^2) Set equal to the broken loop flow area upstream of the pump
ENO	F10	Pump speed before power loss (rpm)

Card No. 25

EM	F10	Density ratio exponent (1.0 is suggested)
C1LOSS	F10	Bearing torque loss coefficient
C2LOSS	F10	Windage torque loss coefficient

If WM = 0.0 on Card No. 19, then the next card to be entered is Card No. 31.

Even if WM ≠ 0.0, Card No. 26 should be skipped in the case of NLOOPS = 0.

Card No. 26

NLGLOOP(1) . . . NLGLOOP(NLOOPS)	I5	Number of series-connected legs in external loop No. 1
NLGTOPR	I5	Number of series-connected legs from the upper plenum junction to the junction where the pressurizer branch is attached

TABLE 4-1 (CONTINUED)

NOTATION	FORMAT	DESCRIPTION
NLGPRES	I5	Number of legs in the pressurizer branch

Card No. 27

JAC1	I5	The leg I.D. No. attached to the accumulator of loop 1, at its last node
JAC1N	I5	The leg I.D. No. attached to the accumulator of loop 1, at its first node
JAC2	I5	
JAC2N	I5	The leg I.D. No. similar to JAC1 and JAC1N connecting to the accumulators of loops 2 and
JAC3	I5	3
JAC3N	I5	
JDELH1	I5	The leg I.D. No. attached to the SIS/Deluge pump of loop 1, at its last node
JDELH1N	I5	The leg I.D. No. attached to the SIS/Deluge pump of loop 1, at its first node
JDELH2	I5	
JDELH2N	I5	The leg I.D. No. similar to JDELH1 and JDELH1N connecting to the SIS/Deluge pumps of loops
JDELH3	I5	2 and 3
JDELH3N	I5	

Card No. 28

LOOP(I,J)	I5	The leg I.D. No. of the J-th leg in the I-th external loop in sequence

Card No. 29

WLOOP	F10	Initial mass flow rate (1b/sec) in a (non-lumped) loop
PPRESS	F10	Initial pressurizer pressure (psia)

If NLOOPS = 0 on Card No. 4, then Card No. 30 should be skipped.

TABLE 4-1 (CONTINUED)

NOTATION	FORMAT	DESCRIPTION
Card No. 30		
LPRESS(I)	I5	The leg I.D. numbers representing the pressurizer surge line. The sequence starts with the pressurizer (I=1) and ends up with the leg (I=NLGPRESS) that connects with the main external loop.

If JCRBYP = 0 (Card No. 18), then Card Nos. 30a and 30b should be skipped.

NOTATION	FORMAT	DESCRIPTION
Card No. 30a		
NBYP	I5	Number of core bypasses (peripheral, former region, etc.)
Card No. 30b		
NLK (N)	I5	No. of legs forming the n-th bypass.
JBYP(N,J) (J=1,NLK)	13I5	Leg I.D. Nos. in sequence from the bottom of the core to the top, in the n-th bypass
*Card Group No. 31		
J	I5	Leg No.
I	I5	Node No.
H(I,J,2)	F10	The abnormal enthalpy at node I of leg J; a card for each abnormal point. To stop reading this data, set J > NOLEG.

If NHEAT = 0 on Card No. 4, then the next card to be prepared is Card No. 39.

NOTATION	FORMAT	DESCRIPTION
Card No. 32		
NROD	I5	Number of fuel rods in the core
NTUBE	I5	Number of tubes in the S.G.
Card No. 33		
RADF	F10	Fuel pellet radius (inches)
RADCL	F10	Outer radius of fuel cladding (inches)
DRCL	F10	Cladding thickness (inches)
RADTUB	F10	Inner radius of S.G. tube (inches)

TABLE 4-1 (CONTINUED)

NOTATION	FORMAT	DESCRIPTION
DRTUBE	F10	S.G. tube thickness (inches)
Card No. 34		
CONF	F10	Thermal conductivity of fuel pellets (Btu/hr · ft · °F)
CONCL	F10	Thermal conductivity of cladding (Btu/hr · ft · °F)
CONTUBE	F10	Thermal conductivity of S.G. tubes (Btu/hr · ft · °F)
CPF	F10	Specific heat of fuel pellets (Btu/hr · ft · °F)
CPCL	F10	Specific heat of cladding (Btu/hr · ft · °F)
CPTUBE	F10	Specific heat of S.G. tubes (Btu/hr · ft · °F)
Card No. 35		
RHOF	F10	Density of fuel pellets (lb/ft^3)
RHOCL	F10	Density of cladding (lb/ft^3)
RHOTUBE	F10	Density of S.G. tubes (lb/ft^3)
Card No. 36		
HFCO	F10	Steady-state heat transfer coefficient at cladding surface (Btu/hr · ft^2 · °F)
HFCSG	F10	Steady-state heat transfer coefficient at the inner surface of S.G. tubes
HFBO	F10	Steam film coefficient at cladding, based on the steady state mass flow rate and the containment pressure
HFBSG	F10	Steam film coefficient at inner surface of S.G. tubes
HGAP	F10	Heat transfer coefficient at the gap between the fuel pellet and the cladding; mean value during blowdown

TABLE 4-1 (CONTINUED)

NOTATION	FORMAT	DESCRIPTION
HSECOND	F10	Heat transfer coefficient at the outer surface of S.G. tubes, mean value during blowdown

Card No. 37

TEMPSG	F10	Average temperature of secondary coolant at S.G. tube outer surface (°F)
POWERC	F10	Steady state reactor power (Btu/sec)
TIMROD	F10	Control rod trip delay time following initiation of blowdown (sec)

Skip Card No. 38 if POWERO > 10^5.

Card No. 38

DTPOW(I)	8F5	Time table (sec) after scram
POWHIST(I)	8F5	Power history table after scram (reactor power = POWER · POWHIST(I))

*Card No. 39

TSEP	F10	Time (sec) when phase separation calculation begins (sputtering effects)
XFRIC	F10	Fluid quality above which the Martinelli-Nelson model is used for frictional pressure drop calculation provided that $p \leq 500$ psia. XFRIC ≤ 0.05 is recommended
VBUB2	F10	Bubble rise velocity (ft/sec) to be used in the phase separation calculation
PCONT	F10	Containment pressure (psia)

If JAC1 = JAC2 = 0 on Card No. 27, skip Card Nos. 40 and 41.

Card No. 40

PGO1	F10	
PGO2	F10	Accumulator initial gas pressure in the external loops 1, 2, and 3, respectively. When this value is set to 0, then that accumulator is inactive.
PGO3	F10	

TABLE 4-1 (CONTINUED)

NOTATION	FORMAT	DESCRIPTION
VAC	F10	Volume of an accumulator (ft^3)
VGO	F10	Initial gas volume of an accumulator
ELAC	F10	Length of pipe connecting the external loop and the accumulator (ft)
ACK	F10	Hydraulic loss coefficient for flow between the loop and the accumulator

Card No. 41

EXPN	F10	Polytropic exponent for the accumulator gas expansion
HAC	F10	Enthalpy of the accumulator water (Btu/lb)

*Card No. 42

JAC4	I5	The core leg number at whose last node a vessel accumulator is attached
LEAK4	I5	Leakage element leg number where the vessel accumulator is attached. If none, set to zero.

If JAC4 = 0, then Card No. 43 should be skipped.

Card No. 43

PGO4	F10	
VAC4	F10	
VGO4	F10	Variables for the vessel accumulator -- same meaning as PGO1, VAC, VGO, ELAC, ACK, and HAC on Card Nos. 40 and 41
ELAC4	F10	
ACK4	F10	
HACK	F10	

*Card No. 44

PDELAC	F10	SIS/Deluge system activation pressure (PDELAC < PGO). This is in case this system is attached to an accumulator

TABLE 4-1 (CONTINUED)

NOTATION	FORMAT	DESCRIPTION
PDELLP	F10	The activation pressure of the SIS/Deluge system that is not attached to an accumulator
TSIS	F10	Delay time (sec) in bringing the SIS/Deluge pump up to speed
DTSIS	F10	Delay time in opening the discharge valve downstream of the SIS/Deluge system

If PDELAC = PDELLP = 0.0, then the next card to be prepared is Card No. 46.

Card Group No. 45a

PD(I) (25 data)	8F10	Pressure (psia) -- corresponding to discharge rate (WD below) -- characteristics for the SIS/Deluge pumps

Card Group No. 45b

WD(I,N) (25 data)	8F10	Discharge flow rate (lb/sec) for the N-th SIS/Deluge pump. The 25 pieces of data are to be provided for N = 1, 2, 3, 4.

*Card No. 46

PCSP	F10	Activation pressure for incore spray system (psia)
HCSP	F10	Enthalpy of incore spray water
RCSP	F10	Density of incore spray water (lb/ft^3)
ELCSP	F10	Length of incore spray water supply pipe (ft)
ACSP	F10	Flow area of the incore spray supply line (ft^2)
CSPK	F10	Hydraulic loss coefficient for the incore spray supply line
OFFSP	I5	Core channel number for which the incore spray will not be activated. Leave blank if not applicable.

If PCSP = 0.0, then Card No. 47 should be skipped.

TABLE 4-1 (CONTINUED)

NOTATION	FORMAT	DESCRIPTION
Card No. 47		
P1CSP	F10	Pressure (psia) - discharge rate (lb/sec) charac-
		teristics of the core spray system. PCSP >
W1CSP	F10	P2CSP > P1CSP. For the pressure at the dis-
		charge point p > PCSP, the flow rate w = 0.
P2CSP	F10	For PCSP > p > P1CSP, w is given by quadratic
		interpolation of (PCSP, 0), (P2CSP, W2CSP),
W2CSP	F10	and (P1CSP, W1CSP). For p < P1CSP, w = W1CSP.
*Card No. 48		
TWHT	F10	Time (sec) after which the wetted wall heat trans- fer calculations can be performed. To ignore such a calculation, set TWHT = 9999.
DTWALL	F10	A fixed time increment to be used in the wetted wall heat transfer calculations. DTWALL = 0.1 sec, is recommended.
DWALL	F10	Wall thickness (inches) of typical legs
PERIM	F10	Length of circumference (ft) of typical legs

If TWHT = 9999., then Card No. 49 should be skipped.

NOTATION	FORMAT	DESCRIPTION
Card Group No. 49		
J	I5	Leg I.D. number
DWALL(J)	F10	Wall thickness of non-typical leg J.
PERIM(J)	F10	Circumference of non-typical leg J
NN	I5	= 0 -- for continued data ≠ 0 -- end of the data group

If NWINDOW ≠ 0 on Card No. 4, the following data for initial conditions on Card Group No. 50, and for predetermined boundary conditions on Card Group No. 51 must be prepared. Otherwise, the next card is No. 52.

NOTATION	FORMAT	DESCRIPTION
Card Group No. 50 (J = 1, NOLEG)		
P	F10	Pressure at the first node of leg J
DP	F10	Pressure increment per node in leg J
G	F10	Mass flow rate in leg J

TABLE 4-1 (CONTINUED)

NOTATION	FORMAT	DESCRIPTION
H	F10	Enthalpy at the first node of leg J
DH	F10	Enthalpy increment per node

Card Group No. 51a

| TTBL(I) (21 data) | 7F10 | The time table |

Card Group No. 51b

| WTBL(I) (21 data) | 7F10 | The table for total mass flow rate (lb/sec). Usually, they are negative values (NND2 = 13). |

Card Group No. 51c

| HTBL(I) (21 data) | 7F10 | The table for the enthalpy of in-flow water (NND2 = 13) |

Card Group No. 51d

| PTBL(I) (21 data) | 7510 | The table for pressure (NND2 = 12) |

If PTBL(21) $\geq$ 4000, prepare steady state oscillation data.

Card Group No. 51e

| AMP | F10 | Pressure boundary condition is |
| ØMG | F10 | p = AMP · sin (OMG · t) |

IØSTYP=1,2

(a,c)

Card Group No. 52

| MAXITER | I5 | Number of iterations for fluid-structure calculations (=5, suggested) |

4-28

TABLE 4-1 (CONTINUED)

NOTATION	FORMAT	DESCRIPTION
NSEG	I5	
IØSTYP	I5	Type of analysis (=1 or 2)
NINPLA	I5	

(a,c)

(a,c)

Card Group No. 53

One blank card

Card Group No. 54 (one blank card at the end of this group)

K	I5	Wall number (in sequence)
JCHAN(K)	I5	Leg number on one side of wall
LCHAN(K)	I5	Leg number on other side of wall
NWALL(K)	I5	Wall number across JCHAN(K)
		= 0, For JCHAN(K) to be surrounded by flexible wall K and a rigid wall
FLEX1	F10	
FLEX2	F10	
FLEX3	F10	
FLEX4	F10	
FLEX5	F10	

(a,c)

Card Group No. 55

| ETA | F10 | |

Card Group No. 56

| IYMAX | I5 | |
| ISKPRP | I5 | |

(a,c)

4-29

TABLE 4-1 (CONTINUED)   20

NOTATION	FORMAT	DESCRIPTION
KRIP	I5	
J2CHØK	I5	
GCHØK	F10	
J2BC	I5	
TJ2BC	F10	

(a,c)

Card Group No. 57 (*IKMAX)

KKK1(I)	I5	}
KKK2(I)	I5	
WDISP1(I)	F10	}
WDISP2(I)	F10	
FACTK1(I)	F10	}
FACTK2(I)	F10	
FACTK3(I)	F10	

(a,c)

Card Group No. 58

KRIP	I5	
JRIP	I5	
DIRRIP	F10	
ARIP	F10	
WIDTH	F10	
HRIP	F10	

(a,c)

TABLE 4-1 (CONTINUED)

NOTATION	FORMAT	DESCRIPTION
	$I\emptyset STYP=3,4,53,54$	

Card Group No. 52

| MAXITER | I5 | Number of iterations for fluid-structure cal-
culations (=5, suggested) |
| NSEG | I5 | |

(a,c)

| IØSTYP | I5 | Type of analysis (=3,4,53 or 54) |
| NINPLA | I5 | |

(a,c)

Card Group No. 53

| DELTA | 12F5 | Half the angle (in degrees) subtended by each
wall along the core circumference; used in
curvature correction. For symmetric cores,
=360./(2. * NSEG). For asymmetric cores,
=22.5. |

Card Group No. 54 (one blank card at the end of this group)

K	I5	Wall number (in sequence)
JCHAN(K)	I5	Leg number on one side of wall
LCHAN(K)	I5	Leg number on other side of wall
NWALL(K)	I5	Wall number across JCHAN(K)
FLEX1	F10	For IØSTYP=3 or 4, mass in lb_m
FLEX2	F10	
FLEX3	F10	
FLEX4	F10	
FLEX5	F10	

4-31   (a,c)

TABLE 4-1 (CONTINUED)

NOTATION	FORMAT	DESCRIPTION
Card Group No. 55		
MASPNT	I5	
IEFF	I5	
		(a,c)
Card Group No. 55a		
EFFMAS(J) J=1,MASPNT	7F10	
		(a,c)
Card Group No. 56		
FREQ(J) J=1,MASPNT	7F10	
		(a,c)
Card Group No. 57		
((PHI)I,J) I=1,MASPNT) J=1,MASPNT)	7F10	
		(a,c)
Card Group No. 58		
ETA	F10	
		(a,c)
Card Group No. 59		
NLBC	I5	
		(a,c)
Card Group No. 60		
PHIB(N.J) J=1,MASPNT	7F10	Weighted relative mode shapes (Weighted Relative Displacements - ψ_n)
		(a,c)

TABLE 4-1 (CONTINUED)

NOTATION	FORMAT	DESCRIPTION
Card Group No. 61		
RPHIB(N,J) J=1,MASPNT	7F10	
Card Group No. 62		
XKLIN(N)	F10	
XFJUMPO(N)	F10	
XJMP(N)	F10	
XFJMP(N)	F10	
XCNL(N)	F10	
SLIDEF(N)	F10	
Card Group No. 63		
GAP1(N)	F10	
XKNL1(N)	F10	
GAP2(N)	F10	
XKNL2(N)	F10	

(a,c)

IØSTYP=5,55

Card Group No. 52		
MAXITER	I5	Number of iterations for fluid-structure cal- culations (=5, suggested)
NSEG	I5	

(a,c)

TABLE 4-1 (CONTINUED)

NOTATION	FORMAT	DESCRIPTION
IØSTYP	I5	Type of analysis (=5 or 55)
NINPLA	I5	

(a,c)

Card Group No. 53

DELTA	12F5	Half the angle (in degrees) subtended by each wall along the core circumference; used in curvature correction.

Card Group No. 54 (one blank card at the end of this group)

K	I5	Wall number (in sequence)
JCHAN(K)	I5	Leg number on one side of wall
LCHAN(K)	I5	Leg number on other side of wall
NWALL(K)	I5	Wall number across JCHAN(K)
FLEX1	F10	
FLEX2	F10	
FLEX3	F10	
FLEX4	F10	
FLEX5	F10	

(a,c)

Card Group No. 55

MASPNT	I5	
NBEAM2	I5	
NBEAM1	I5	

(a,c)

4-34

TABLE 4-? (CONTINUED)

NOTATION	FORMAT	DESCRIPTION
Card Group No. 56		
(YFREQ(J),J=1,MASPNT)	7F10	
(YFREQ(J),J=1,MASPNT)	7F10	
Card Group No. 57		
(MNLAST(I),I=1 (NBEAM2-NBEAM1))	14I5	

(a,c)

Card Group No. 58		
(PHI(I,J),I=1, number of mass points in this beam)	7F10	

(a,c)

Card Group No. 59		
(PHI(I,J),I=1, number of mass points in this beam)	7F10	

(a,c)

Card Group No. 60		
ETA	F10	

(a,c)

(a,c)

TABLE 4-1 (CONTINUED)

NOTATION	FORMAT	DESCRIPTION	
		[IOSTYP=9]	

Card Group No. 52

MAXITER	I5	Number of iterations for fluid-structure calculations (=5, suggested)	
NSEG	I5		
IØSTYP	I5	Type of analysis (=9, required)	(a,c)
NINPLA	I5		
			(a,c)

Card Group No. 53

| DELTA | 12F5 | Half the angle (in degrees) subtended by one wall along the core circumference; used in curvature correction (=22.5, required) | |

Card Group No. 54 (one blank card at the end of this group)

K	I5	Wall number (in sequence)	
JCHAN(K)	I5	Leg number on one side of wall	
LCHAN(K)	I5	Leg number on other side of wall	
NWALL(K)	I5	Not used (=0, required)	
FLEX1	F10		
FLEX2	F10		
FLEX3	F10		
FLEX4	F10		
FLEX5	F10		
			(a,c)

Card Group No. 55

NWINL1	I5		
JSEG	I5		
			(a,c)

4-36

TABLE 4-1 (CONTINUED)

NOTATION	FORMAT	DESCRIPTION

Card Group No. 55 (Continued)

SRATIØ   F10

IPREP   I5

                                            (a,c)

Card Group No. 56

(JINWL1 (I,K) I=1,JSEG)   5I5

                                            (a,c)

Card Group No. 57

(RATWA (I,K) I=1,JSEG)   5F10

                                            (a,c)

IOSTYP=10,60

                                            (a,c)

Card Group No. 52

MAXITER	I5	Number of iterations for fluid-structure calculations (=5, suggested)
NSEG	I5	
IØSTYP	I5	Type of analysis (=10 or 60, corresponding to a 2-dimensional beam analysis of 5 or 55, respectively) (a,c)
NINPLA	I5	(a,c)

4-37

TABLE 4-1 (CONTINUED)

NOTATION	FORMAT	DESCRIPTION
Card Group No. 53		
DELTA	12F5	Half the angle (in degrees) subtended by one wall along the core circumference; used in curvature correction (=22.5, required)
Card Group No. 54 (one blank card at the end of this group)		
K	I5	Wall number (in sequence)
JCHAN(K)	I5	Leg number on one side of wall
LCHAN(K)	I5	Leg number on other side of wall
NWALL(K)	I5	Not used (=0, required)
FLEX1	F10	
FLEX2	F10	
FLEX3	F10	
FLEX4	F10	
FLEX5	F10	

(a,c)

Card Group No. 55		
MASPNT	I5	
NBEAM2	I5	
NBEAM1	I5	
Card Group No. 56		
(FREQ(J),J=1,MASPNT)	7F10	
(YFREQ(J),J=1,MASPNT)	7F10	

4-38

(a,c)

TABLE 4-1 (CONTINUED)

NOTATION	FORMAT	DESCRIPTION
Card Group No. 57		
(MNLAST(I),I=1, (NBEAM2+NBEAM1))	14I5	
		(a,c)
Card Group No. 58		
(PHI(I,J),I=1, number of mass points in this beam)	7F10	
		(a,c)
Card Group No. 59		
(PHI(I,J),I=1, number of mass points in this beam)	7F10	
		(a,c)
Card Group No. 60		
ETA	F10	
Card Group No. 61		
NWINL1	I5	
JSEG	I5	
SRATIØ	F10	
		(a,c)

4-39

TABLE 4-1 (CONTINUED)

NOTATION	FORMAT	DESCRIPTION
IPREP	I5	

Card Group No. 62

  (JINWL1 (I,K) I=1,JSEG)   5I5

(a,c

Card Group No. 63

  (RATWA (I,K) I=1,JSEG)   5F10

(a,c

Card Group No. 64

To run DIRPLT as a part of MULTIFLEX, one input card is necessary. This card must follow all structural input data and be the last card in the deck. Its format is:

IØPT	I5	= 1 if modal analysis is to be performed = 0 if no modal analysis is to be performed
N	I5	Structural data is read from TAPE4 at every N-th timestep
BEGIN	F10	Start time (in seconds) of range of data to be plotted
END	F10	End time (in seconds) of range of data to be plotted

If no plotting is desired, the above card should be left blank.

TABLE 4-2

SENSITIVITY STUDY FOR DOWNCOMER NETWORK MODEL
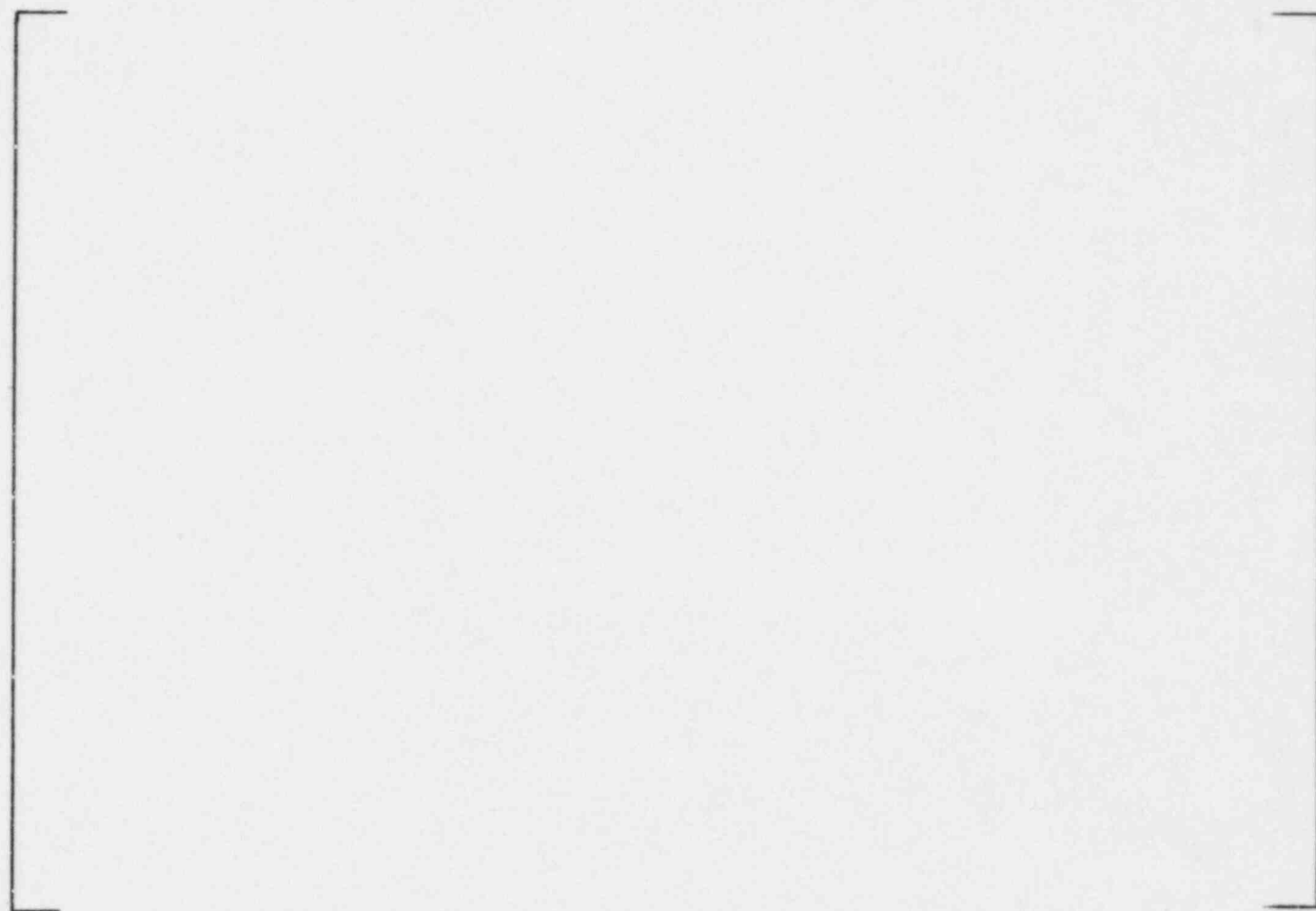
4-41

(a,c)

TABLE 4-3

NODAL ELEVATION OF WECAN, MULTIFLEX, And LATFORC

4-42

(a,c)

(a,c)

TABLE 4-4 STRUCTURAL INPUT DATA OBTAINED BY RELATIVE MODAL ANALYSES

[ ] (a,c)
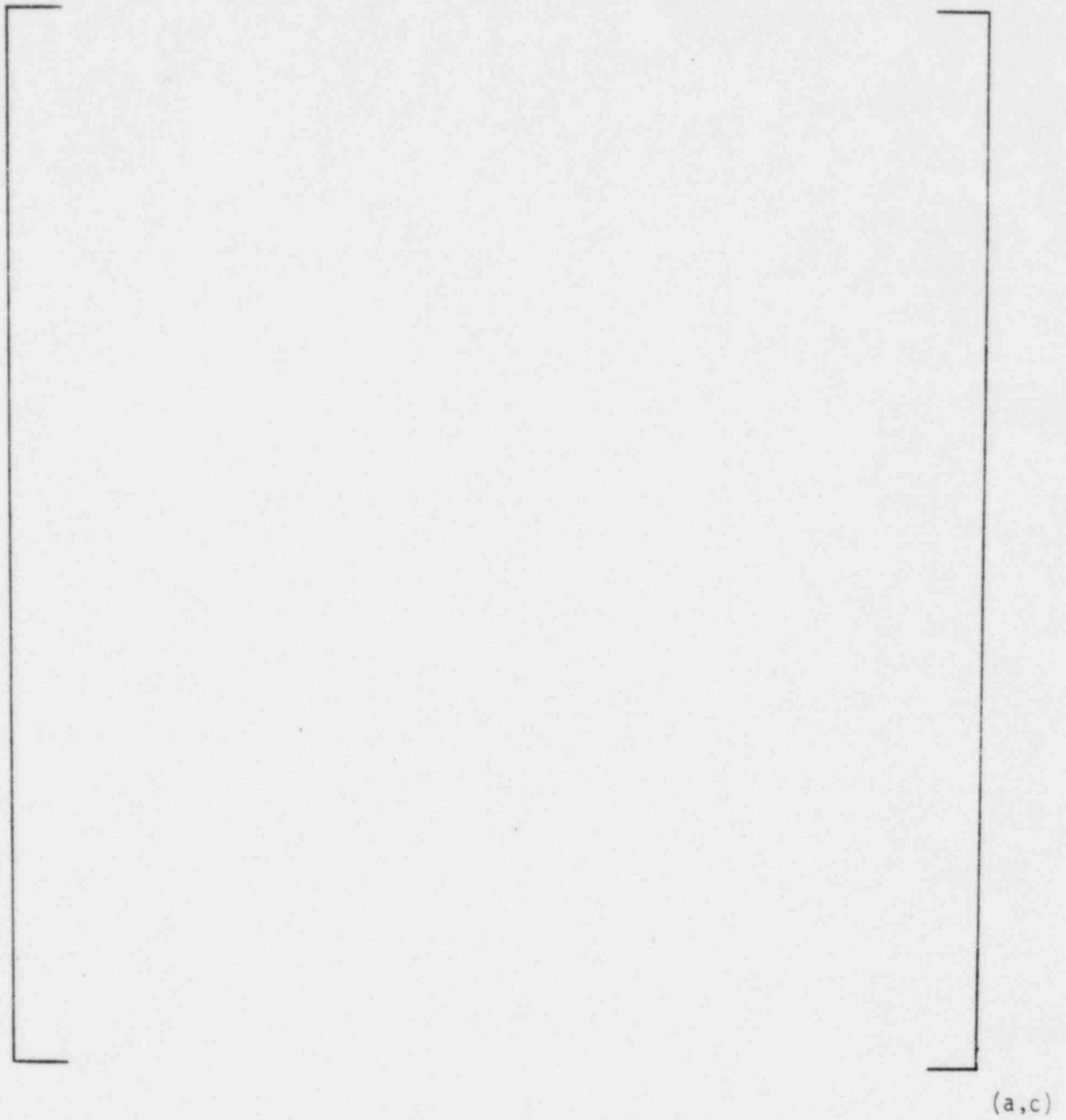
Figure 4-1. Hydraulic Modeling of Downcomer Annulus

(a,c)
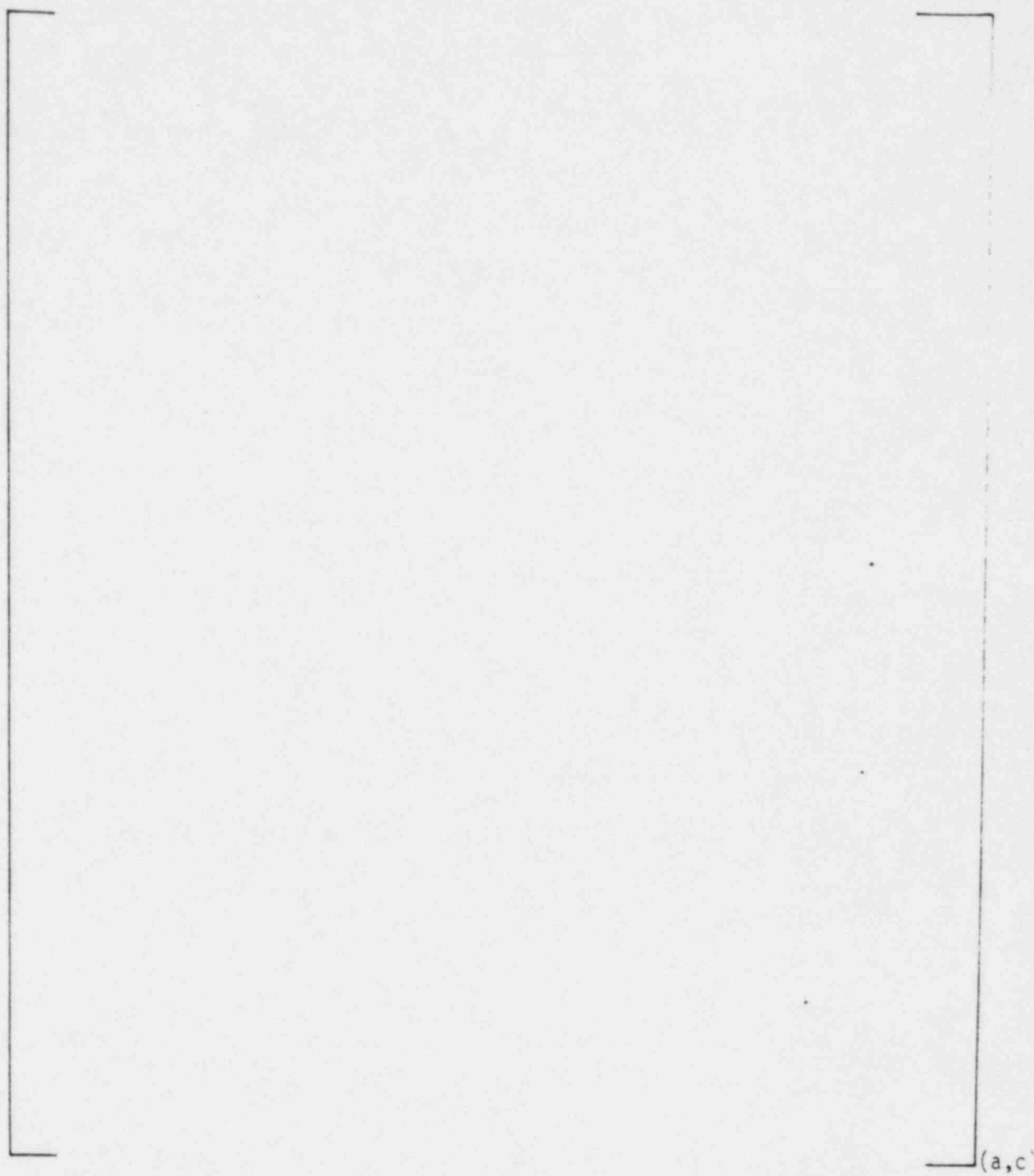
Figure 4-2. Downcomer Network for a Three-Loop Thermal Shield Plant

(a,c)
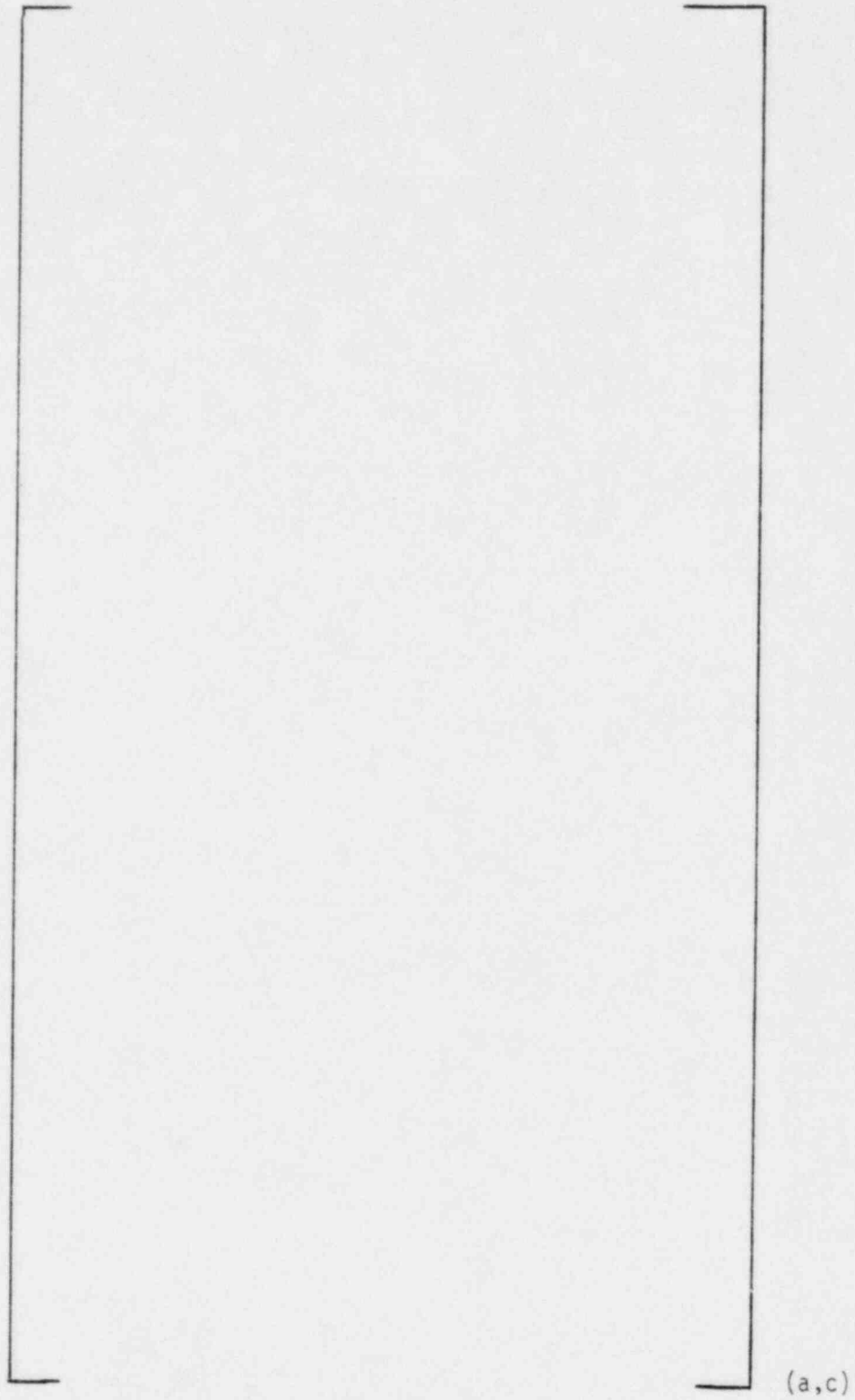
Figure 4-3. Results of Sensitivity Study for the Downcomer Model
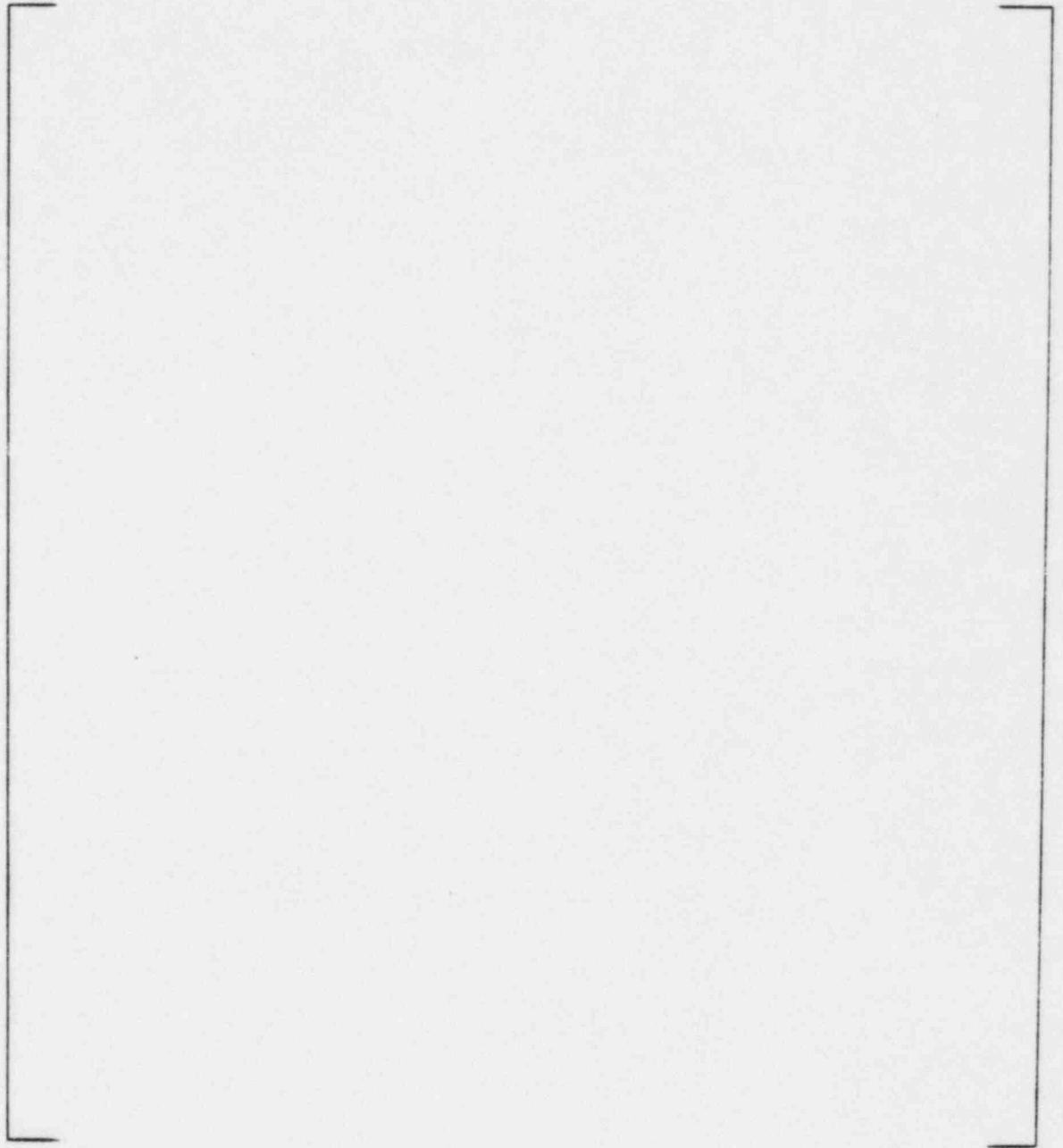
$$(a,c)$$

Figure 4-4. Interface Modeling of Downcomer Annulus Element

(a,c)
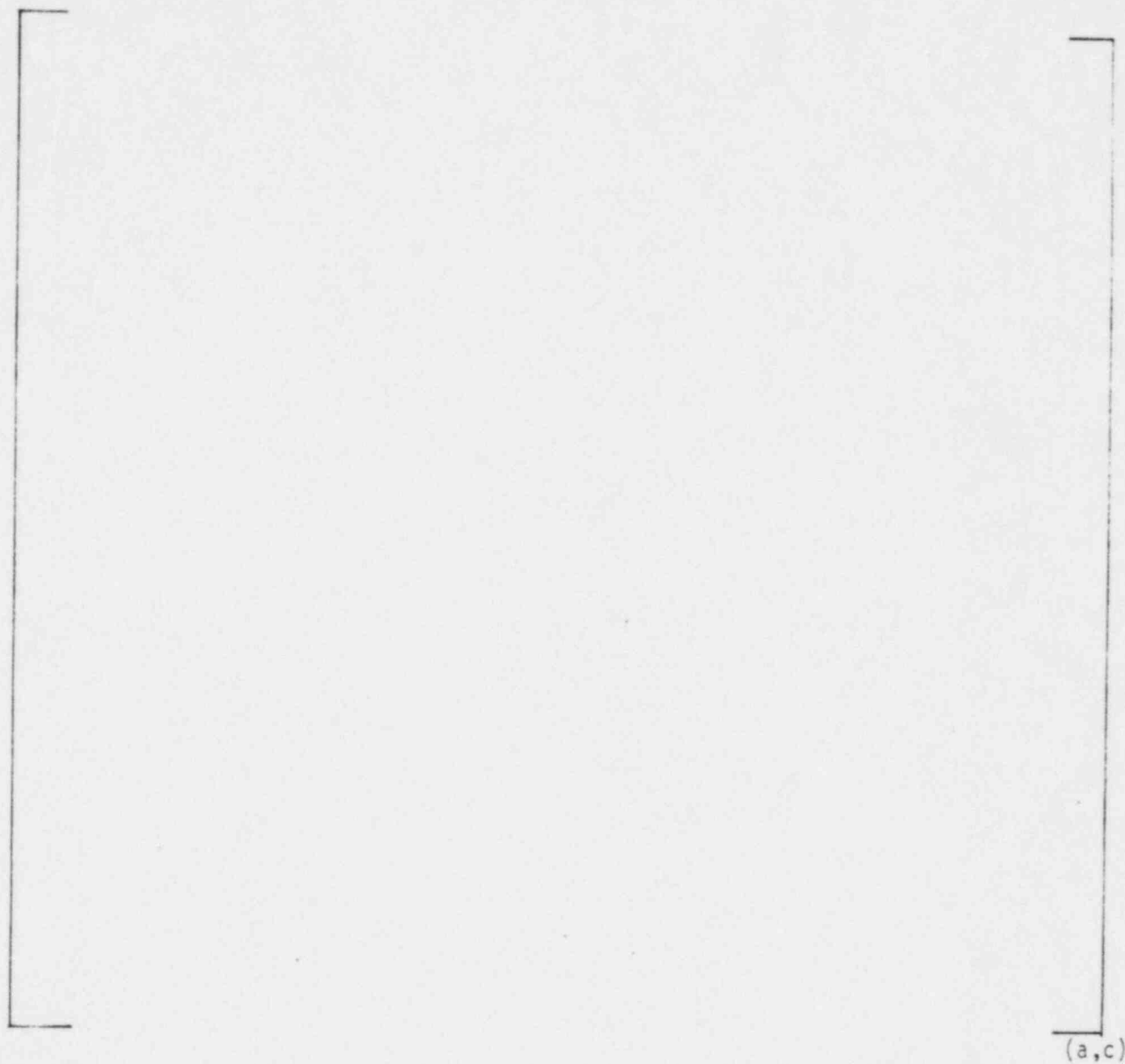
Figure 4-5. Interface Modeling of the Flexible Walls and the Hydraulic Network
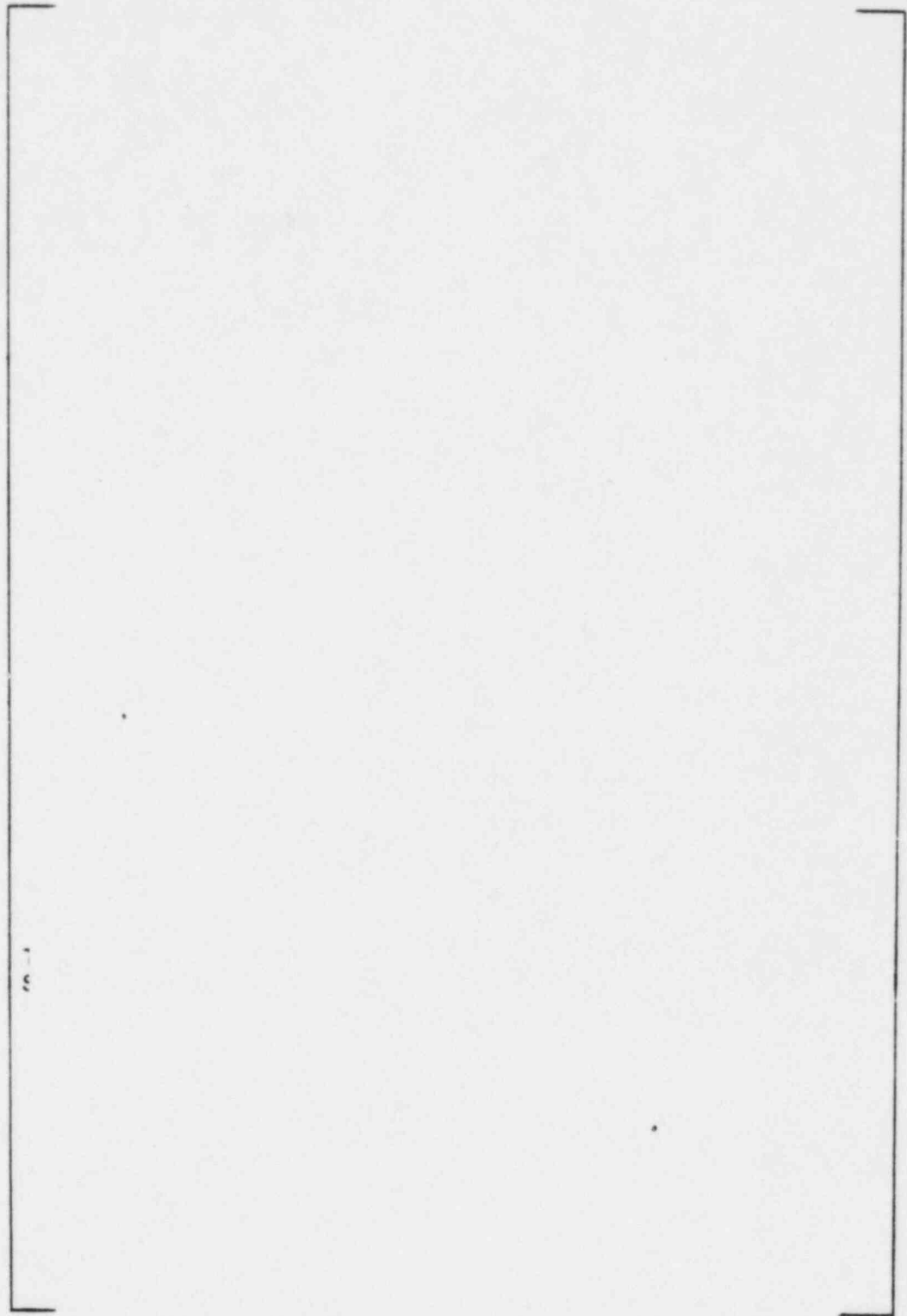
Figure 4-6. Structural Model for WECAN Modal Analysis

(a,c)

(a,c)
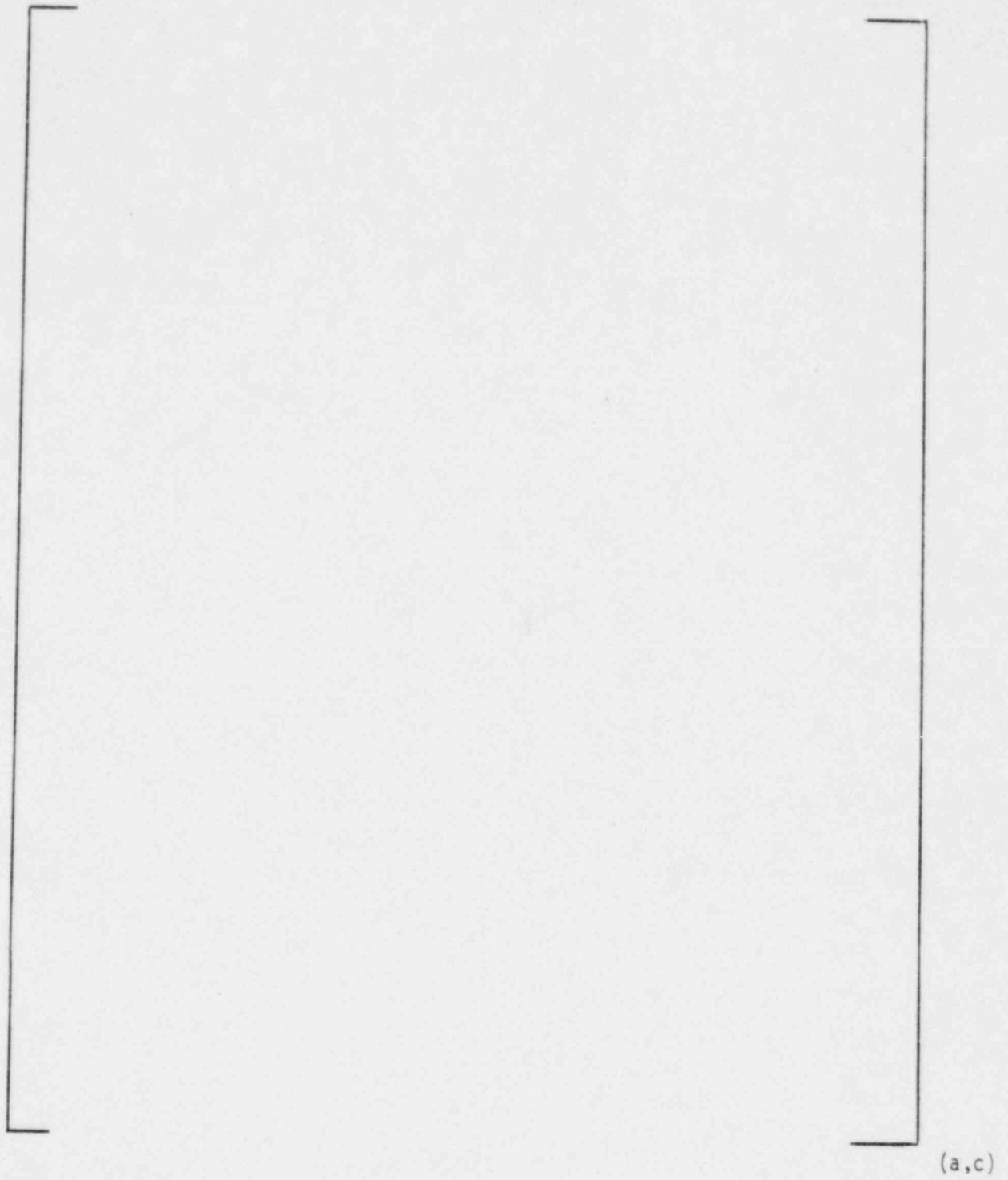
Figure 4-7. Force Displacement Relation at Barrel
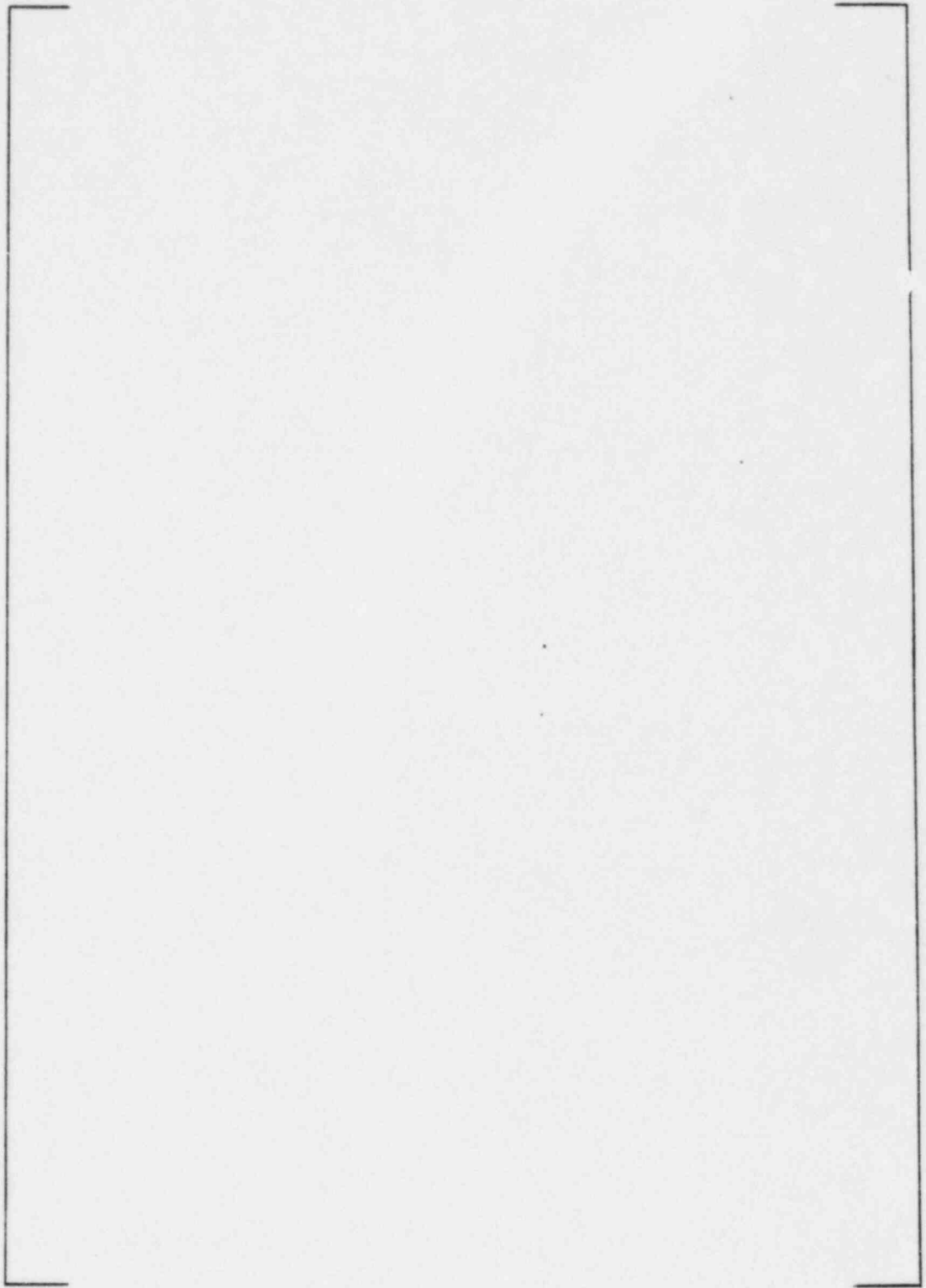
Figure 4-8. Force-Displacement Relations at Core Support Plate

(a,c)

5.0 STRUCTURAL INPUT AND NON-LINEAR BOUNDARY CONDITIONS

As stated elsewhere, structural input data for the advanced beam model are the relative mode shapes, generalized masses, model frequencies, and the data for non-linear boundary conditions. Basic assumptions and the methodology of generating the non-linear boundary conditions in terms of load-deformation relationships are discussed in Section 5.1. Preparation of the modal analysis data in terms of eigenvalues, relative eigenvectors and generalized masses are discussed in Section 5.2.

5.1 Reactor Vessel And Core Barrel Boundary Conditions

There are three non-linear boundaries in the beam model illustrated in Figure 2-3; the upper core barrel flange support, the hot leg nozzles, and the lower radial key restraints. It should be noted that the nozzle support has negligible effects on the overall system response and, therefore, is not included in the MULTIFLEX beam model. However, for the relative modal analysis, the vessel supported at the node of the inlet nozzle/downcomer joint is included in the model.

5.1.1 Upper Core Barrel Flange Boundary Conditions

Upper boundary conditions as shown in Figure 2-3 consist of a horizontal non-linear spring and a linear rotary spring between the core barrel flange and the reactor vessel flange. The non-linearities here are due to (1) the mechanical gaps and (2) load dependent deformation of the barrel flange. During horizontal LOCA excitations, the core barrel flange impacts the reactor vessel flange when the radial clearance between the two flanges is closed. In the following, we describe briefly the basic assumptions and the finite element models of core barrel flange to develop the top boundary conditions.

The core barrel flange is modeled as a circular ring by thirty-six (36) three-dimensional beams (STIF4) of WECAN code[27]. In determining the number of beams to represent the barrel flange as a ring, the finite element solution was compared to a classical solution[36]. The results show that the finite element approximation to the ring is within one percent[37] of the classical solution and thus the 36 beam representation of the barrel flange should adequately describe the deformation of the structure. Figure 5.1 shows the beam representation of the core barrel flange.

Figure 5-2a shows the simply supported cross-section of the core barrel flange; whereas Figure 5.2b represents rigid cross beams ($E \backsimeq \infty$) that have been connected from the simply supported location to the center of the barrel shell through the centroid of the flange. Figure 5-3 shows the finite element model of the flange and shell structure.

The radial clearance which exists between the core barrel flange and the reactor vessel flange, is reprsented by 3-D dynamic element (STIF37) of WECAN code[27]. Figure 5-4 shows the top view of the barrel-vessel flanges with the 3-D dynamic element. For a given lateral load, the core barrel flange first contacts the vessel at one point and then deflects conforming to the I.D. of the vessel flange with a constant radius of curvature. Figure 5-5 shows the deflected shape of the barrel flange. The contact arc length between the vessel and barrel flanges; and the corresponding stiffness depends on the magnitude of the lateral load.

In the analysis it is assumed that:

(1) The applied load to the barrel flange is one of the tangential shear with

$$Fx = A \sin^2 \theta \qquad , \qquad Fy = A \sin\theta \cos\theta$$

(2) Out-of-plane deformations of the flange are not permitted.

Using the finite element model described above, typical force-displacement relations for two, three, and four loop core barrel flange are shown in Figure 4-7.

5.1.2 Core Barrel Bottom Boundary Conditions

The bottom boundary supports for the core barrel and the reactor vessel are at the lower radial key restraints level. The force-displacement relationship for this boundary support is calculated using the concept of unit load analysis. The basic assumptions made here are:

(a) Vessel, clevises, and inserts are considered rigid,
(b) Two side keys are loaded at the same time,
(c) Deformation in the side keys is due to shear only.

Then using the stress-strain relationship for the material, dimensions of the radial keys and the procedure outlined in Reference 37, the load-deformation curve can be constructed. Figure 4-8 illustrates the force-displacement relationship for a typical 3-loop standard plant.

5.2 Normal Mode Analysis

Structural input data required for MULTIFLEX consist of generalized masses, eigen-
frequencies, relative mode shapes, weighted and non-weighted relative boundary
shapes. This input data can be computed from WECAN[27] two-dimensional or three-
dimensional structural model using normal mode analysis option. A typical three-
dimensional WECAN finite element model of PWR vessel support, pressure vessel,
and internal components for a thermal shield type plant is shown in Figures 5-6
and 5-7. Here, the core barrel, thermal shield and the reactor vessel are repre-
sented by concentric pipes (STIF7). The fuel assemblies are represented by 3-D
beams. The upper support assembly consisting of guide tubes, upper support
columns and the deep beam is represented by mass and stiffness matrices (STIF27)
obtained via sub-structuring technique. For a detailed description of the finite
element model, the reader is referred to Reference 38.

It is important that the WECAN structural model should be consistent with the
MULTIFLEX model in the sense that elevations of barrel-vessel mass points in the
MULTIFLEX model are coincident with the barrel-vessel node points of WECAN model.
Also, the linear springs at the top and bottom barrel-vessel supports used in
WECAN normal mode analysis should be identical to those used in MULTIFLEX pseudo
force method (see Section 2.2.3.1).

The WECAN output for reduced modal analysis is cataloged on TAPE22. From the re-
sults of modal analysis, a maximum number of ten (10) modes counted from the
lowest are selected. The barrel-vessel response is the only criterion for selec-
tion of these modes and can either be made by visual inspection of mode shapes
or by harmonic response analysis. Once the selection of these modes is made, the
data on TAPE22 is attached to be input to RELMODE subroutine described in Appendix
A. The results of RELMODE for input to MULTIFLEX consist of:

- Generalized Masses
- Eigenfrequencies
- Relative Mode Shapes
- Weighted Relative Boundary Shapes
- Non-weighted Relative Boundary Shapes

The input data instructions for RELMODE subroutine are given in Appendix A. Table
A-2 shows a typical output from RELMODE to be used in MULTIFLEX.
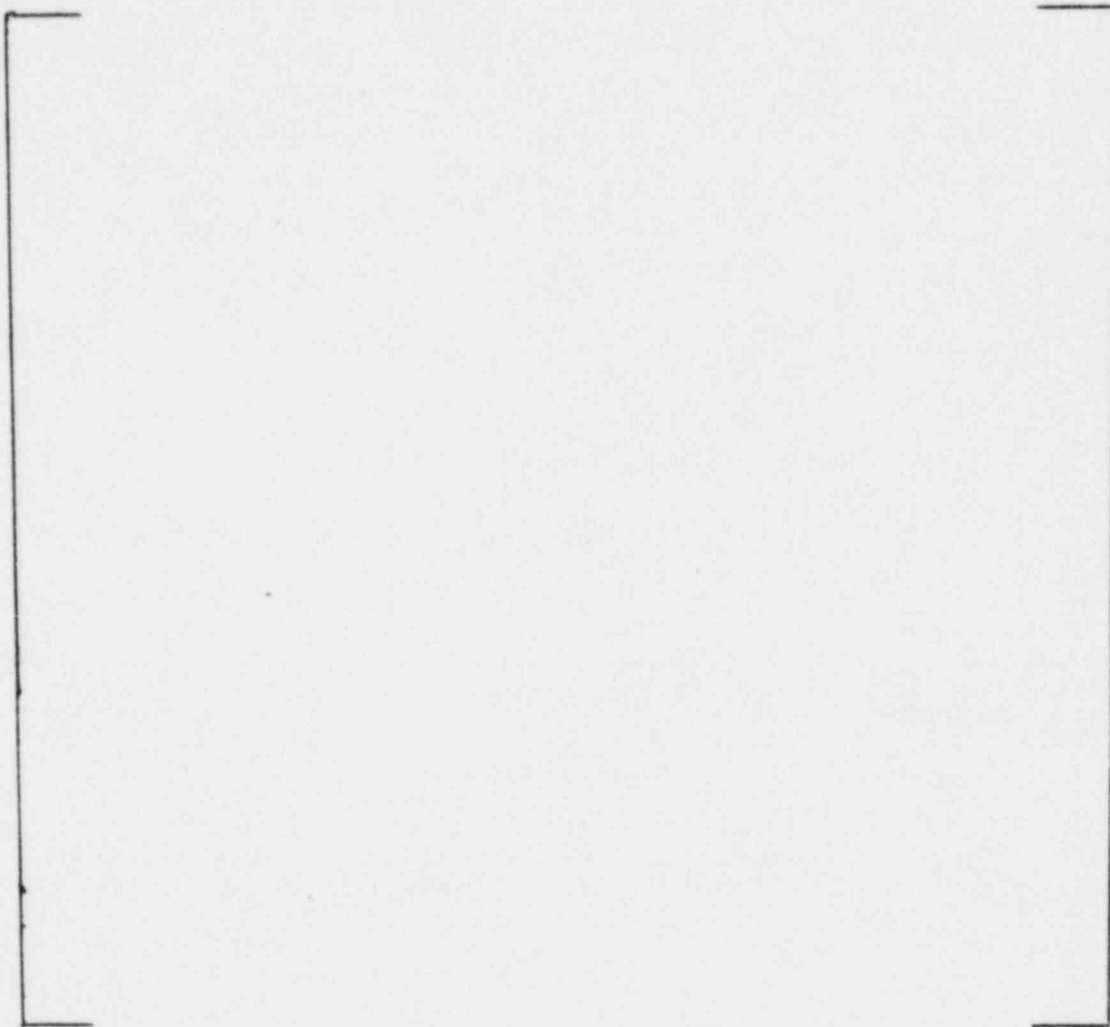
(a,c)

FIGURE 5-1   Finite Element Ring Approximation
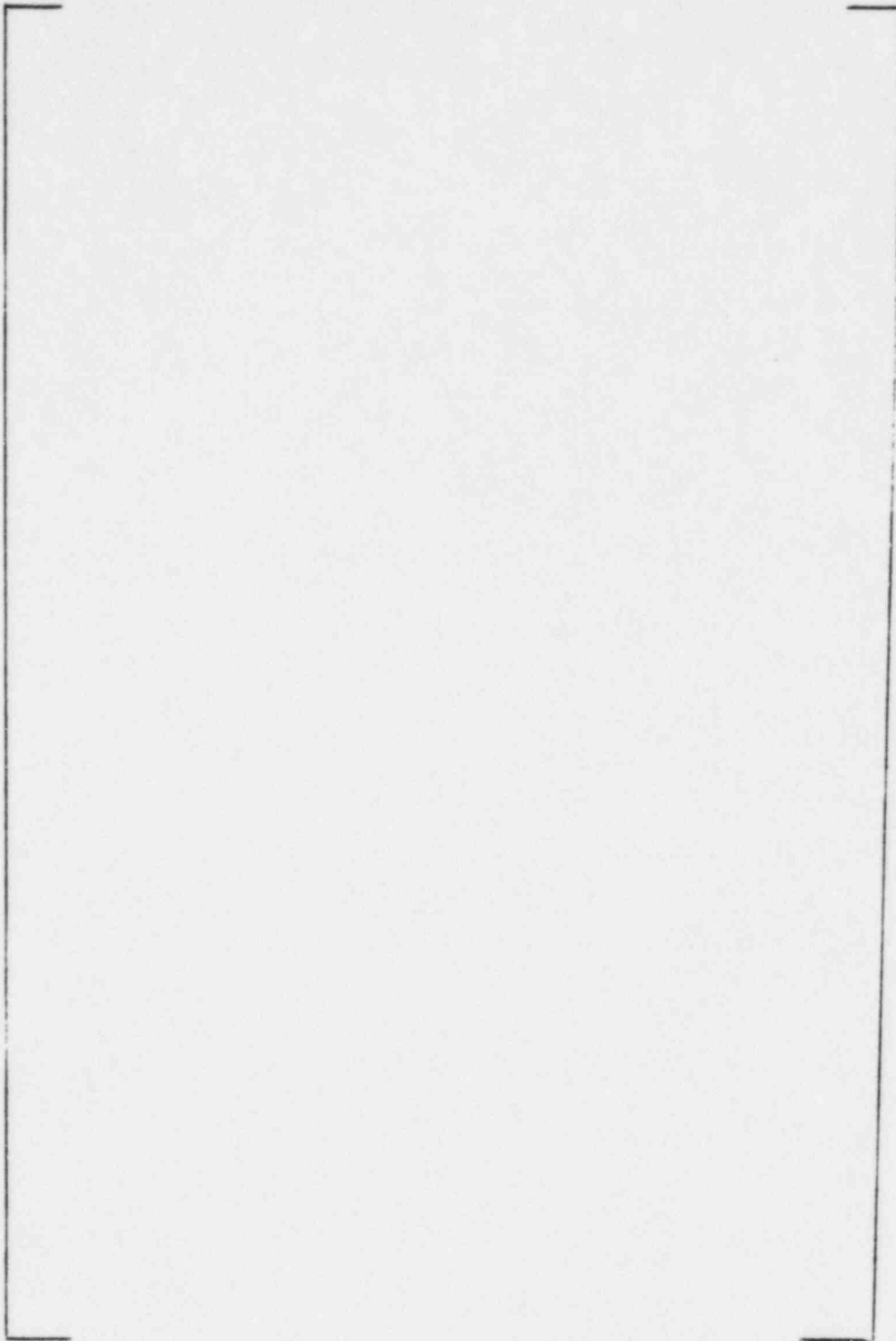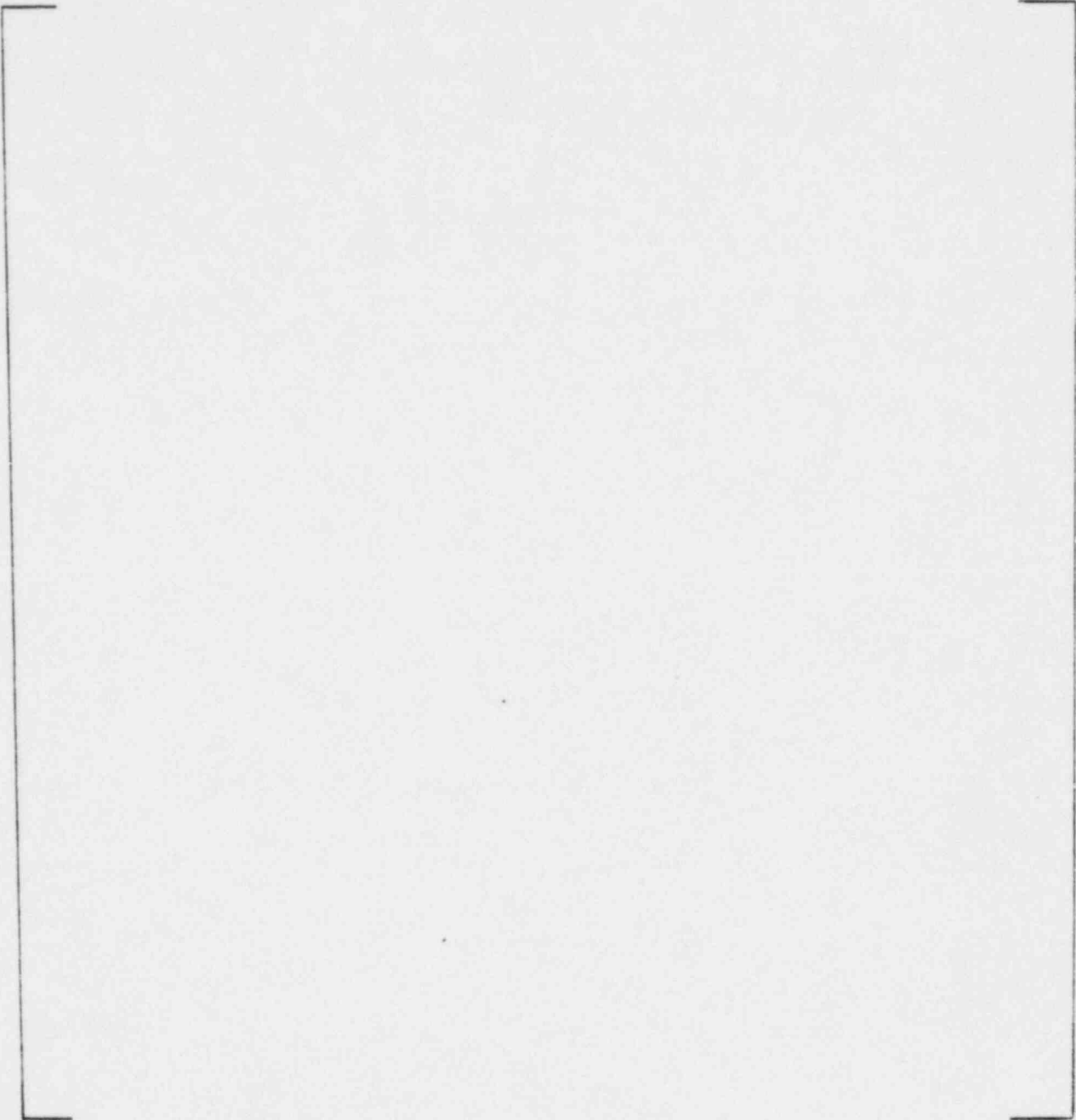Of The Core Barrel Flange

FIGURE 5-2   Core Barrel Flange   (a,c)
              Cross-Section And Simulated Simply
              Supported Boundary Conditions

5-5

(a,c)

FIGURE 5-3   Finite Element Barrel
Shell & Flange Representation
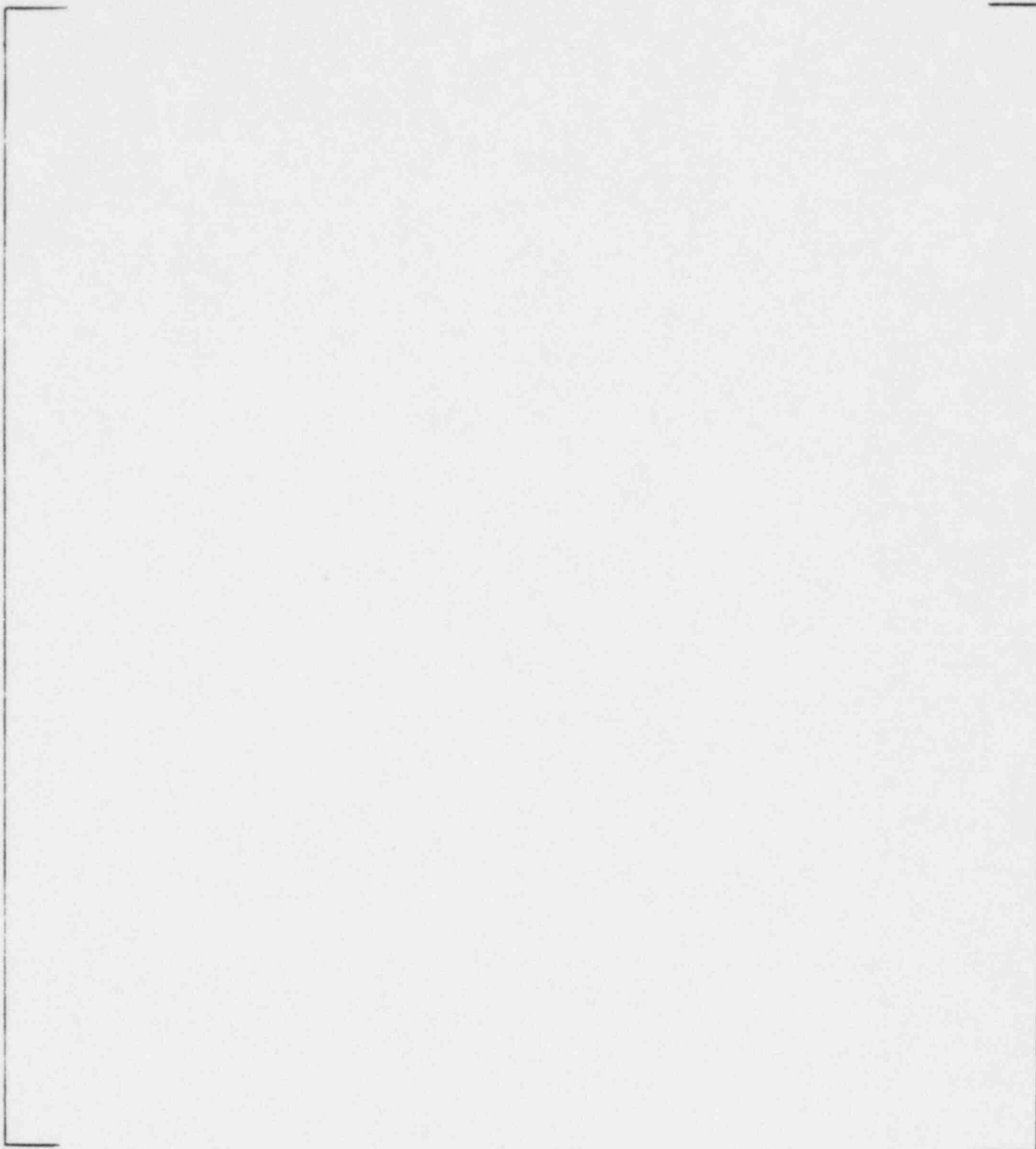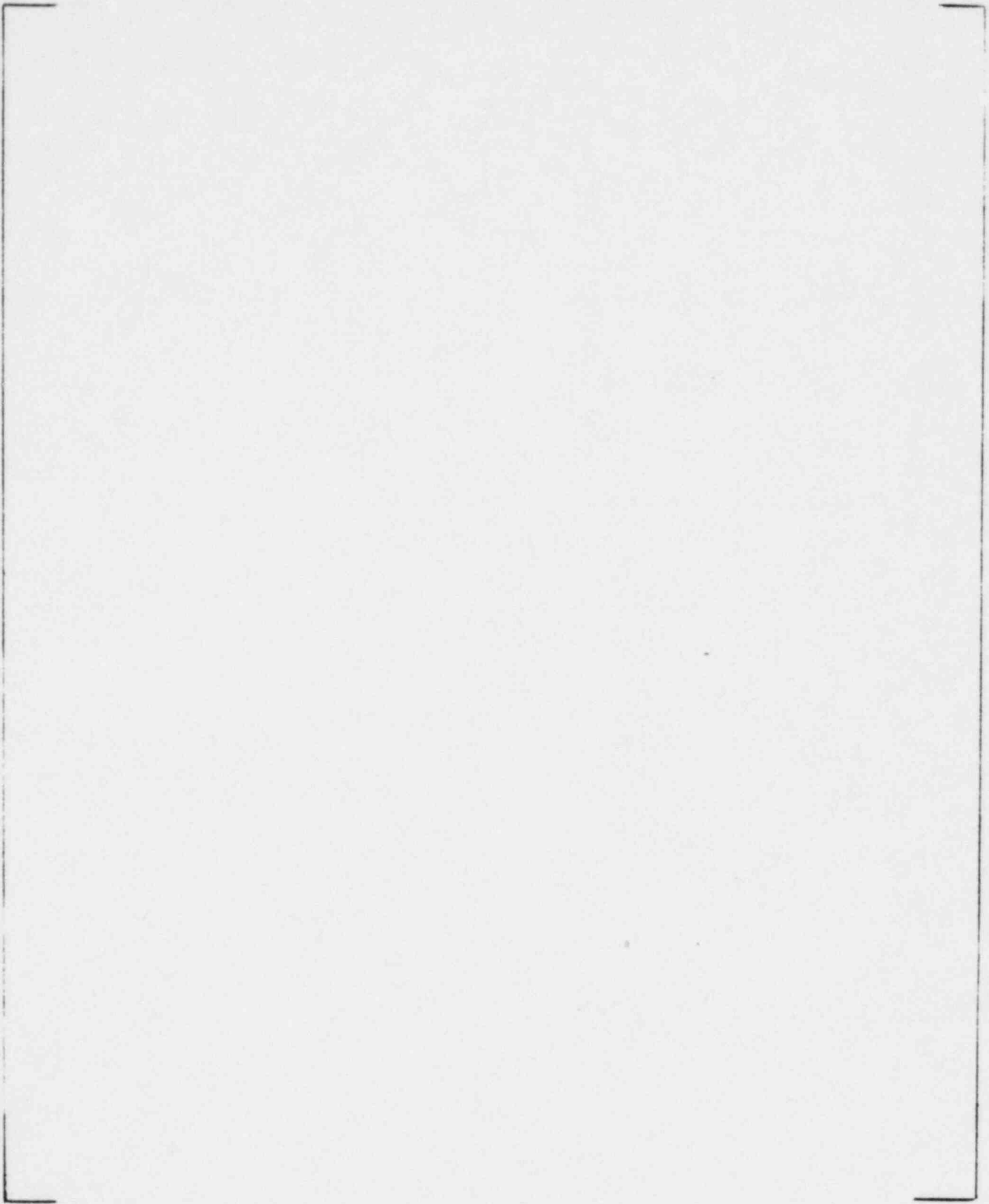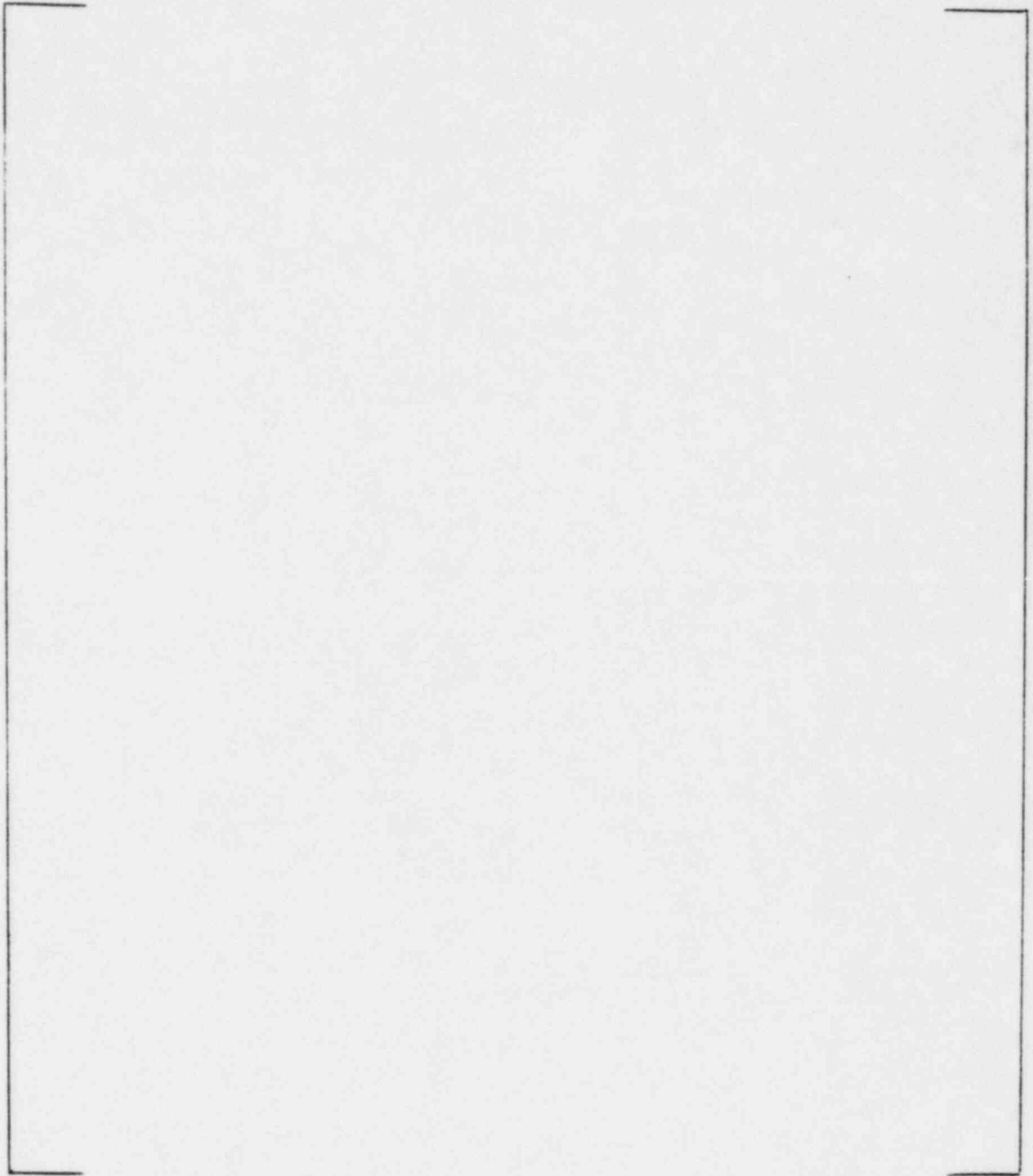
5-6

FIGURE 5-4   Top View Of Barrel Flange &
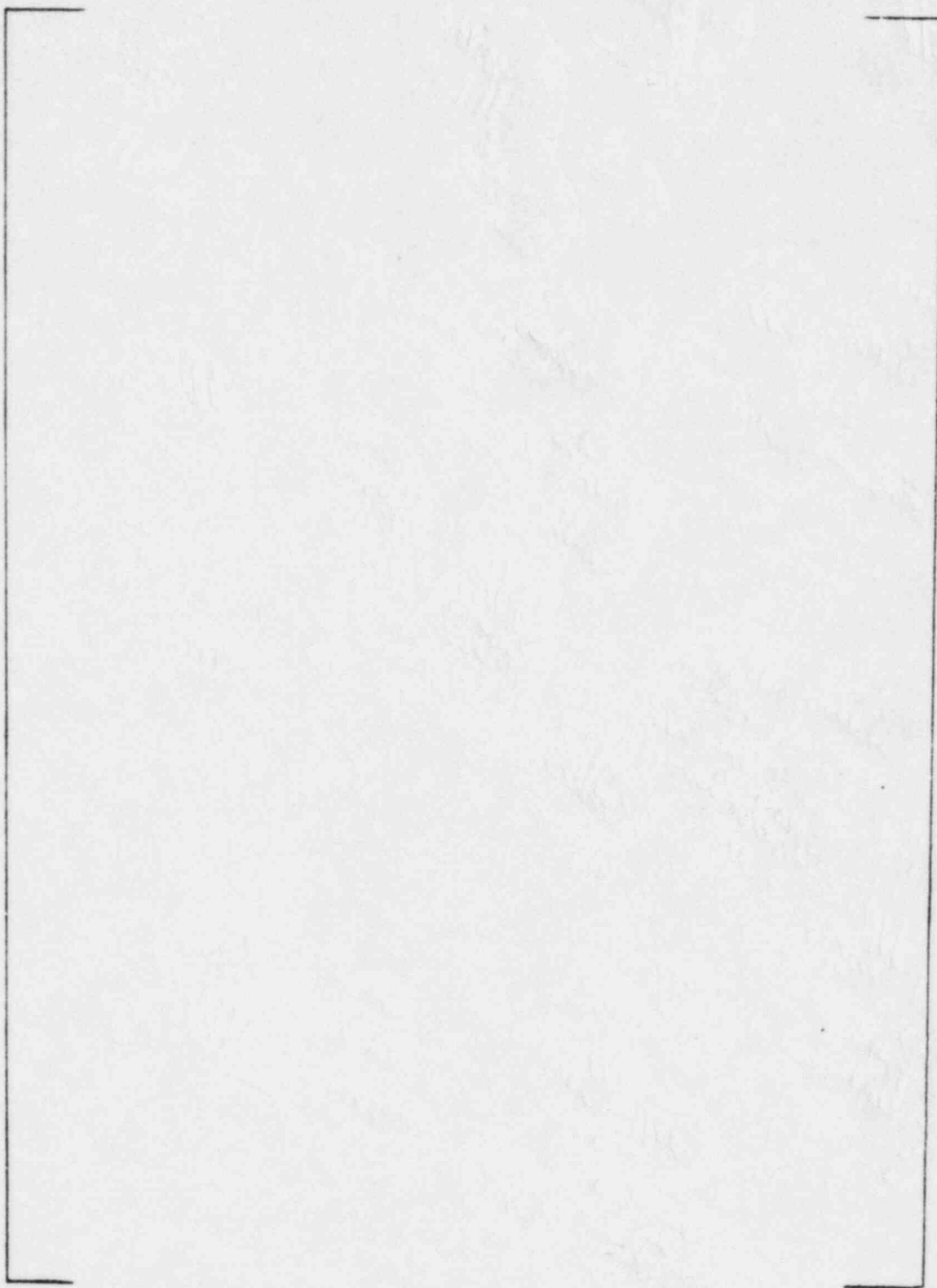   Vessel With Non-Linear
              Spring Elements

(a,c)

(a,c)

FIGURE 5-5   Deflected Shape Of The Barrel Flange

[   ]

(a,c)

Figure 5-6. 3-D Model of Vessel Support

Figure 5-7. 3D Beam Model of Vessel and Reactor Internals

(a,c)

6.0 APPLICATION TO THREE-LOOP THERMAL SHIELD PLANT

Sample analyses of a three-loop thermal shield plant are performed by the use of the advanced beam model. The methods are described in the previous Section 4.2 and the actual input data and analyses results are shown in this chapter. The input data are discussed in Section 6.1 and the results of computations are discussed in Section 6.2

6.1 Input Data

The advanced beam modeling of the hydraulic and structural systems and their interface are described in Section 4.2. The hydraulic model of the external loops and the barrel interior (the core region, the upper plenum and the upper head) is identical to the one shown in WCAP-8708[8]. The downcomer annulus is modeled by a half downcomer model the same as before but with the one-dimensional network equivalent to two-dimensional fluid structure interactions; see Figures 4-2 and 4-5. The method of network formation is discussed in Section 4.2 and the obtained input data are shown in Table 6-1.

The structural input data are computed by the use of the reduced modal analysis of a three-dimensional structural model; Figure 5-6 for the vessel support and Figure 5-7 for the reactor vessel internals. In order to carry out the modal analysis, linear stiffnesses $\bar{k}_\ell = 15 \times 10^6$ lb_f/in and $\bar{k}_\ell = 10 \times 10^6$ lb_f/in are chosen respectively for the top (between nodes 2 and 5) and bottom (between nodes 4 and 11) boundaries. The modal analysis is performed with the WECAN code, condensing all the dynamic degrees of freedom other than linear displacement along the x-axis and rotation around the z-axis.

The computed results stored on TAPE22 are input to RELMØDE code (see Appendix A) to obtain the relative mode shapes. Among them, important modes for fluid-structure interactions are selected to be input to MULTIFLEX code (see the flexible wall data in Table 6-1).

6.2 Results Of Computation And Barrel/Vessel Relative Displacements

After obtaining a steady state condition with the MULTIFLEX model, a LOCA transient is initiated by opening a break area 1 ft^2 in 1 ms at the RPV inlet nozzle inside the biological shield.

The computed pressure histories inside the pressure vessel are stored on TAPE1

which are then used to calculate the hydraulic forces by the use of the LATFØRC code, as discussed in Section 4.2.3.1. The hydraulic forces are applied to the WECAN dynamical model shown in Figures 5-6 and 5-7.

In order to verify MULTIFLEX non-linear advanced beam model, the barrel/vessel relative displacements computed by MULTIFLEX are compared with those of WECAN code, in Figures 6-1a-e. The MULTIFLEX results are shown by solid curves and the WECAN results by dotted curves. There is another case indicated by dashed curves which are computed by MULTIFLEX taking into account the sliding friction of the core barrel flange on the vessel flange. The effect of such friction is impor- tant to upper barrel displacements but not so much to the lower part of the barrel. Is is also seen that the solid curves agree fairly well with the dotted curves, verifying that the MULTIFLEX non-linear model is consistent with the WECAN model.

6.3 Fuel Grid Loads And Vessel Support Loads

Since validity of the MULTIFLEX advanced beam model has been found to be satis- factory, a sensitivity study of some parameters is carried out. The sensitivity is evaluated by means of the maximum fuel grid impact load and the pressure vessel support load. To clarify the studied cases, the advanced beam model is tentatively defined to be comprised of 1) network downcomer model, 2) the realistic boundary conditions with impact damping, 3) the relative modal analysis for vessel motion, and 4) the sliding friction (0.1 Mlb_f) at the vessel/barrel flange. The external loads are not applied to the MULTIFLEX model, unless otherwise so stated.

Cases A-E are calculated by the standard design procedure: The hydraulic force computed by MULTIFLEX is applied to the WECAN structural model which computes the time histories of upper and lower core plate displacements and of the barrel dis- placement at the level of the upper core plate. These displacements are used as input to the WEGAP code.[18] At the same time, WECAN computation yields the maximum vessel support loads which is proportional to the maximum vessel support displace- ment. The grid impact force for the above cases is also shown in Table 6-2.

Case A is the conventional MULTIFLEX computation with closed gap model, discussed in Reference 8. Cases B and D are the advanced beam model, respectively, with and without the external loads applied to the WECAN dynamic model. In cases C and E, the fluid-structure interaction is represented by the Fritz formula for hydrodynamic mass matrix but the virtual mass term is adjusted to fit MULTIFLEX structural deformation. Such mass matrices (Fitted Mass) are added to

the 3-D structural model in Figures 5-6 and 5-7, which is subjected to rigid wall hydraulic forces generated by rigid wall MULTIFLEX (or BLØDWN-2A). Cases C and E are calculated with and without external loads, respectively.

From the computed data of the above cases, the following conclusions are reached regarding the vessel support loads:

(a,c)

The conclusions about the maximum fuel grid loads are as follows:

(a,c)

4. The Fitted mass method also underestimates the grid loads compared to the advanced beam model (B vs. C and D vs. E).

(a,c)

TABLE 6-1   Input Data For A Three-Loop Thermal Shield Plant

(a,c)

TABLE 6-1 (Continued)

(a,c)

TABLE 6-1 (Continued)

6-6

$\rfloor$(a,c)

TABLE 6-1 (Continued)

$\rule{0.3cm}{0.3pt}$ (a,c)

TABLE 6-1 (Continued)

6-8

$\rfloor^{(i,c)}$

TABLE 6-1 (Continued)

6- 9

(a,c)

TABLE 6-1 (Continued)

(a,c)

TABLE 6-1 (Continued)

6- 11

$\overline{(a,c)}$

TABLE 6-1 (Continued)

(a,c)

TABLE 6-1 (Continued)

(a,c)

TABLE 6-1 (Continued)

6-14

$$\left[\right]^{(a,c)}$$
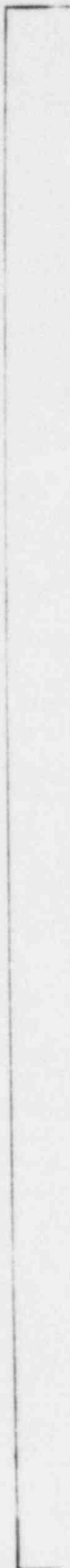
TABLE 6-1 (Continued)

WALL DISPLACEMENT (INCHES)
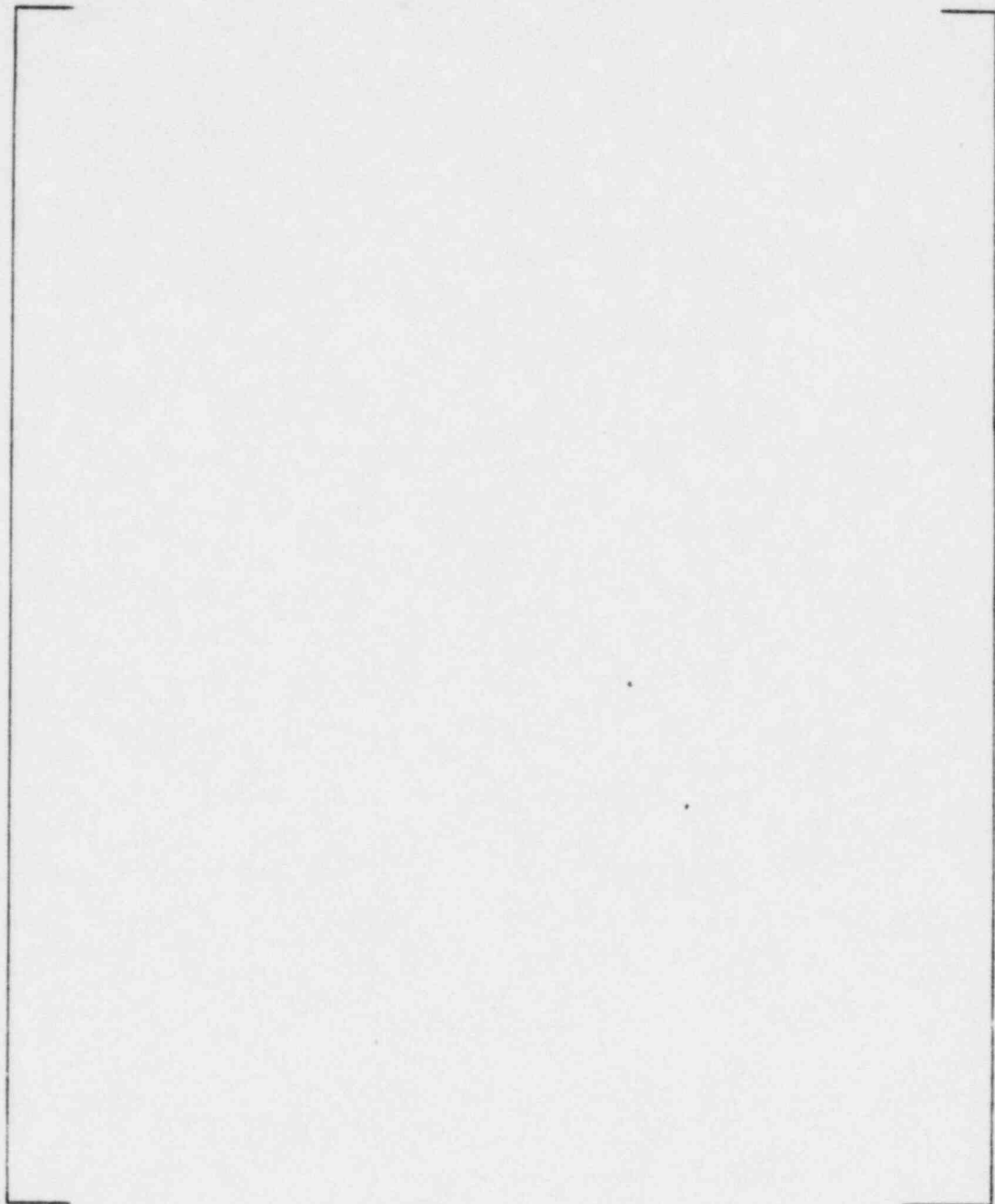
TIME (SECONDS)   (a,c)

FIGURE 6-1a Barrel/Vessel Relative Displacements At
            The Top Level

WALL DISPLACEMENT (INCHES)
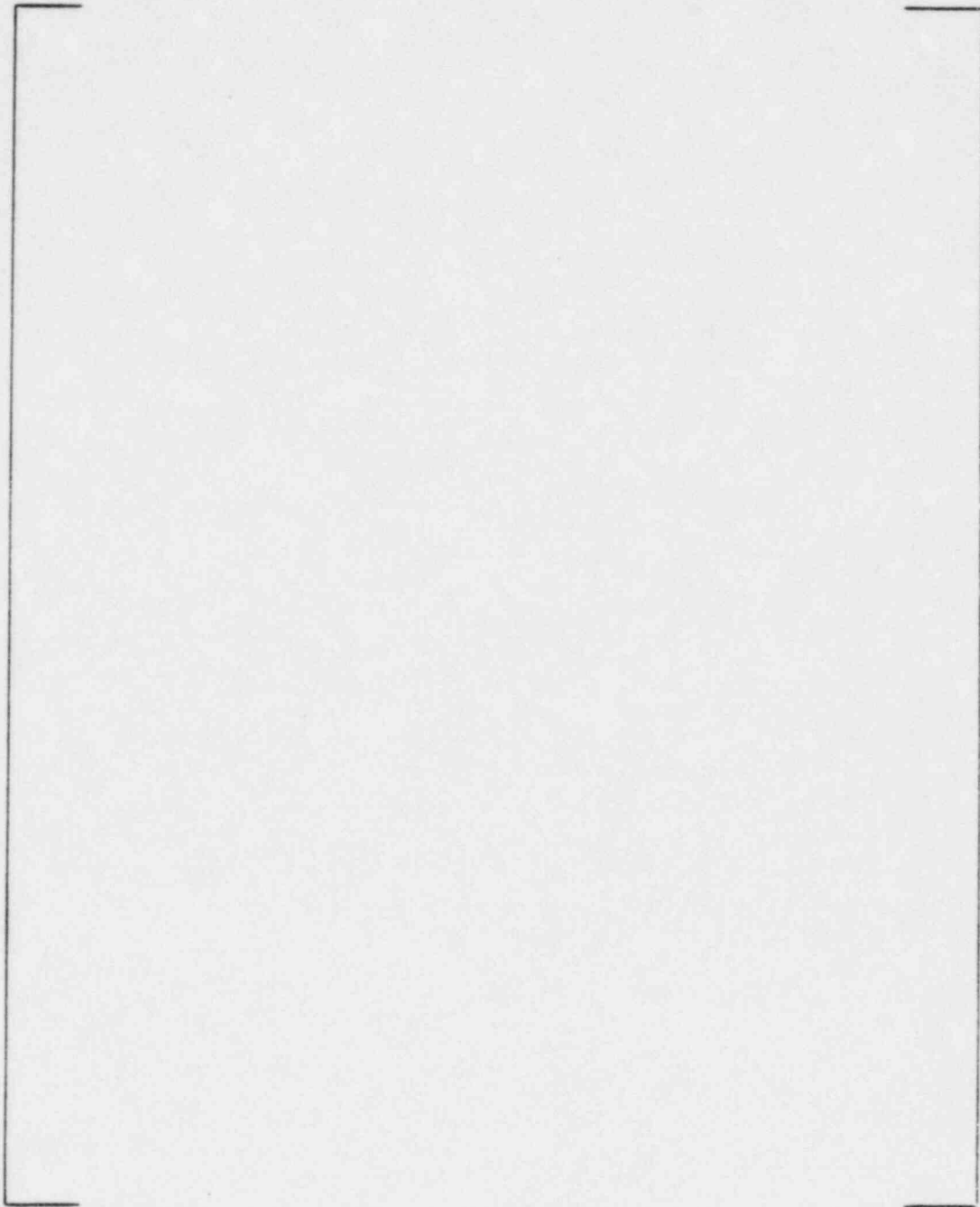
TIME (SECONDS)

(a,c)

FIGURE 6-1b Barrel/Vessel Relative Displacements At The
Inlet Nozzle Elevation

WALL DISPLACEMENT (INCHES)
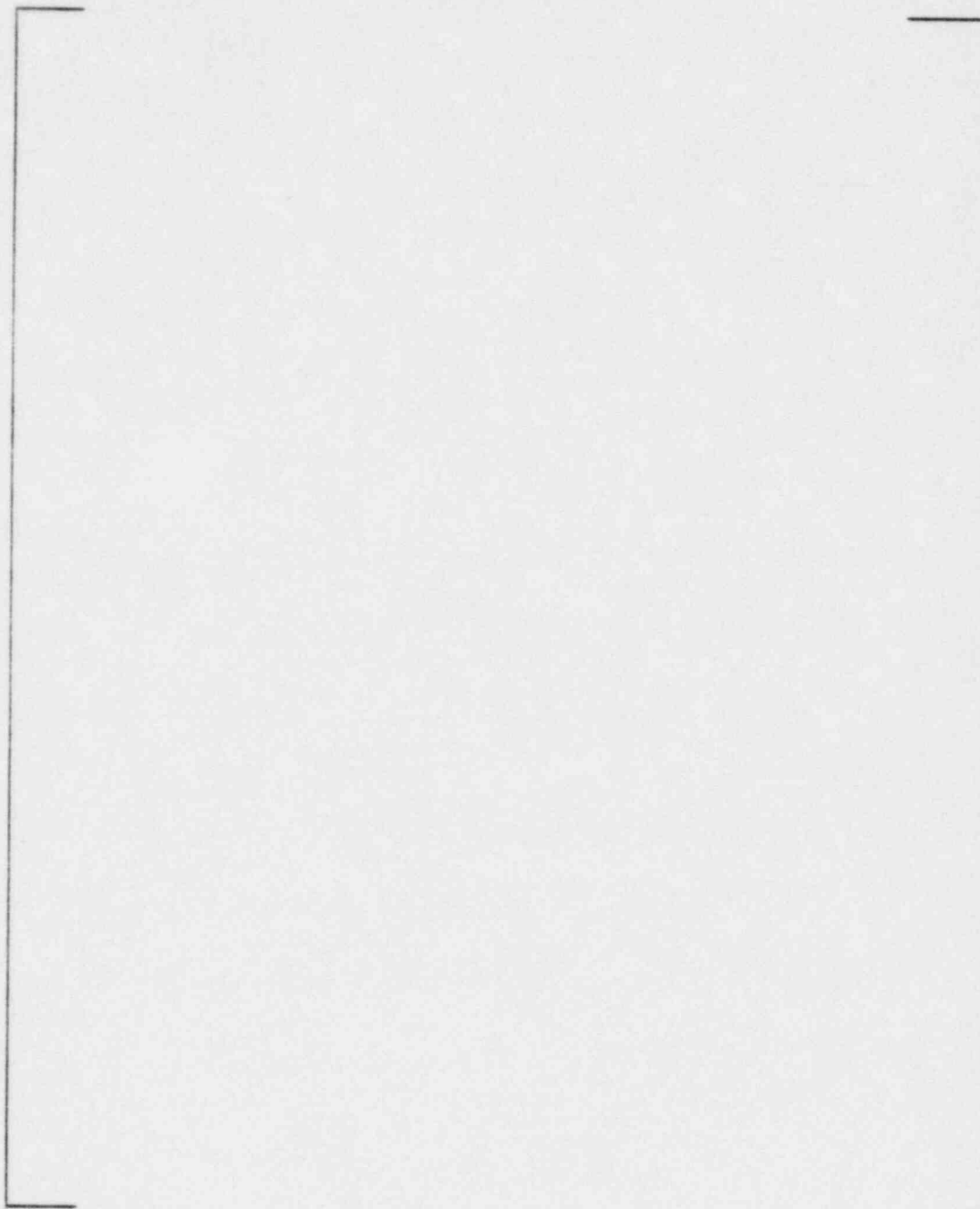
TIME (SECONDS)

(a,c)

FIGURE 6-1c   Thermal Shield/Vessel Relative Displacements
At The T.S. Top Elevation

WALL DISPLACEMENT (INCHES)

TIME (SECONDS)

(a,c)
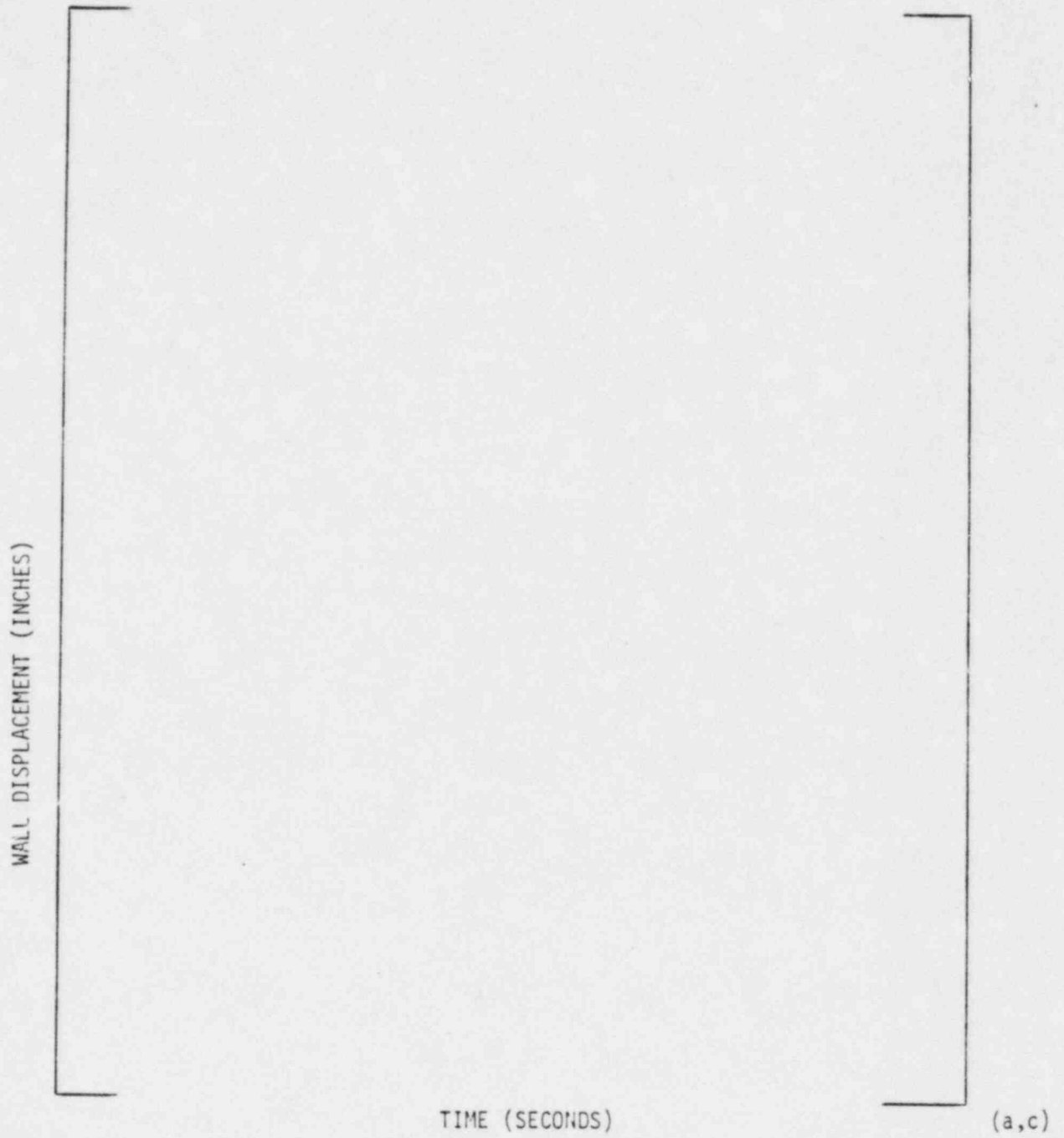
FIGURE 6-1d   Thermal Shield/Vessel Relative Displacements
At The T.S. Middle Elevation

6 - 19

WALL DISPLACEMENT (INCHES)

TIME (SECONDS)

(a,c)
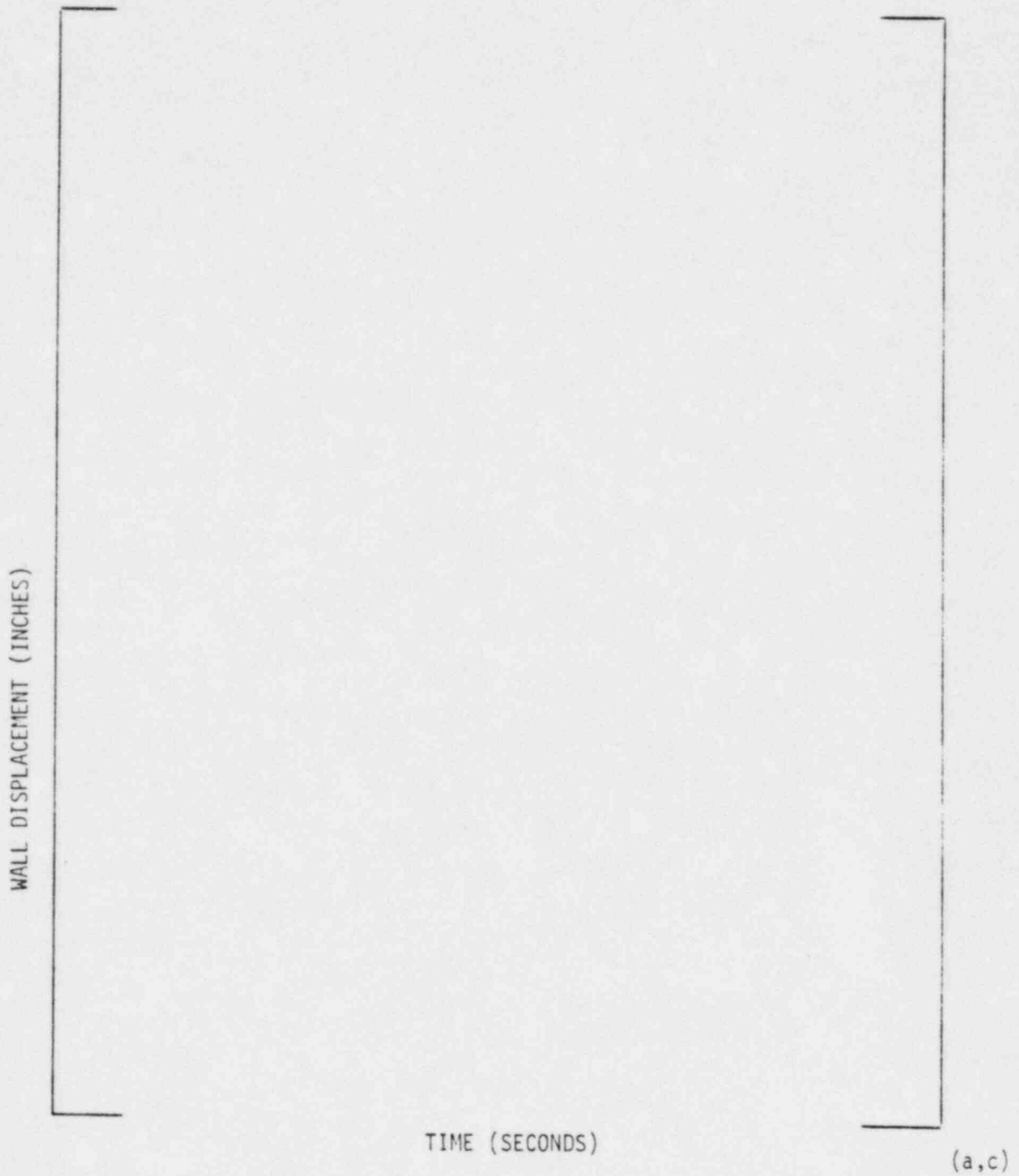
FIGURE 6-1e Thermal Shield/Vessel Relative Displacements
At The T.S. Bottom Elevation

6 - 20

TABLE 6-2
SENSITIVITY STUDY ON MAXIMUM GRID
IMPACT LOADS AND VESSEL SUPPORT LOADS

CASES		DESCRIPTION	MAXIMUM GRID LOAD (lb_f) (Sec.)		VESSEL SUPPORT DISPLACEMENT (in.)
MFX → WECAN → WEGAP	A	Conventional MFX External Loads (WECAN)			
	B	Advanced Beam External Loads (WECAN)			
	C	Fitted Mass External Loads (WECAN)			
	D	Advanced Beam W/O External Loads			
	E	Fitted Mass W/O External Loads			

(a,c)

Advanced Beam = (1) Network DC
                 (2) Realistic BC With Realistic Impact Damping
                 (3) Vessel Motion (Rel. Modal)
                 (4) Sliding Friction Loss (0.1 Mlb_f)

6 - 21

7.0 APPLICATION TO THREE LOOP PLANT WITH NEUTRON PADS

As a further example of code application, the analyses of the RPV internals hydraulic forcing functions (h.f.f.), resulting from a postulated loss-of-coolant accident (LOCA) in a PWR primary coolant loop, will be illustrated for the case of a three-loop plant with neutron pads. The pipe break considered in this example is a limited-displacement guillotine rupture, located at the safe end of the RPV inlet nozzle. An instantaneous (one millisecond) break opening time has also been assumed.

Section 7.1 provides a description of the hydraulic/structural models for the above three-loop plant, and also gives a listing of the corresponding MULTIFLEX computer program input data. Typical three-loop plant results obtained from a hydraulic force calculation are presented in Section 7.2.

7.1 Description Of Model And Input Data

Figures 7-1 through 7-5 illustrate the MULTIFLEX equivalent piping network representation of the complete primary reactor coolant system for a three-loop plant with neutron pads. The external loop containing the RPV inlet nozzle break is shown in Figure 7-1. The unbroken external loop is portrayed in Figure 7-2, and it represents the combination of the two intact coolant loops. In all plant applications (2-, 3-, and 4-loop plants), the broken and unbroken external coolant loops are represented by a sequence of one-dimensional hydraulic legs, connected end-to-end.

The downcomer annulus region is the volume of fluid between the inside surface of the pressure vessel and the outside surface of the core support barrel. For a three-loop plant with neutron pads, the downcomer region is annular in shape to a certain extent. However, due to the asymmetrical placement of the neutron pads in the annulus region, a vertical center plane of symmetry cannot be drawn, as was done for the case of the three-loop plant with thermal shield. Therefore, it is necessary to represent the entire downcomer annulus region with a hydraulic piping model. Figure 7-3 depicts a "full-downcomer" model developed or straightened into a plane, and represented by a network of equivalent flowpaths. This can be compared with the "half-downcomer" model in Figure 4-2, which represents the annulus region of a three-loop plant with thermal shield.

The hydraulic piping representation of the RPV internals region is shown in Figure 7-4. The hydraulic piping model of the internals region for all types of plants

7-1

is very similar. In all plant applications, the flow paths representing the down-comer annulus/lower plenum interface region join together at a common junction; also, the fluid volume inside the core barrel from the lower support plate to the upper plenum region is modelled by a series of hydraulic legs.

The barrel-baffle region is the volume of fluid between the inside surface of the core support barrel and the outside surface of the core baffle plates. For a three-loop plant with thermal shield, steady-state flow in this region is in the downward direction; flow enters the barrel-baffle region through holes in the core barrel located at an elevation slightly below the upper core plate, and exits this region through a gap between the bottom surface of the baffle plates and the top surface of the lower core plate. The orientation of the steady-state flow in this region for a three-loop plant with neutron pads is in the upward direction; flow enters the barrel-baffle region through a gap between the bottom surface of the baffle plates and the top surface of the lower core plate, and exits this region through a gap between the top surface of the baffle plates and the bottom surface of the upper core plate. By comparing Figure 7-5 with Figure 5-5 (in Reference 8), it is evident that for both types of three-loop plants, regardless of the direction of steady-state flow, the barrel-baffle region is represented by a sequence of one-dimensional hydraulic legs.

Note that in going from the original to the advanced MULTIFLEX beam model, the only hydraulic piping model which had to be modified was that of the downcomer annulus region; the hydraulic models simulating other portions of the reactor coolant system remain unchanged.

For a three-loop plant with neutron pads, the structural surfaces interfacing with the fluid in the downcomer annulus region are the outer surface of the neutron pads and core barrel, and the inner surface of the reactor vessel. The fluid-structure interface is modelled consistently with the network downcomer model. Figure 7-6 shows the interface modeling between the flexible walls and hydraulic piping network for a three-loop plant with neutron pads. This can be compared with Figure 4-5, which represents the interface modeling for a three-loop plant with thermal shield.

Table 7-1 provides a detailed description of the MULTIFLEX program input data, which was utilized to perform this sample problem. In order to prepare this hydraulic and structural data, the standard techniques and nodalization rules des-

cribed in the input data instructions (see Section 4.0) were observed.

7.2 Presentation And Discussion Of Computed Results

This section presents typical three-loop plant results obtained from a design-basis hydraulic force calculation. As noted earlier, the pipe break considered in this sample problem is a limited-displacement guillotine rupture, located at the safe-end of the RPV inlet nozzle.

Figures 7-7 through 7-9 show time-history plots of the average pressure differential applied across the 3rd, 5th, and 7th level mass points in the MULTIFLEX structural model. The core barrel is represented by a ten mass points beam model; as previously demonstrated in Figure 7-6, the application of the MULTIFLEX code to a three-loop plant with neutron pads requires that each mass point be composed of four individual flexible walls. As can be seen from the figures, a relatively large pressure differential is attained early in the blowdown transient. This corresponds to the initial propagation of the depressurization wave into the downcomer annulus region. After this initial pressure pulse, the rarefaction wave travels axially and circumferentially throughout the downcomer region, and at the same time, the fluid in the annulus region is interacting with the core barrel/reactor vessel structures; these phenomena result in a rapid and significant attenuation of the applied pressure differentials.

Figures 7-10 through 7-12 present time-history plots of the MULTIFLEX-computed displacement of the core barrel relative to the reactor vessel at the 3rd, 5th, and 7th level mass points. As expected, at all three elevations, the mass points move towards the RPV inlet nozzle of the broken loop (negative direction).

As the depressurization waves propagate axially (a,c) and circumferentially throughout the downcomer annulus region, the magnitude and direction of the pressure differentials applied across the flexible walls are constantly changing; this produces the well-behaved, oscillatory motion exhibited by the displacement curves. Examination of the MULTIFLEX-predicted displacement time histories, at all three mass point levels, indicates that the core barrel structure is responding at a frequency of approximately [   ] Hz.

(a,c)

For a pipe rupture in the cold leg of the system, the depressurization wave enters the reactor vessel through the inlet nozzle of the broken loop, and propagates in all directions throughout the downcomer annulus region. This produces an asymmetrical pressure distribution in the annulus region which results in a net hori-

zontal thrust on the vessel wall and core barrel. Figure 7-13 provides a typical total horizontal forcing function on the vessel wall for a three-loop plant with neutron pads. A maximum horizontal thrust of about [   ] is attained very early in the accident transient, t ∿ 13 milliseconds; after this peak vessel load is experienced, the hydraulic force undergoes both a rapid and significant attenuation. Examination of the force time-history reveals that the major forcing function frequency is approximately equal to 14 Hz.

(a,c)

TABLE 7-1 LIST OF INPUT DATA FOR MULTIFLEX COMPUTER

PROGRAM - 3 LOOP (NEUTRON PADS) PLANT
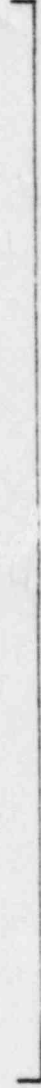
(a,c)

(a,c)

TABLE 7-1 (CONTINUED)

[

]

(a,c)

TABLE 7-1 (CONTINUED)

(a,c

TABLE 7-1 (CONTINUED)

TABLE 7-1 (CONTINUED)

[

]
(a,c)

TABLE 7-1 (CONTINUED)

[(a,c)

TABLE 7-1 (CONTINUED)

] (a,c)

7-11

(a,c)

TABLE 7-1 (CONTINUED)

7-12

(a,c)

TABLE 7-1 (CONTINUED)

(a,c)

TABLE 7-1 (CONTINUED)

[

]

(a,c)

TABLE 7-1 (CONTINUED)

7-15

$\rfloor$(a,c)

TABLE 7-1 (CONTINUED)

7-16

TABLE 7-1 (CONTINUED)

7-17

TABLE 7-1 (CONTINUED)   (a,c)

7-18

(a,c)

FIGURE 7-1 EQUIVALENT PIPING NETWORK REPRESENTATION OF 3 LOOP (NEUTRON
PADS) PLANT - BROKEN LOOP - RPV INLET NOZZLE BREAK

(a,c)

FIGURE 7-2 EQUIVALENT PIPING NETWORK REPRESENTATION OF

3 LOOP (NEUTRON PADS) PLANT - INTACT LOOP

(a,c)

FIGURE 7-3 EQUIVALENT PIPING NETWORK REPRESENTATION OF 3 LOOP (NEUTRON

PADS) PLANT - VESSEL DOWNCOMER ANNULUS REGION

(a,c)
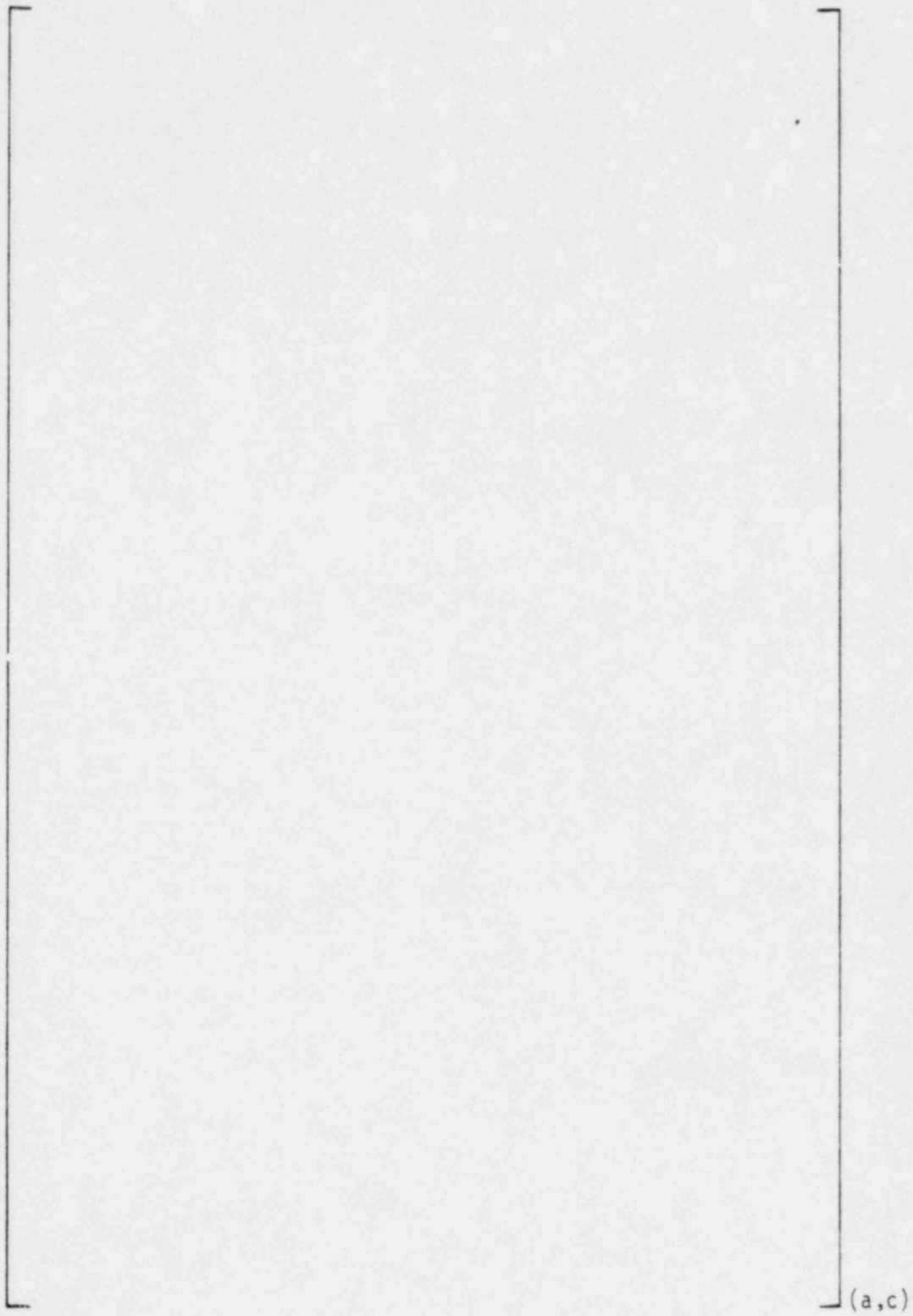
FIGURE 7-4 EQUIVALENT PIPING NETWORK REPRESENTATION OF 3 LOOP (NEUTRON

PADS) PLANT - REACTOR PRESSURE VESSEL INTERNALS REGION
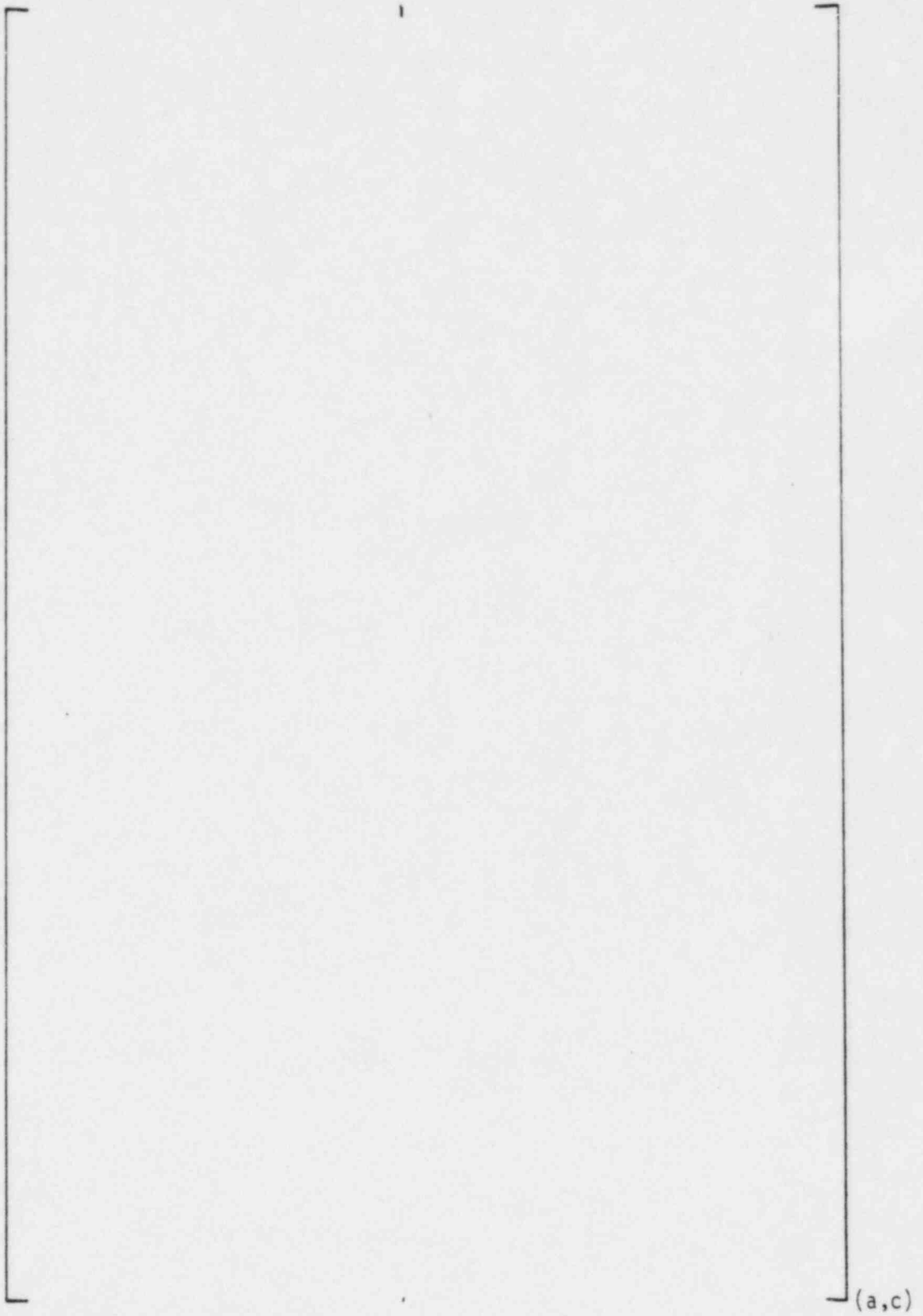
FIGURE 7-5 EQUIVALENT PIPING NETWORK REPRESENTATION OF 3 LOOP

(NEUTRON PADS) PLANT - BARREL/BAFFLE REGION - UPFLOW

(a,c)

FIGURE 7-6 INTERFACE MODELING BETWEEN FLEXIBLE WALLS AND HYDRAULIC

PIPING NETWORK - 3 LOOP (NEUTRON PADS) PLANT
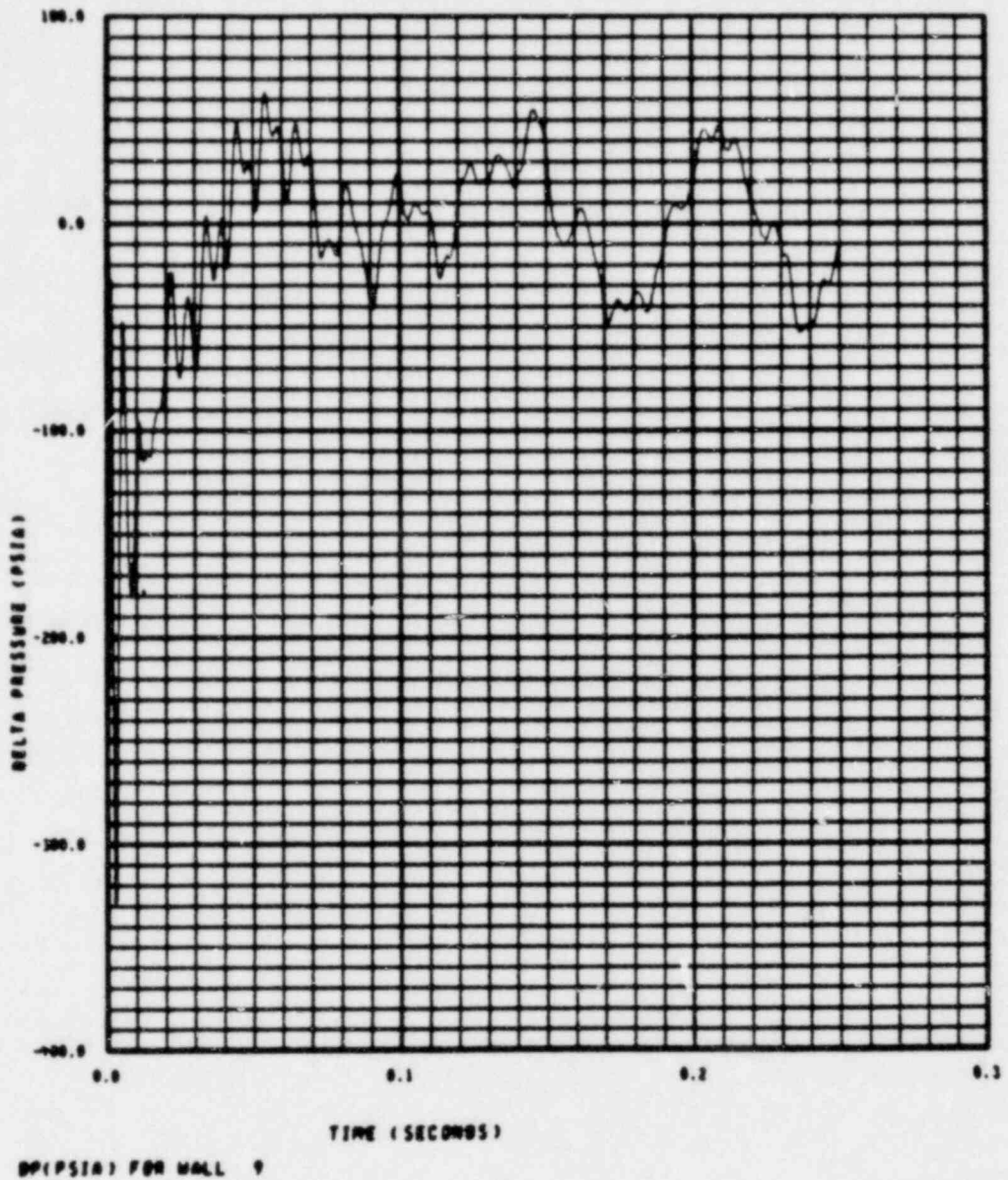
FIGURE 7-7 AVERAGE PRESSURE DIFFERENTIAL ACROSS 3RD LEVEL MASS POINT
(WALL NOS. 9-12) - 3 LOOP (NEUTRON PADS) PLANT
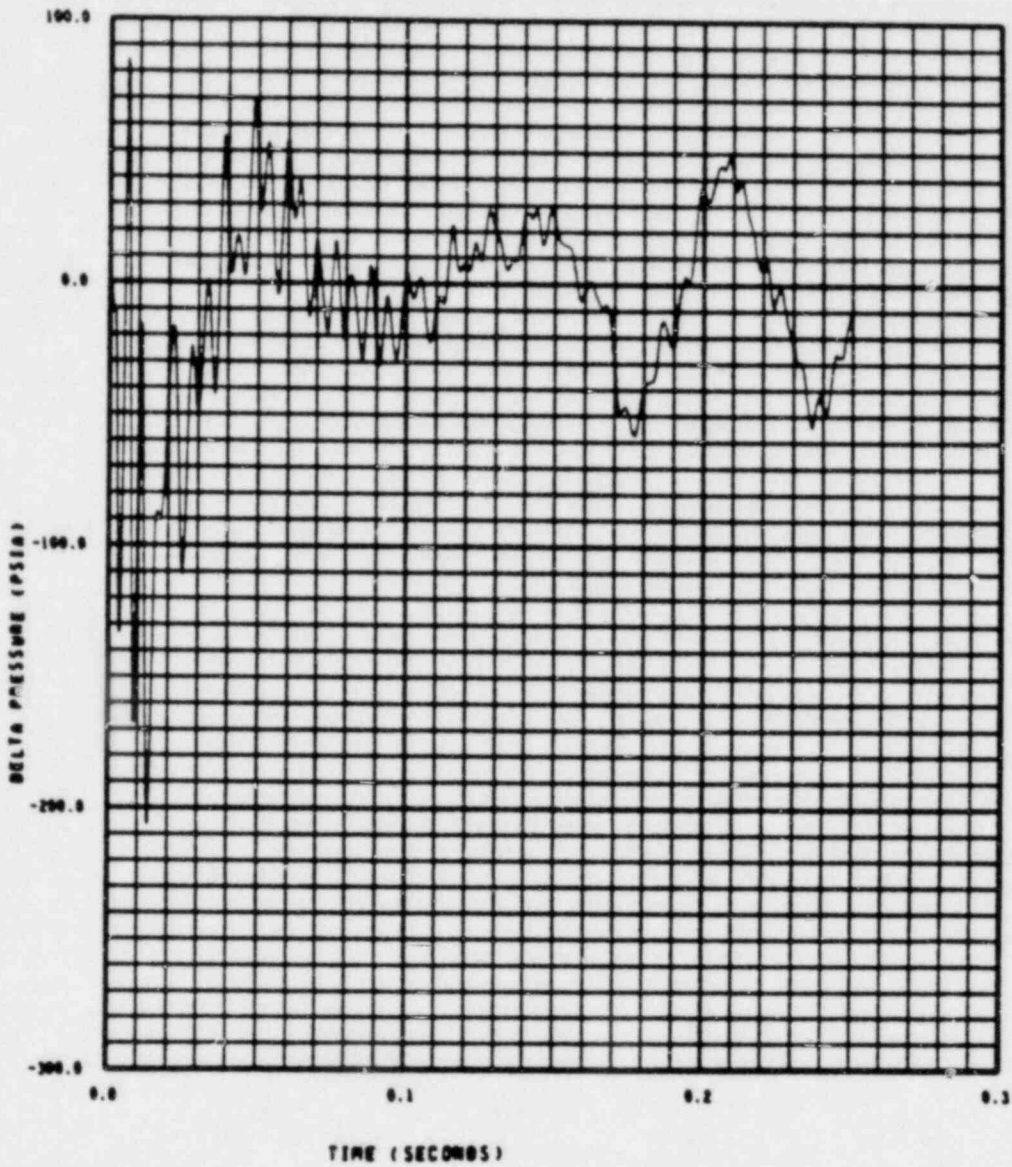
FIGURE 7-8 AVERAGE PRESSURE DIFFERENTIAL ACROSS 5TH LEVEL MASS POINT
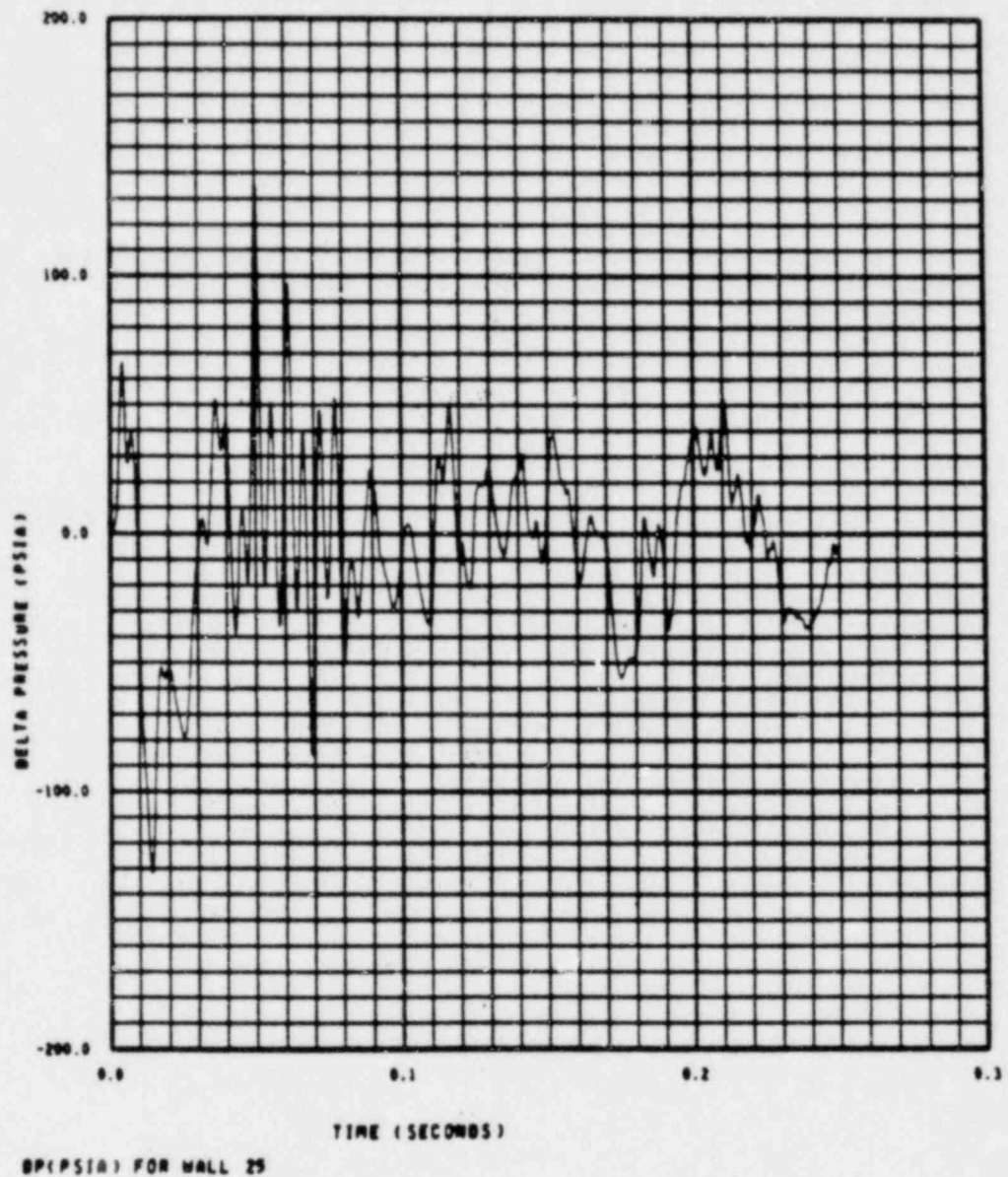(WALL NOS. 17-20) - 3 LOOP (NEUTRON PADS) PLANT

FIGURE 7-9 AVERAGE PRESSURE DIFFERENTIAL ACROSS 7TH LEVEL MASS POINT
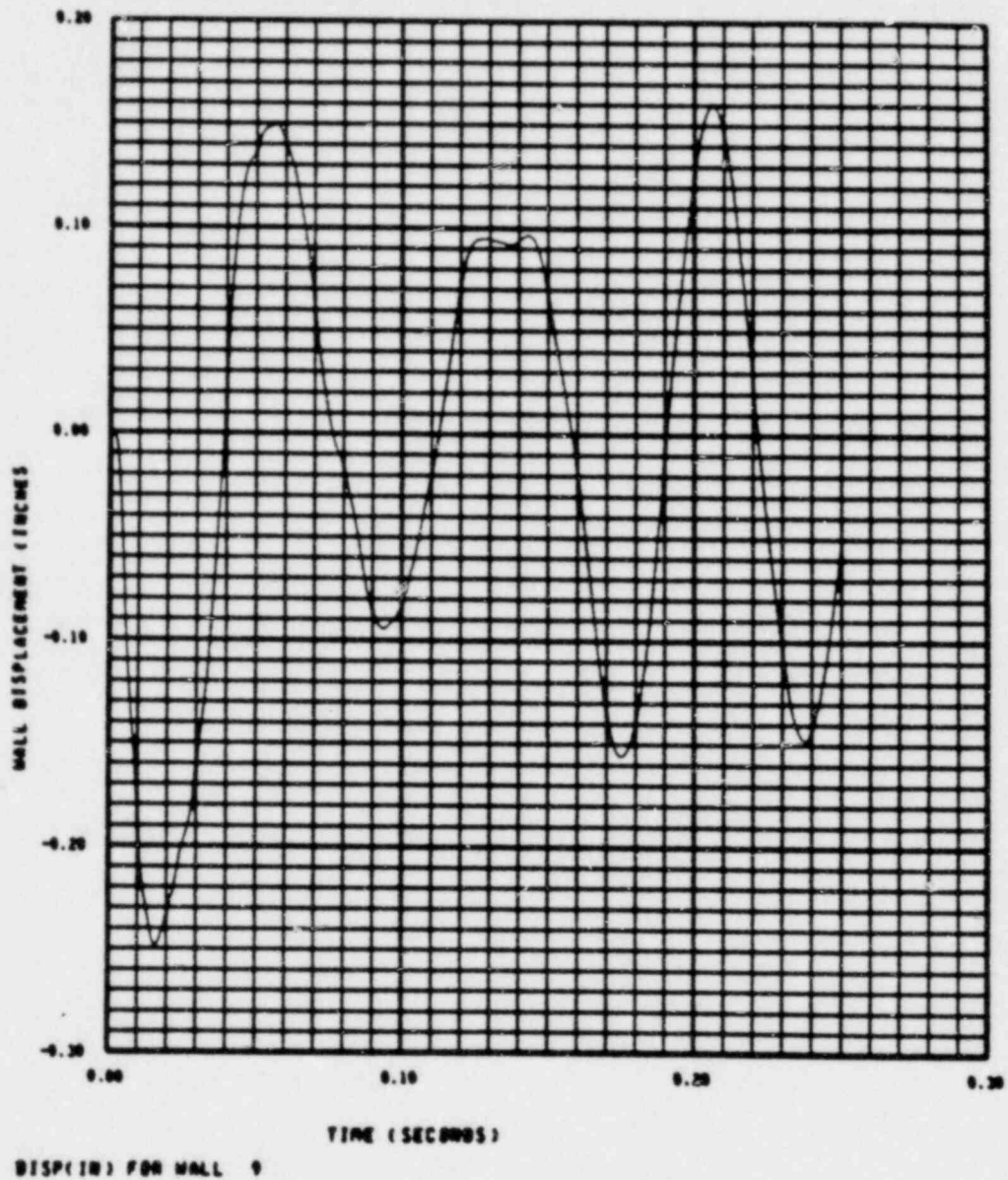(WALL NOS. 25-28) - 3 LOOP (NEUTRON PADS) PLANT

FIGURE 7-10 DISPLACEMENT OF CORE BARREL RELATIVE TO REACTOR VESSEL - 3RD LEVEL
MASS POINT (WALL NOS. 9-12) - 3 LOOP (NEUTRON PADS) PLANT
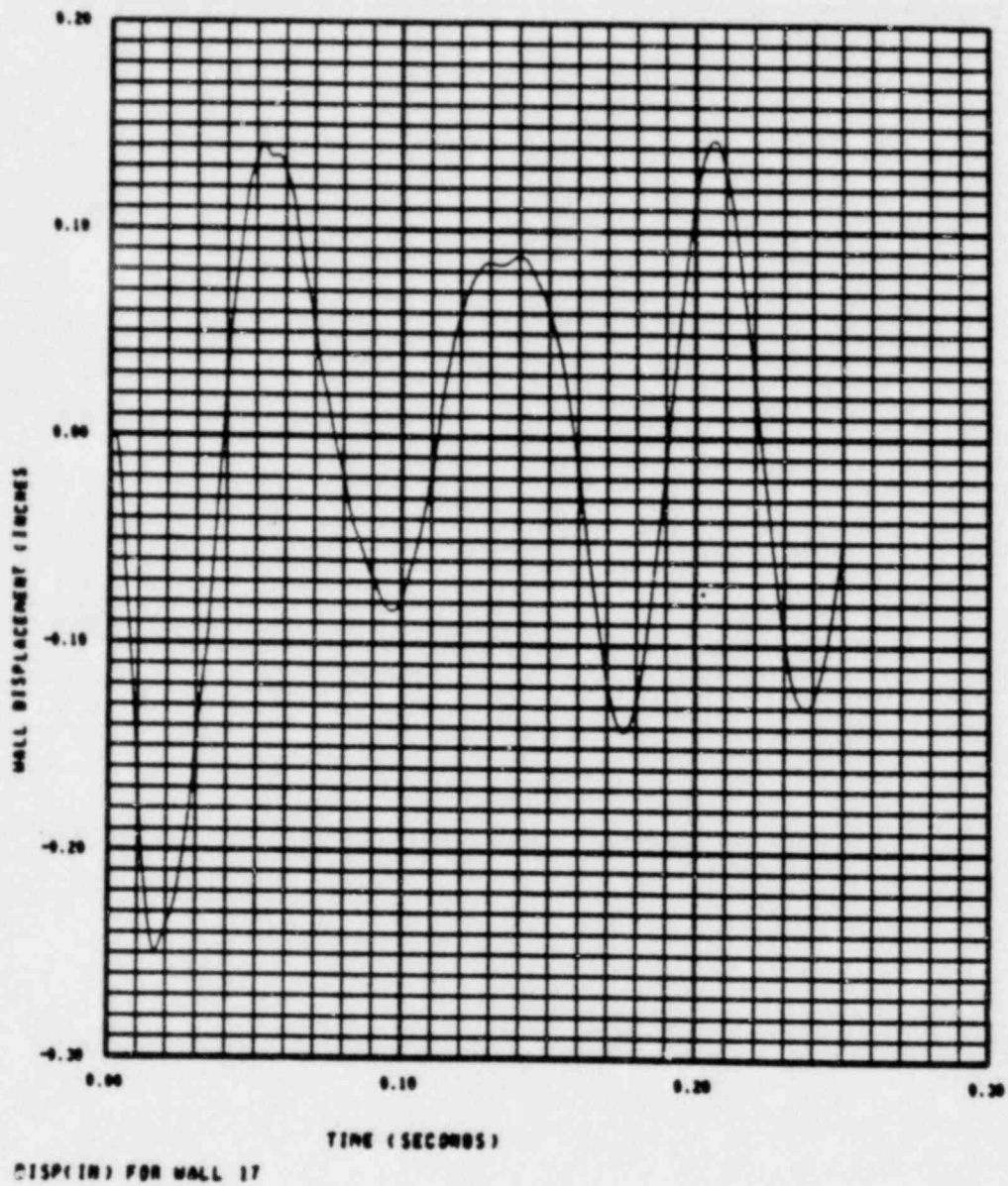
7-28

FIGURE 7-11 DISPLACEMENT OF CORE BARREL RELATIVE TO REACTOR VESSEL - 5TH LEVEL
MASS POINT (WALL NOS. 17-20) - 3 LOOP (NEUTRON PADS) PLANT
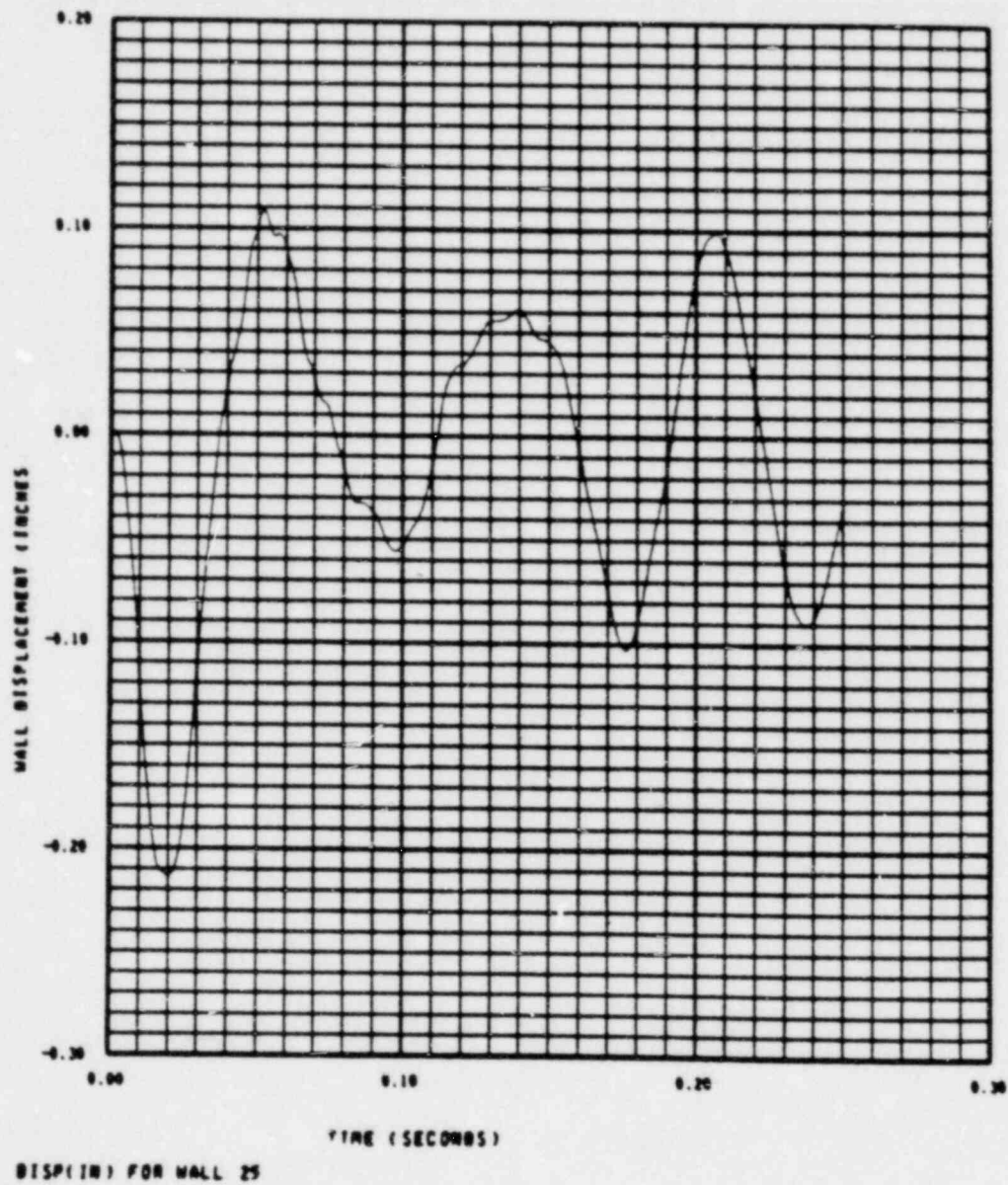
FIGURE 7-12 DISPLACEMENT OF CORE BARREL RELATIVE TO REACTOR VESSEL - 7TH LEVEL MASS POINT (WALL NOS. 25-28) - 3 LOOP (NEUTRON PADS) PLANT

(a,c)

FIGURE 7-13 TOTAL SPATIALLY-INTEGRATED HORIZONTAL FORCE ON VESSEL
WALL IN X-DIRECTION - 3 LOOP (NEUTRON PADS) PLANT

8.0 REFERENCES

1. Fabic, S., "Description of the BLØWDN-2 Computer Code", WCAP-7593 (1970).

2. Wallis, G. B., "One-Dimensional Two-Phase Flow", McGraw-Hill Book Company, Inc., New York (1969).

3. Landau, L. D., and Lifshitz, E. M., "Fluid Mechanics", Pergamon Press, London (1959).

4. Courant, R., and Hilbert, D., "Methods of Mathematical Physics", Vol. II, Interscience Publishers, New York (1962).

5. Takeuchi, K., "BLØWDN-3, A FORTRAN-IV Computer Program for Analyzing Short Term Transient Thermal-Hydraulic Systems", WCAP-8519 (1975).

6. Richtmyer, R. D., and Morton, K. W., "Difference Methods for Initial-Value Problems", Interscience Publishers, New York (1967).

7. Fabic, S., "Feedline Break Analysis for Model-D Steam Generator", WCAP-8158 (1973).

8. Takeuchi, K., Kowalski, D. J., Esposito, V. J., and Bordelon, F. M., "MULTIFLEX, A FORTRAN-IV Computer Program for Analyzing Thermal-Hydraulic-Structural System Dynamics", WCAP-8708 (1976).

9. Takeuchi, K., "Verification of MULTIFLEX --- Pressure Wave Propagation and Hydro-Structural Interaction", WCAP-8781 (1976).

10. Takeuchi, K., and Bhandari, D. R., "MULTIFLEX, A FORTRAN-IV Computer Program for Analyzing Thermal-Hydraulic-Structural System Dynamics (II) --- Shell Model And Projector Method", WCAP-8920 (1977).

11. Takeuchi, K., "Hydraulic Force Calculation with Hydro-Structural Interactions", Nuclear Technology 39 (1978) 155.

12. Kowalski, D. J., "MULTIFLEX Code (Beam Version) Sensitivity Studies", WCAP-8974 (1978).

REFERENCES (Continued)

13. Kuenzel, A. J., and Nahavandi, A. N., "Vertical and Transverse Vibration Of Reactor Internal Structures", WCAP-8134 (1973).

14. Takeuchi, K., "One-Dimensional Network for Multi-Dimensional Pressure Wave Propagation with Hydro-Structural Interactions", Trans. Am. Nucl. Soc. 30 (1978) 210.

15. Takeuchi, K., "One-Dimensional Network for Multi-Dimensional Fluid-Structural Interactions", Nucl. Sci. and Eng. 72 (1979) 322.

16. Takeuchi, K., and De Santo, D., "Shell Model In-Water Frequencies of the Core Barrel", ANS/ASME Conference (1980).

17. Takeuchi, K., "Intermediate Pseudo-Force Method for Non-Linear Boundaries", MD-THM-391 (1979).

18. Takeuchi, K., "Modal Analysis on a Relative Coordinate System", MD-THM-376 (1979).

19. Takeuchi, K., and Squarer, D., "Analysis of Experiments of Feedline Break in a 1:10 Steam Generator Preheater Scale Model", WCAP-9480 (1979).

20. Takeuchi, K., and Squarer, D., "Analysis of a Blowdown Experiment of 1/10 Scale Steam Generator Model", To Be Published in ASME PVP Conference (1980).

21. Kowalski, D., and Esposito, V. J., "Application of Fluid-Structure Interaction for Steam Generator Force Analysis," Nuclear Technology 46 (1979) 536.

22. Bogard, W. T., "Dynamic Analysis of Reactor Pressure Vessel for Postulated Loss-Of-Coolant Accidents: North Anna Units 1 and 2", WCAP-8748 (1976).

23. Advanced Engineering Analysis, "Generic Stress Report of Four Loop Standard Reactor Core Support Structures", WNEP-70702, Section 6.5, June (1977).

24. Takeuchi, K., "Dynamic Analysis of Hydraulic Pressure Wave Propagation in A Plastically Deforming Pipe", ANS tr. 26 (1977) 360.

REFERENCES (Continued)

25. Molnar, A. J., Vashi, K. M., and Gay, G. W., "Application of Normal Mode Theory and Pseudo-Force Methods to Solve Problems With Non-Linearities", J. of Pressure Vessel Tech. (1976) 151.

26. Shah, V. N., Bohm, G. J., and Nahavandi, A. N., "Modal Superposition Method for Computationally Economical Non-Linear Structural Analysis", J. of Pressure Vessel Tech. (1979) 134.

27. WECAN, Westinghouse Electric Computer Analysis User's Manual, Vols. 1 and 2 (1976).

28. Bohm, G. J., and Lafaille, J. L., "Reactor Internals Response Under a Blowdown Accident", Proceedings of the First International Conference on Structural Mechanics in Reactor Technology, Berlin, Germany (1971).

29. Bohm, G. J., and Nahavandi, A. N., "Dynamic Analysis of Reactor Internal Structures and Impact Between Components", Nucl. Sci. Eng. 47, 391 (1972).

30. Burnett, A. J., Takeuchi, K., "New Downcomer Model For MULTIFLEX", MD-THM-377 (1979).

31. Takeuchi, K., "Network Downcomer Model For Beam Analysis Of Operating Plants", MD-THM-404 (1979).

32. Bhandari, D., "Non-Linear Boundary Conditions", PE-PEA-69/80 (1980).

33. Bhandari, D., "Impact Damping For Non-Linear Boundary Conditions", PE-PEA-70/80 (1980).

34. Morrone, A., Nahavandi, A. N., Brussalis, W. G., "Scram And Non-Linear Reactor System Seismic Analysis For A Liquid Metal Fast Reactor", Nucl. Eng. And Design 38 (1976) 555.

35. Bhandari, D., "Sliding Friction Force For Non-Linear Boundary Condition", PE-PEA-71/80 (1980).

REFERENCES (Continued)

36. Roark, R. J., "Formulas For Stress And Strain", McGraw-Hill Book Company, N.Y.
    (1965).

37. "3 Loop (DRL) Generic Structural & Fatigue Analysis", WNEP 7801, Pensacola,
    Florida (March 1978).

38. "Westinghouse Owner's Group Asymmetric LOCA Loads Evaluation Phase C", WCAP-
    9748 (June 1980).

39. R. J. Fritz, "The Effects Of Liquids On The Dynamic Motion Of Immersed Solids",
    Trans. ASME, J. Eng. Industry (1972) 167.

40. V. L. Streeter and E. B. Wylie, "Hydraulic Transients", McGraw-Hill, N.Y.
    (1967).

APPENDIX A   RELMØDE

Program RELMØDE computes relative modal data for the advanced beam model. A
brief description and non-linear boundary data for the code usage is given in
this appendix. The code can be attached by the statement,

ATTACH(RELMØDE,RELMØDE).

The structural input data are computed by WECAN (2d or 3d) reduced modal analy-
ses and the results on TAPE22 are cataloged. These data are attached on TAPE22
to be input to RELMØDE. The RELMØDE results which are required for input to
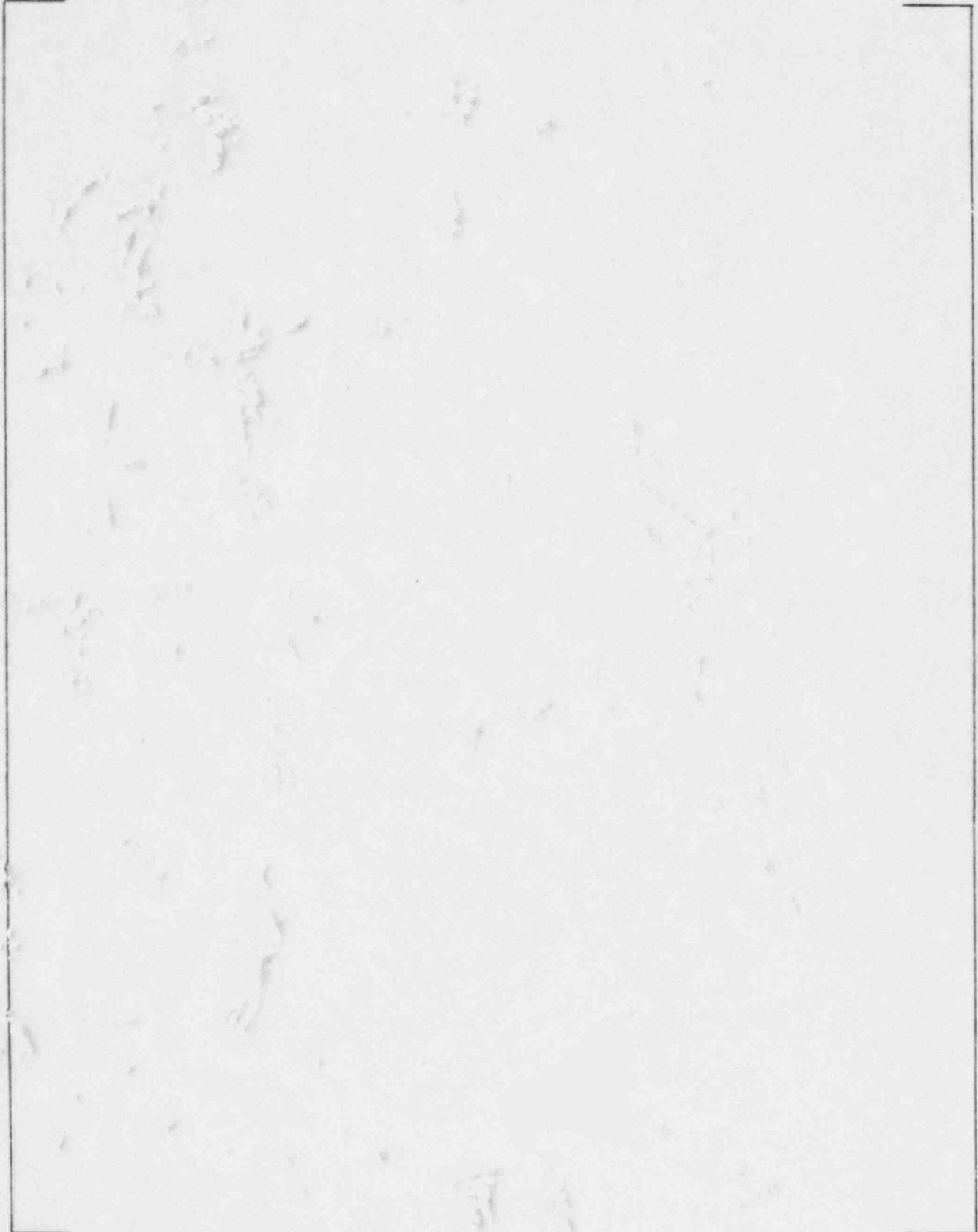MULTIFLEX are punched on cards. The card outputs are:

> Generalized Masses
> Eigenfrequences
> Mode Shapes
> Weighted Relative Boundary Shapes
> Non-Weighted Relative Boundary Shapes
> Absolute Displacement Shapes

The input data instructions are given in Table A-1 and additional notes are:

* In WECAN modeling, node numbers should be consecutive in sequence. A skip
  in node numbering must be avoided.

* If the WECAN model has nodes constrained to each other, the smallest node
  number must be used for WECAN node identifications in this RELMØDE input
  data.

TABLE A-1

INPUT DATA INSTRUCTIONS FOR RELMØDE

A-2

(a,c)
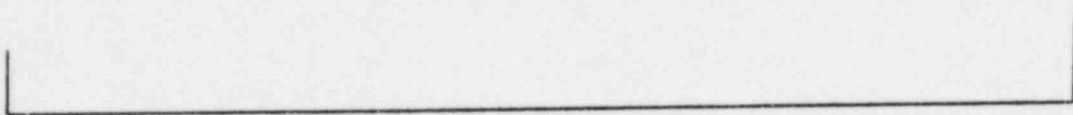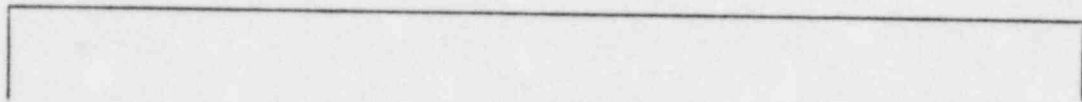
(a,c)

TABLE A-2 Punched Cards As Input Data To MULTIFLEX

A-3